THE ROLE OF ALDH1A2 IN HEAD AND NECK SQUAMOUS CELL CARCINOMA

A Dissertation

Presented to the Faculty of the Weill Cornell Weill Graduate School

of Medical Sciences

in Partial Fulfillment of the Requirements for the Degree of

Doctor of Philosophy

by

Abigail Kathryn Horstmann

June 2017

THE ROLE OF ALDH1A2 IN HEAD AND NECK SQUAMOUS CELL CARCINOMA

Abigail Kathryn Horstmann, Ph.D.

Cornell University 2017

Head and neck squamous cell carcinomas (HNSCC) are one of the most common cancers worldwide. The patient 5-year survival rate has remained approximately 50% for decades, necessitating discovery of novel therapies and targets. To date, all-*trans* retinoic acid (RA) and its isoforms – retinoids – are some of the most-studied and most-active agents in the treatment and prevention of HNSCC. A key enzyme involved in catalyzing the synthesis of endogenous RA from retinol (vitamin A), aldehyde dehydrogenase 1a2 (ALDH1a2), has previously been shown to act as a tumor suppressor in human prostate cancer. Among HNSCC patients, high ALDH1a2 protein expression correlates with better overall survival. Our primary objective was to delineate the role of ALDH1a2 in HNSCC carcinogenesis; further study into the proteins involved in endogenous retinoid synthesis and signaling, such as ALDH1a2, could reveal new and more effective strategies for retinoid therapy. We found that ALDH1a2 transcript levels are dramatically reduced in RNA data sets from over 300 human HNSCC samples, as well as in SCC tumor tissue from mice subjected to the 4-nitroquinoline 1-oxide (4-NQO)-induced murine model of human oral carcinogenesis developed in our lab. Through retroviral gene transduction, we overexpressed ectopic ALDH1a2 in human HNSCC cell lines SCC-4, SCC-9, and SCC-25. We observed that ALDH1a2 overexpression affects the phenotype of these transformed cells *in vitro*, decreasing both proliferation and clonogenicity. In addition, we created transgenic mice that inducibly express transgenic ALDH1a2 specifically in select, stratified epithelial tissues including the tongue, skin, and esophagus. These

mice underwent 4-NQO treatment, to determine whether ectopic ALDH1a2 expression can suppress oral cavity carcinogenesis *in vivo*. We found that the expression of ectopic ALDH1a2 during 4-NQO-induced carcinogenesis reduced the tongue protein expression of enhancer of zeste homolog 2 (EZH2) and vimentin, two markers of epithelial-to-mesenchymal transition (EMT) and tumor migration in this disease. This work provides evidence that ALDH1a2 has tumor suppressive functions in HNSCC and has furthered our understanding of retinoid signaling and cancer chemoprevention.

BIOGRAPHICAL SKETCH

Abigail Kathryn Horstmann was born in Poughkeepsie, New York, on September 27th, 1988. Early on, her parents instilled in her a love of science, learning, and problem-solving, leading Abigail to pursue a Bachelor of Science degree in Biochemistry and Molecular Biology from Pennsylvania State University. During her time as an undergraduate, Abigail had the opportunity to explore several fields of scientific research. Her first laboratory experience – including learning how to pipette – was at JRS Pharma, where she developed chemical assays for use with novel excipient products as a research and development intern. She then worked as a chemical research intern at Keystone Nano, trying to chemically synthesize nanoparticles for use as encapsulates for cancer therapeutics. Throughout the latter part of her undergraduate career, Abigail worked in the laboratory of Dr. Squire J. Booker. There she expressed, purified, and characterized the *Mycobacterium tuberculosis* lipoyl synthase enzyme, a potential future antibiotic target in multi-drug resistant tuberculosis. This research comprised her undergraduate thesis, which earned her a Bachelor of Science with Honors in 2010 and was later published in *Biochemistry* in 2016.

Eager to contribute further to biomedical research, Abigail began her graduate studies in the Pharmacology program at Weill Cornell Graduate School of Medical Sciences. She joined the laboratory of Dr. Lorraine J. Gudas as a Ph.D. Candidate to study cancer and its molecular mechanisms, and continue her work of characterizing potential therapeutic targets in human disease. Here she was awarded a Ruth L. Kirschstein Institutional National Research Service Award (T32) and a Ruth L. Kirschstein Predoctoral Individual National Research Service Award (F31) through the National Institutes of Health to fund her thesis research. Abigail's thesis project is

focused on the retinoic acid synthesis pathway and its function in head and neck squamous cell carcinoma – in particular the role of the enzyme aldehyde dehydrogenase 1a2. This research brings us one step closer to finding new and more effective forms of therapy for this disease. Her years working in the Gudas Laboratory have been exceptionally rewarding, and Abigail leaves with invaluable scientific skills, fond memories, and lifelong friendships to take with her into the next stage of her scientific career and beyond.

ACKNOWLEDGMENTS

There are many people I would like to thank for their contributions to my thesis work, without whom this day may not have been possible. Above all, I would like to express my deepest gratitude to my advisor, Dr. Lorraine J. Gudas. Mentoring a graduate student is no easy (or short) task, yet she did so with positivity and patience throughout. Her expertise and scientific aptitude are an inspiration, and helped guide me during our time working together. I will forever cherish the memory of when I realized we had begun conversing like colleagues rather than strictly as student/teacher, a true mark of how far I had come with her mentorship. While I will miss our conversations, lab trips, and laughs, I look forward to a future of applying everything she taught me, both on and off the bench.

I would also like to thank my Special Committee members Dr. Lonny Levin and Dr. Paraskevi Giannakakou for their guidance over the years. Their scientific discussion and insight given at my committee meetings were instrumental to the progress of this project. In addition, I would like to thank Dr. Yueming Li and Dr. Heidi Stuhlmann for graciously agreeing to be on my thesis examining committee. It is an honor to present my thesis work to such a distinguished group of scientists.

I would also like to thank Dr. Theresa Scognamiglio for generously performing histopathological analysis for this project. In addition, I would like to thank those at the Weill Cornell Electron Microscopy and Histology Core Facility for their tireless efforts in preparing the tissue sections that were so critical to my mouse work. The research herein was made possible by funding through a NIH F31 Predoctoral Fellowship, awarded by the National Institute of Dental and Craniofacial Research (4

F31 DE023273-03), and a NIH T32 Training Grant in Developmental Biology (5 T32 HD060600-04). I am honored and grateful to have been selected for these awards.

I cannot thank my fellow Gudas lab members – past and present – enough for the privilege of working with them. Dr. Gudas has cultivated a laboratory made up of scientists who are as brilliant as they are kind, and their willingness to help was invaluable to me and my research. I would especially like to thank Dr. Xiao-Han Tang for his boundless expertise on retinoic acid signaling and head and neck cancer, and for performing the groundwork on the 4-NQO mouse model that made my project possible. A special thank you to Dr. Leiping Fu, who served as an unofficial mentor while sharing our desk. I am very fortunate to have been seated next to you, as our friendship and our discussions – both scientific and otherwise – were truly a highlight of my time here. I would also like to thank Dr. Kristian Laursen and Dr. Frances Gratacos for mentoring me during my early days as a fledgling scientist in the lab (and beyond). In addition, I am grateful to Dr. Alison Urvalek, Dr. Kwame Osei-Sarfo, and Dr. Steven Trasino for their guidance and scientific input over the many years we worked together.

I would also like to thank my fellow graduate students for the pleasure of learning alongside them in the Gudas Lab. It would have been a very different journey without Dr. Denise Minton, my peer and partner in crime, by my side. We have certainly come a long way from our days as first-years. I will always be grateful that we ended up working together, and I look forward to a lifetime of friendship to come. I would also like to thank Dr. Kasia Marcinkiewicz for being an exceptional role model and guide while a senior graduate student in the lab. Lastly, to the junior graduate students in the lab: Jocelin Kalish, Cynthia Quintero, Ryan Serio, and Jaclyn Kubala, I thank you for the opportunity to pass along my knowledge and to see you

grow as scientists over the last few years. Though I will miss our innumerable coffee runs, walks home, and lunch chats, this isn't the last you'll see of me and I look forward to keeping in touch!

A special thank you goes to Tamara Weissman, Daniel Stummer, and Viral Patel, for the countless ways they helped me over the years. Whether it was aid writing and submitting a grant, ordering key supplies, or teaching me protocols, their efforts helped make all of this possible.

Last but certainly not least, I would like to thank my family and friends for their endless support and encouragement over the years. To my wonderful parents Susan and Paul Horstmann – it is difficult to put into words just how grateful to you I am, but suffice it to say I could not have done this without you. Thank you for raising me to be intellectually curious and open-minded, and to dream big. This is *our* accomplishment. In addition, thank you to my sister Christina Horstmann, another scientist, for always inspiring me to reach higher, do better, and take chances. Finally, to my fiancé Greg, thank you for helping me to be my very best, and for believing in me even when I don't believe in myself. I am incredibly lucky to have you by my side. Graduate school may be coming to an end but our story is only just beginning. To Greg and my family, I give you my love and my thanks from the very bottom of my heart.

TABLE OF CONTENTS

LIST OF FIGURES

LIST OF TABLES

LIST OF ABBREVIATIONS

4N+Dox	4-NQO + Doxycycline
4-NQO	4-Nitroquinoline 1-Oxide
5-Aza	5-Aza-2'-Deoxycytidine
13-cRA	13-*cis*-Retinoic Acid
ALDH1a2	Aldehyde Dehydrogenase 1 Family, Member A2
ADH	Alcohol Dehydrogenase
COX-2	Cyclooxygenase-2
CRABP2	Cellular Retinoic Acid Binding Protein 2
CSC	Cancer Stem Cell
CYP26	Cytochrome P450 Family 26
DMEM	Dulbecco's Modified Eagle Medium
Dox	Doxycycline
EGFR	Epidermal Growth Factor Receptor
EMT	Epithelial-Mesenchymal Transition
EV	Empty Vector
EZH2	Enhancer Of Zeste Homolog 2

FABP5	Fatty Acid Binding Protein 5
FBS	Fetal Bovine Serum
HDAC	Histone Deacetylase
HNSCC	Head and Neck Squamous Cell Carcinoma
HPRT1	Hypoxanthine Phosphoribosyltransferase 1
HPLC	High-performance Liquid Chromatography
HPV	Human Papilloma Virus
K1	Cytokeratin 1
K14	Cytokeratin 14
KRT	K14-rtTA$^{+/-}$
KRT/ALDH	K14-rtTA$^{+/-}$/TRE-ALDH1a2$^{+/-}$
LRAT	Lecithin:retinol Acyl Transferase
NCoR	Nuclear Receptor Co-Repressor
OSCC	Oral Squamous Cell Carcinoma
PBS	Phosphate-Buffered Saline
PPAR	Peroxisome Proliferator-Activated Receptor
PRC2	Polycomb Repressive Complex 2
RA	All-*trans* Retinoic Acid

RALDH2	ALDH1a2 (Formerly Retinaldehyde Dehydrogenase 2)
RAR	Retinoic Acid Receptor
RARE	Retinoic Acid Response Element
RBP4	Retinol Binding Protein 4
RDH	Retinol Dehydrogenase
RT-PCR	Reverse Transcription-PCR
rtTA	Reverse Tetracycline-Controlled Transactivator
RXR	Retinoid X Receptor
SCC	Squamous Cell Carcinoma
SMRT	Silencing Mediator of Retinoic Acid and Thyroid Hormone Receptor
SPT	Second Primary Tumors
STRA6	Stimulated By Retinoic Acid 6
TBST	Tris-Buffered Saline + 0.1% TWEEN 20
TG ALDH1a2	Transgenic (Ectopic) Aldehyde Dehydrogenase 1A2
TRE	Tetracycline Response Element
VC+Dox	Vehicle Control + Doxycycline

CHAPTER ONE

INTRODUCTION

HEAD AND NECK CANCER

Incidence and overview

Head and neck cancers, which affect tissues of the upper aerodigestive tract, represent one of the most common and lethal malignancies worldwide. It is estimated that in 2016 there will be approximately 61,760 new cases (45,330 men and 16,430 women) and 13,190 deaths (9,800 men and 3,390 women) in the United States alone[1]. The vast majority (>90%) of head and neck cancer cases are squamous cell carcinomas (HNSCC) originating in the epithelial mucosa of various tissues, including the oral and nasal cavities, throat (oropharynx, larynx, or hypopharynx), and upper digestive tract[2, 3]. Globally, there are an estimated 550,000 new cases of HNSCC each year, and around 300,000 deaths[4]. The 5-year survival rate is less than 55%, and has remained relatively constant for decades, illuminating the dire need for continued research into HNSCC chemotherapy and chemoprevention[3]. My thesis research addresses this need; by broadening our understanding of HNSCC at the molecular level, I hope to help identify novel targets for more effective strategies for therapy.

The primary etiological factors of HNSCC are long term and excessive tobacco and/or alcohol use, which can act synergistically during carcinogenesis[2]. Repeated exposure of the oral cavity to these carcinogens results in the accumulation of genetic mutations and epigenetic changes in cells in the basal and suprabasal layers of the epithelium, eventually leading to aberrations in cellular differentiation and morphology. Since large areas of tissue are affected by tobacco and/or alcohol

exposure simultaneously, tissues exhibit "field cancerization" in which tumor development is a multifocal process throughout the exposed region[3, 5]. Field cancerization contributes to a high rate of second primary tumors (SPT) and local recurrences among HNSCC patients, complicating treatment and increasing mortality. Our lab's research focuses on tobacco and alcohol-induced carcinomas; however, there exists a subgroup of HNSCC cases that is caused by infection with high-risk types of human papilloma virus (HPV)[2, 3]. HPV-positive HNSCC differs genetically and molecularly from HPV-negative HNSCC, often occurs in the oropharynx, and generally has a more favorable prognosis[6].

Histological and molecular changes observed in HNSCC

During oral cavity carcinogenesis, striking phenotypic changes occur in the stratified squamous epithelium. This tissue is normally a highly-ordered structure characterized by multiple layers of cells (keratinocytes) exhibiting distinct patterns of differentiation ranging from the inner, basal layer to the outer, cornified layer (Figure 1.1)[7]. The basal layer, which adjoins the basement membrane, is highly proliferative and contains a basal stem cell population. As these cells undergo terminal differentiation, they move upward through the suprabasal and superficial layers before eventually dying and being sloughed off. Each layer of keratinocytes represents a different state of differentiation and is characterized by the expression of specific structural proteins which play a critical role in maintaining the integrity of the epithelium[8]. However, this strict organization is lost during carcinogenesis, as cells of the basal and surprabasal layers start exhibiting aberrant differentiation and morphology[8]. Histologically, these changes to the epithelium first manifest as oral premalignant lesions (e.g. leukoplakia), before progressing through hyperplasia and

dysplasia to become oral squamous cell carcinoma (OSCC) and eventually, metastatic cancer[9].

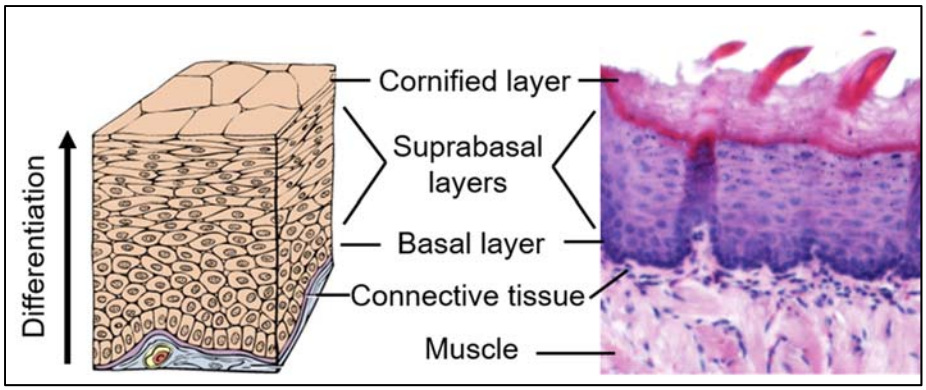

Figure 1.1: Structure of the stratified squamous epithelium. The stratified squamous epithelium, such as that found in the tongue, is composed of multiple layers of cells representing different stages of keratinocyte terminal differentiation. The basal layer contains a highly proliferative stem cell population that maintains the regenerating epithelium. As cells in the basal layer undergo differentiation, they move upwards through the suprabasal layers before eventually dying and sloughing off. Left panel: adapted from John Wiley & Sons, Inc. Right panel: 7µm paraffin-embedded mouse tongue stained with hematoxylin & eosin (200X).

On the molecular level, epithelial cells exhibit changes in many key biological pathways including cellular proliferation, cell survival, squamous epithelial differentiation, and invasion/metastasis[10]. Studies of HNSCC have identified genetic abnormalities in many well-known tumor suppressor genes and oncogenes, some of which will be briefly described here. The tumor suppressive p53 pathway is compromised in up to 80% of HNSCC cases, either through inactivating mutations or other mechanisms[3]. In addition, nearly 94% of HNSCCs exhibit alterations in either *CDKN2A* or *CCND1*, the genes encoding p16 and cyclin D1, respectively[11]. *CDKN2A* is often inactivated, and *CCND1* often amplified or gained, greatly contributing to aberrant cellular proliferation and survival[3]. EGFR overexpression is another common characteristic in HNSCC, and is associated with an unfavorable clinical outcome[11].

HNSCC cells also exhibit a characteristic increase in some squamous differentiation markers (e.g. involucrin, transglutaminase I, cytokeratin 1 (K1)), as well as decreased levels of E-cadherin[3, 12]. These are just some of the many molecular changes that have been identified in HNSCC.

Current treatment strategies

While treatment of early-stage primary tumors with radiation and/or surgery is often successful, SPT, recurrence, and metastasis necessitate additional treatments, of which there are currently few options of only limited clinical efficacy. Currently the gold standard for treatment is a combination therapy comprised of a platinum-based drug (e.g. cisplatin), fluorouracil (FU) or a taxane, and cetuximab, which is a monoclonal antibody that inhibits EGFR[13, 14]. To date, this regimen has demonstrated the greatest clinical activity, and yet still only results in a median survival of 10 months[13]. This underscores the dearth of effective chemotherapies available to HNSCC patients and the need for novel approaches to treatment and prevention. Therefore, my thesis research is focused on a particular signaling pathway that has emerged as a compelling target for new therapies in both preclinical and clinical studies: the retinoid signaling pathway.

THE RETINOIC ACID SYNTHESIS AND SIGNALING PATHWAY

Overview of retinoid signaling

Vitamin A (retinol) and its natural and synthetic derivatives, retinoids, are perhaps some of the most studied and most active agents tested in the treatment and prevention of SPT and HNSCC progression[15]. Endogenous retinoid signaling plays a critical role in the regulation of many key cellular events, including embryonic development, differentiation, proliferation, and apoptosis[16, 17]. Retinol is an essential

micronutrient obtained from the diet, and cannot be synthesized by vertebrates *de novo*[18]. Retinol is transported in the blood while complexed to serum retinol-binding protein (RBP4), and is taken up by certain types of target cells (such as epidermal keratinocytes) via the membrane receptor STRA6 (stimulated by retinoic acid 6) (Figure 1.2)[19, 20].

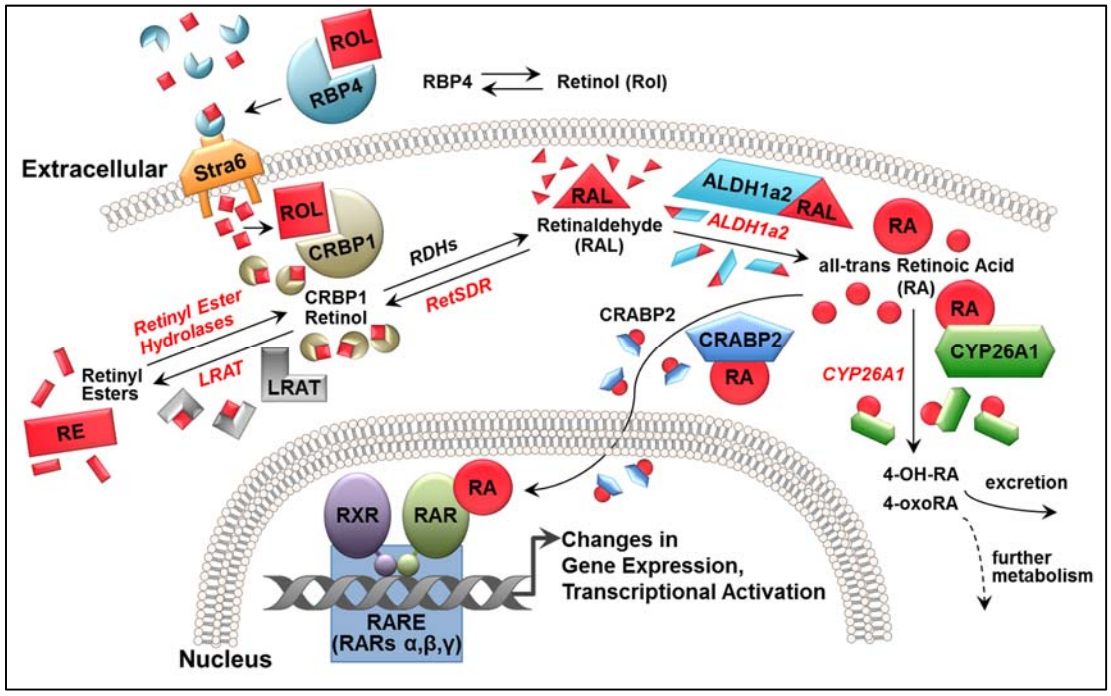

Figure 1.2: Simplified schematic of chief pathways of retinoid signaling and metabolism in mammalian cells. Retinol enters the cell via interactions with RBP4 and Stra6, whereupon it is converted into a variety of metabolites. It can be converted into retinyl esters by LRAT, or into retinaldehyde through the activity of RDHs. ALDH1a2, otherwise known as RALDH2, then catalyzes the synthesis of RA from retinaldehyde. RA is translocated to the nucleus by binding to CRABP, and affects gene expression through its binding and activation of nuclear receptor heterodimers. Figure created by Daniel Stummer and adapted from Mongan & Gudas, 2007.

Upon reaching target cells, intracellular retinol has two possible fates. It can either be converted to retinyl esters for storage by the enzyme lecithin:retinol acyl transferase (LRAT), or it can be metabolized to an active metabolite, the most

biologically active of which is all-*trans* retinoic acid (RA)[17]. RA synthesis from retinol occurs through a series of two enzymatic steps. First, all-*trans* retinol is reversibly oxidized by alcohol dehydrogenases (ADHs) or retinol dehydrogenases (RDHs) to form all-*trans* retinaldehyde. Aldehyde dehydrogenases (ALDHs) then irreversibly oxidize all-*trans* retinaldehyde to form RA[21]. Free cytoplasmic RA can then be translocated to the nucleus by cellular retinoic acid binding protein 2 (CRABP2), whereupon RA exerts its biological effect by binding to and activating specific nuclear receptors – retinoic acid receptors (RARs) and retinoid X receptors (RXRs)[22]. These receptors function as RAR/RXR heterodimers, and are bound to specific DNA sequences known as retinoic acid response elements (RAREs) in order to control the transcription of a wide assortment of downstream genes (Figure 1.2)[23]. Activation of RAR/RXR by a retinoid agonist causes the dissociation of co-repressors and recruitment of co-activators, inducing transcription[24]. In addition, RXRs can dimerize with other nuclear receptors, such as the peroxisome proliferator-activated receptor (PPARβ/δ), to initiate transcriptional changes and cellular responses distinct from those initiated by RAR/RXR[25, 26].

Besides acting as classical transcription factors, retinoid receptors can also affect gene expression by inducing epigenetic changes that modify the chromatin structure[27, 28]. For example, our lab has demonstrated that in the presence of a retinoid agonist, RAR-regulated genes acquire H3K4/9ac activation marks and lose H3K27me3 marks, stimulating transcriptional activation[29-31]. Such epigenetic changes occur as a result of the action of numerous co-regulators associated with the retinoid receptors, and these modifications can be long-term and stable[32]. Co-repressors inhibit transcriptional activation by retinoid receptors until an agonist is present, at which point they disassociate to allow for binding of co-activators. Known co-repressors include the nuclear receptor co-repressor (NCoR) and the silencing mediator of

retinoic acid and thyroid hormone receptor (SMRT), which mediate the recruitment of repressor complexes that contain histone deacetylases (HDACs)[33]. Research in our lab has shown that the polycomb repressive complex (PRC2), an epigenetic silencing complex that contains histone methyltransferase (HMT) activity and is responsible for H3K27me3, is also displaced from RAREs by RA signaling[29, 34, 35]. Notable co-activators include proteins with histone acetyltransferase activity, e.g. p300/CBP, pCAF, and p160 co-activators[17]. Thus, retinoids are potent signaling biomolecules that can have pleiotropic effects by modulating the transcription and epigenetic status of many important and diverse genes[16-18].

Retinoid signaling is disrupted in cancer

Aberrations in retinoid signaling and metabolism are frequently observed in human epithelial cancers, including HNSCC[17]. Prostate, skin, colon, kidney, and breast cancers also often exhibit alterations in this pathway[25, 36-39]. Since one of the physiological functions of retinoid signaling is to maintain normal cell growth and differentiation, it follows that aberrations in this pathway would disrupt this regulation and promote the malignant cellular dysregulation observed in HNSCC. Changes in this pathway that have been observed in HNSCC include reductions in LRAT, RARγ, RARβ$_2$, and CRABP2 mRNA and protein levels, as well as increases in cytochrome P450 26A1 (CYP26A1), which is the enzyme that catalyzes the first step of RA degradation (Figure 1.2)[6, 17, 40-45]. In the case of RARβ$_2$, expression is lost via hypermethylation of the promoter (rather than genetic mutation), and is believed to be an early event in carcinogenesis[46, 47]. In addition, early studies (first reported in 1925 by Wolbach and Howe) found that vitamin A deficiency induces squamous metaplasia in the mucosa of the upper aerodigestive tract, similar to premalignant events in the mucosa of heavy smokers[46, 48]. Conversely, epidemiologic studies found that a high

dietary intake of vitamin A is associated with slower progression of carcinogenesis of several cancers, including OSCC[49]. This inverse association between cancer development and retinoid status and signaling illustrates the importance of the endogenous retinoid pathway in maintaining proper endogenous differentiation and preventing malignant transformation.

Retinoid use in cancer treatment and prevention

Restoration of retinoid signaling is therefore an attractive therapeutic strategy to reinstate the normal pathway of differentiation and inhibit the malignant phenotype. Clinically, retinoids have been a chemotherapeutic and chemopreventative focus for decades and are already used in a number of successful treatment regimens for various malignancies[17, 25, 50]. Most notably, acute promyelocytic leukemia (APL), which used to have a high mortality rate, is now the most curable subtype of acute myelocytic leukemia[51, 52]. This is due to the addition of RA treatment to the standard anthracycline-based chemotherapy, which increased the long-term survival from just 40% to above 80%[51, 52]. Recently, a phase III clinical trial was able to increase this survival rate even further; the combination of RA and arsenic trioxide demonstrated a two-year event-free survival rate of 97% (versus 86% seen with RA and chemotherapy)[53]. This application exemplifies the use of retinoids as differentiation therapy, as treatment with RA causes abnormal promyelocytic leukemia cells to differentiate into normal granulocytes, preventing further proliferation[25, 54].

In the context of squamous cell carcinoma, modulating retinoid signaling has yielded promising results in cell culture and xenograft studies. Transfection of RARβ into the human esophageal squamous cell carcinoma line TE-8, which does not express RARβ, induced apoptosis and inhibited proliferation and colony formation[47, 55]. This induction of RARβ also suppressed the expression of cyclooxygenase (COX)-

2, an enzyme that shows increased expression in HNSCC and has been linked to carcinogenesis and metastasis. In addition, a skin cancer study showed that loss of RARγ predisposed epidermal keratinocytes to Ras-induced squamous cell carcinoma *in vivo* in xenograft experiments, suggesting that RARγ acts as a tumor suppressor in this cell type[56]. Both of these studies link loss of retinoid signaling to epithelial tumorigenesis.

Furthermore, a large body of work has explored the effectiveness of treatment with exogenous retinoids, either alone or in combination, in HNSCC. Treatment of many different human HNSCC cell lines with RA inhibits cell proliferation and decreases mRNA and protein levels of squamous differentiation markers that are aberrantly overexpressed in HNSCC: transglutaminase type 1, involucrin, and K1[12, 57]. In contrast, culturing the HNSCC cell line 1483 in delipidized serum, from which endogenous retinoids have been extracted, increased the expression of these same three differentiation markers[58]. Recent work has found evidence that RA treatment inhibits the growth of HNSCC cancer stem cells (CSCs) by inducing differentiation and suppressing Wnt/β-catenin signaling[59]. RA given alone or in combination with sodium butyrate was found to inhibit cell growth and to induce cell cycle G1 arrest and its associated markers (cyclin-dependent kinase 6, p21, and p27) in human OSCC cell lines SCC-1 and SCC-9[60]. In the human tongue SCC line Tca8113, treatment with RA and antisense oligonucleotides against hTR had a synergistic anti-tumor effect, inducing apoptosis *in vitro* and inhibiting tumor growth in xenograft experiments[61]. Interestingly, retinoid administration also enhances the cytotoxic effects of cisplatin in cell culture and xenograft experiments[62].

Retinoid use in a murine model of OSCC

Studies conducted in our lab using a carcinogen-induced murine model of OSCC have further elucidated an anti-tumorigenic role for retinoids and retinoid signaling. In this mouse model, which was first developed in our lab by Tang et al., mice are administered the carcinogen 4-nitroquinoline 1-oxide (4-NQO) in the drinking water[63]. Similar to tobacco and its related carcinogens, 4-NQO causes DNA adduct formation, resulting in adenosine substitution for guanosine[63, 64]. 4-NQO-treated mice develop carcinomas that resemble human HNSCC morphologically, histologically, and molecularly, making this an excellent animal model for experimentation[63]. Our lab found that treatment with RA in combination with 5-Aza-2'-deoxycytidine (5-Aza), a DNA methyltransferase inhibitor, reduced oral cavity carcinogenesis and increased RARβ_2 mRNA levels in 4-NQO treated mice (relative to mice treated with 4-NQO + PBS)[65]. Researchers in our lab also reported that treatment with bexarotene (a RXR agonist) and CD1530 (a RARγ agonist) reduced oral cavity carcinogenesis in this mouse model[66]. Lastly, in a model of 4-NQO-induced carcinogenesis in rats, Choi et al. found that a single injection of RA-loaded microspheres was able to suppress oral carcinogenesis[67]. Together, these animal studies reveal that retinoid treatment can inhibit oral carcinogenesis in mice *in vivo*.

Retinoid-based therapies: clinical trials

The early clinical successes of retinoid treatment in suppressing epithelial carcinogenesis helped to define the modern concept of clinical cancer chemoprevention[68]. In HNSCC, much of the focus has been on the use of 13-*cis*-RA (13-cRA, also known as isotretinoin), a naturally occurring isomer of RA that has more favorable pharmacokinetic properties[15]. In initial clinical trials, high-dose 13-cRA was efficacious in suppressing oral premalignant lesions (leukoplakia) and SPT

in HNSCC patients[69, 70]. Furthermore, researchers reported that treatment with 13-cRA restored RARβ mRNA expression, and that restoration of RARβ mRNA was associated with clinical response[71]. However, in a subsequent large-scale randomized phase III clinical trial, low-dose 13-cRA given orally as a single drug was not effective in preventing SPT or recurrence in early-stage HNSCC patients[72]. This result was likely affected by the inclusion of "current smokers" in this and related trials; it has been reported that when compared to "former" and "never" smokers, current smokers have a statistically significantly higher rate of SPT and mortality[68, 72]. In addition, this randomized phase III trial tested a much lower dose of 13-cRA than previous trials (30 mg/day vs. 50-100 mg/m^2/day), prioritizing patient tolerance over chemopreventative efficacy[70].

These limited but promising clinical results have prompted further study into the pharmacology of retinoids in HSNCC and investigation into novel retinoid therapy options. Combination therapy is one attractive option that is currently being explored. Treatment of advanced HNSCC patients with a combination of 13-cRA, interferon-α2a, and chemotherapy has yielded promising results and is awaiting further confirmation by randomized studies[52]. Another research interest is the additional characterization of the proteins involved in the endogenous retinoid signaling pathway and their roles in potentially preventing HNSCC. Such studies could yield new insights and inspire new and more effective strategies for therapy to complement or improve upon existing treatments with exogenous retinoids.

ALDH1A2: A PUTATIVE TUMOR SUPPRESSOR

One enzyme in the endogenous retinoid synthesis and signaling pathway that is currently of interest in the field is ALDH1a2, or aldehyde dehydrogenase family 1 member A2 (previously known as RALDH2; Gene ID: 8854). ALDH1a2 is a

cytosolic, NAD-dependent enzyme that catalyzes the final step of RA synthesis: the irreversible oxidation of all-*trans*-retinaldehyde to yield RA (Figure 1.2)[21, 73]. The cloning of mouse, human, and chick ALDH1a2 homologs revealed 94-98% amino acid sequence similarity, indicating that ALDH1a2 is highly evolutionarily conserved[74]. Much of the research on ALDH1a2 to date has been in the context of normal prenatal development, as an ALDH1a2 gene knockout is embryonic lethal in developing mice due to defects in heart morphogenesis[75, 76]. This reflects the importance of embryonic RA synthesis from retinol. Research on zebrafish has also identified an intriguing role for ALDH1a2 in tissue regeneration; ALDH1a2 transcripts are highly induced after amputation of the adult fin, larval fin, and heart, and inhibition of ALDH1a2 using a small molecule inhibitor or morpholino prevented organ regeneration[27, 77].

In cancer studies, ALDH1a2 has emerged as a candidate tumor suppressor. The first work suggesting this was conducted by Kim *et al*., in which they found that the ALDH1a2 promoter is hypermethylated in the majority of human prostate tumors, and that ALDH1a2 is expressed in normal but not tumor prostate epithelium (Figure 1.3A)[78]. Restoration of ALDH1a2 expression, either through transfection with exogenous ALDH1a2 or treatment with 5-Aza, suppressed colony formation of human prostate cancer cell lines (Figure 1.3C,D)[78]. In addition, mouse studies in our lab revealed that ALDH1a2 protein levels were significantly lower in prostate tissue in a transgenic mouse model of prostate cancer as compared to control mice[79]. Loss of ALDH1a2 expression has also been reported in human ovarian cancer cells, contributing to an overall reduction in retinol metabolism[80]. Additionally, high ALDH1a2 mRNA levels correlate with better overall survival for breast cancer patients[81].

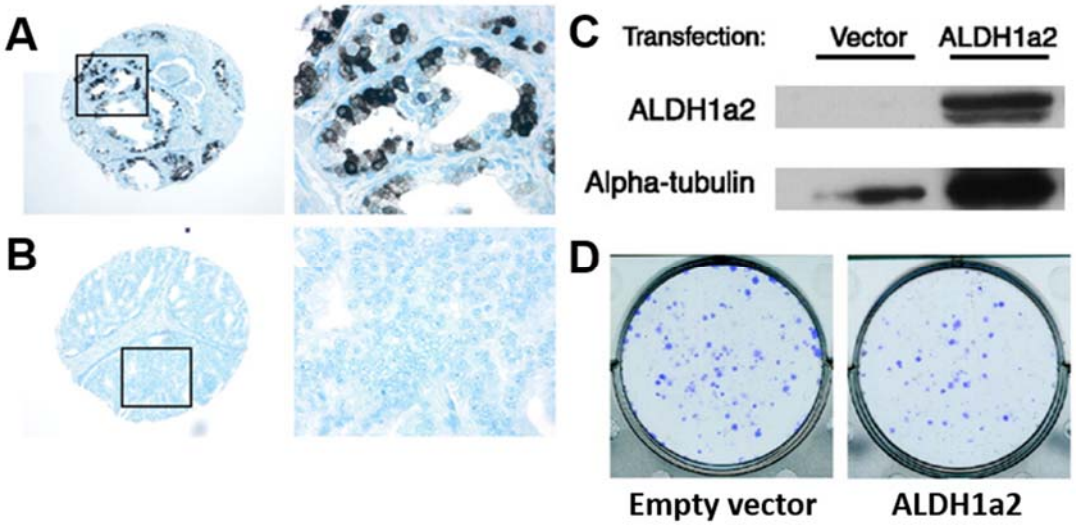

Figure 1.3: ALDH1a2 is expressed in normal, but not tumor, prostate epithelium, and its reexpression inhibits colony formation in prostate cancer cells *in vitro* (adapted from Kim *et al.*, 2005). (A,B) ALDH1a2 immunostaining of a tissue microarray comprised of n=21 primary prostate tumors and matched normal prostate specimens. Images were taken at 100X (left panels) and 400X (right panels). (A) Representative images from a normal prostate epithelium and (B) matched prostate tumor from the same individual. (C) Western blot analysis verifying ALDH1a2 overexpression in prostate cancer cell line DU145 24-hours after transfection . α–tubulin was used as a loading control. (D) Representative colony formation assay of empty-vector- and ALDH1a2-transfected DU145 cells.

Research on ALDH1a2 in the context of HNSCC is more recent. Because HNSCC patients with HPV-driven tumors show a favorable prognosis compared to patients with non-HPV-driven tumors, researchers used an array-based approach to identify differences in promoter methylation that might contribute to this difference in clinical response. In 2013 they reported that hypermethylation of the ALDH1a2 promoter was a common feature of tumors from patients with non-HPV-driven HNSCC and that there was a strong correlation between ALDH1a2 protein levels and a favorable clinical outcome, independent of HPV status (Figure 1.4)[6]. The same group further extended these observations using cell culture and xenograft-based

studies. They treated the human HNSCC cell lines FaDu and Detroit562 with WIN18.446, a bisdichloroacetyldiamine that is a known inhibitor of ALDH1a2, and with BMS493, an inverse agonist of pan-RAR which enhances NCoR interaction with RARs[82, 83]. They observed that treatment of these cells with WIN18.446 or BMS493 resulted in a loss of cell-to-cell junctions and the formation of more poorly-defined clusters, indicative of a loss of epithelial morphology. In addition, they detected a significant increase in the transcript levels of the mesenchymal markers vimentin and N-Cadherin in FaDu cells following treatment with either inhibitor. These results suggest that the inhibition of ALDH1a2-RAR signaling in HNSCC cells results in a loss of cell adhesion and a gain of a mesenchymal-like phenotype. Moreover, in a mouse xenograft model they found that silencing ALDH1a2 using shRNA accelerated tumor growth *in vivo* and resulted in increased tumor vimentin expression, again reflecting a more mesenchymal tumor phenotype (Figure 1.5)[82]. These studies confirmed a link between ALDH1a2 signaling (or lack thereof) and the pathogenesis of HNSCC, however this relationship is still poorly defined.

In the research described herein, we investigated the role of ALDH1a2 in HNSCC tumorigenesis. First we explored the effects of ALDH1a2 expression in transformed human SCC cell lines to delineate the effects of ALDH1a2 on the preexisting malignant phenotype. We then generated a novel transgenic mouse line that showed inducible and tissue-specific expression of ALDH1a2 to determine whether or not ALDH1a2 induction could attenuate the development or progression of oral cavity carcinogenesis in the 4-NQO mouse model. In total, we explored the therapeutic and preventative potential of the enzyme ALDH1a2 in HNSCC.

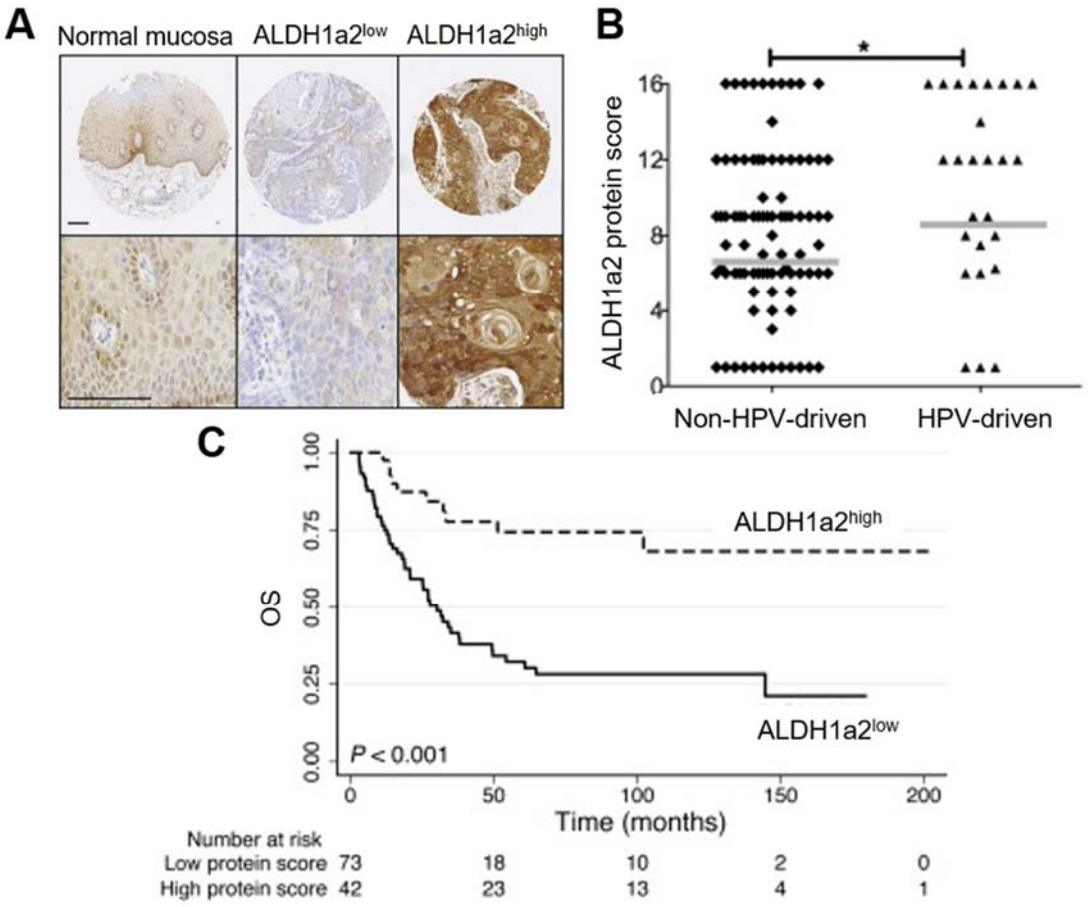

Figure 1.4: ALDH1a2 protein expression correlates with better clinical outcome of HNSCC patients (adapted from Kostareli, *et al.*, 2013). (A) Immunostaining of tissue microarrays generated from primary tumors of n=115 HNSCC patients with known HPV status (n=89 non-HPV-driven; n=29 HPV-driven). They observed low-to-moderate staining for ALDH1a2 protein in keratinocytes in the healthy oral mucosa as well as in n=73 (63.5%) primary tumors ("ALDH1a2^{low}"). High ALDH1a2 protein levels were detected in n=42 (36.5%) primary tumors ("ALDH1a2^{high}"). Tissues were counterstained with hematoxylin (blue nuclear stain). Scale bar represents 100µm). (B) Higher ALDH1a2 protein expression was detected in HPV-driven tumors compared to non-HPV-driven. Bars denote medians. Data was analyzed using a 2-tailed Mann-Whitney *U* test. (C) Kaplan-Meier plot for overall survival (OS) with respect to ALDH1a2 protein level in n=115 HNSCC patients. A log-rank/Mantel-Cox test was used to determine *p* values.

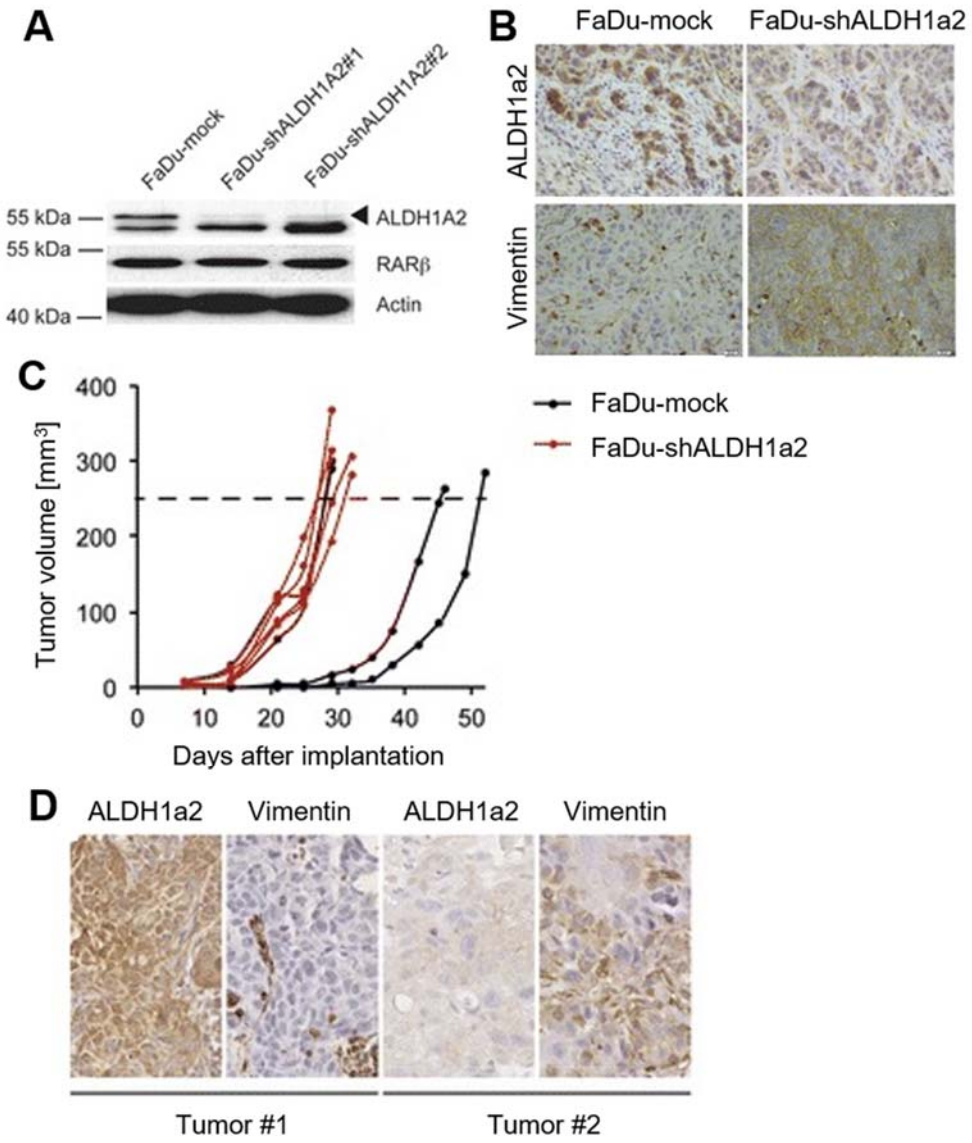

Figure 1.5: Silencing ALDH1a2 accelerated tumor growth and increased tumor vimentin expression in a mouse xenograft model (adapted from Seidensaal, *et al.*, 2015). (A) Western blot analysis demonstrating shRNA-mediated silencing of ALDH1a2 expression in human SCC cell line, FaDu. FaDu-mock cells were used as a negative control. (B) Representative images of IHC staining of tumor sections from FaDu-mock or FaDu-shALDH1a2-injected xenografts to analyze ALDH1a2 and vimentin expression. Increased vimentin expression was observed in FaDu-shALDH1a2 tumors. (C) Quantfication of tumor volume (in mm^3) in mice (n=4 per group) at various times following implantation with FaDu-mock or FaDu-shALDH12 cells. Tumor growth was homogeneous among FaDu-shALDH1a2-implanted mice, however 50% of FaDu-mock tumors exhibited slower growth. (D) Inverse expression of ALDH1a2 and vimentin expression was observed in primary tumors via IHC of serial tumor sections.

REFERENCES

1. Cancer Facts & Figures - 2016, American Cancer Society, 2016.

2. Curado MP, Hashibe M. Recent changes in the epidemiology of head and neck cancer. Curr Opin Oncol. 2009;21: 194-200.

3. Leemans CR, Braakhuis BJ, Brakenhoff RH. The molecular biology of head and neck cancer. Nat Rev Cancer. 2011;11: 9-22.

4. Jemal A, Bray F, Center MM, Ferlay J, Ward E, Forman D. Global cancer statistics. CA Cancer J Clin. 2011;61: 69-90.

5. Mohan M, Jagannathan N. Oral field cancerization: an update on current concepts. Oncol Rev. 2014;8: 244.

6. Kostareli E, Holzinger D, Bogatyrova O, et al. HPV-related methylation signature predicts survival in oropharyngeal squamous cell carcinomas. J Clin Invest. 2013;123: 2488-2501.

7. Squier CA, Kremer MJ. Biology of oral mucosa and esophagus. J Natl Cancer Inst Monogr. 2001: 7-15.

8. Presland RB, Dale BA. Epithelial structural proteins of the skin and oral cavity: function in health and disease. Crit Rev Oral Biol Med. 2000;11: 383-408.

9. El-Naggar AK. Pathobiology of head and neck squamous tumorigenesis. Curr Cancer Drug Targets. 2007;7: 606-612.

10. Rothenberg SM, Ellisen LW. The molecular pathogenesis of head and neck squamous cell carcinoma. J Clin Invest. 2012;122: 1951-1957.

11. Pezzuto F, Buonaguro L, Caponigro F, et al. Update on Head and Neck Cancer: Current Knowledge on Epidemiology, Risk Factors, Molecular Features and Novel Therapies. Oncology. 2015;89: 125-136.

12. Lotan R. Suppression of squamous cell carcinoma growth and differentiation by retinoids. Cancer Res. 1994;54: 1987s-1990s.

13. Sacco AG, Cohen EE. Current Treatment Options for Recurrent or Metastatic Head and Neck Squamous Cell Carcinoma. J Clin Oncol. 2015;33: 3305-3313.
14. Vermorken JB, Mesia R, Rivera F, et al. Platinum-based chemotherapy plus cetuximab in head and neck cancer. N Engl J Med. 2008;359: 1116-1127.
15. Lee JJ, Wu X, Hildebrandt MA, et al. Global assessment of genetic variation influencing response to retinoid chemoprevention in head and neck cancer patients. Cancer Prev Res (Phila). 2011;4: 185-193.
16. Bushue N, Wan YJ. Retinoid pathway and cancer therapeutics. Adv Drug Deliv Rev. 2010;62: 1285-1298.
17. Mongan NP, Gudas LJ. Diverse actions of retinoid receptors in cancer prevention and treatment. Differentiation. 2007;75: 853-870.
18. Blomhoff R, Blomhoff HK. Overview of retinoid metabolism and function. J Neurobiol. 2006;66: 606-630.
19. Laursen KB, Gudas LJ. Crossing the barrier: STRA6 in epidermal differentiation. J Invest Dermatol. 2014;134: 1504-1506.
20. Laursen KB, Kashyap V, Scandura J, Gudas LJ. An alternative retinoic acid-responsive Stra6 promoter regulated in response to retinol deficiency. J Biol Chem. 2015;290: 4356-4366.
21. Napoli JL. Physiological insights into all-trans-retinoic acid biosynthesis. Biochim Biophys Acta. 2012;1821: 152-167.
22. Napoli JL, Boerman MH, Chai X, Zhai Y, Fiorella PD. Enzymes and binding proteins affecting retinoic acid concentrations. J Steroid Biochem Mol Biol. 1995;53: 497-502.
23. Gudas LJ. Retinoids and vertebrate development. J Biol Chem. 1994;269: 15399-15402.

24. Wei LN. Retinoid receptors and their coregulators. Annu Rev Pharmacol Toxicol. 2003;43: 47-72.

25. Tang XH, Gudas LJ. Retinoids, retinoic acid receptors, and cancer. Annu Rev Pathol. 2011;6: 345-364.

26. Schug TT, Berry DC, Shaw NS, Travis SN, Noy N. Opposing effects of retinoic acid on cell growth result from alternate activation of two different nuclear receptors. Cell. 2007;129: 723-733.

27. Gudas LJ. Emerging roles for retinoids in regeneration and differentiation in normal and disease states. Biochim Biophys Acta. 2012;1821: 213-221.

28. Urvalek A, Laursen KB, Gudas LJ. The roles of retinoic acid and retinoic acid receptors in inducing epigenetic changes. Subcell Biochem. 2014;70: 129-149.

29. Gillespie RF, Gudas LJ. Retinoid regulated association of transcriptional co-regulators and the polycomb group protein SUZ12 with the retinoic acid response elements of Hoxa1, RARbeta(2), and Cyp26A1 in F9 embryonal carcinoma cells. J Mol Biol. 2007;372: 298-316.

30. Kashyap V, Gudas LJ, Brenet F, Funk P, Viale A, Scandura JM. Epigenomic reorganization of the clustered Hox genes in embryonic stem cells induced by retinoic acid. J Biol Chem. 2011;286: 3250-3260.

31. Kashyap V, Laursen KB, Brenet F, Viale AJ, Scandura JM, Gudas LJ. RARγ is essential for retinoic acid induced chromatin remodeling and transcriptional activation in embryonic stem cells. J Cell Sci. 2013;126: 999-1008.

32. Gudas LJ. Retinoids induce stem cell differentiation via epigenetic changes. Semin Cell Dev Biol. 2013;24: 701-705.

33. Urvalek AM, Gudas LJ. Retinoic acid and histone deacetylases regulate epigenetic changes in embryonic stem cells. J Biol Chem. 2014;289: 19519-19530.

34. Benoit YD, Laursen KB, Witherspoon MS, Lipkin SM, Gudas LJ. Inhibition of PRC2 histone methyltransferase activity increases TRAIL-mediated apoptosis sensitivity in human colon cancer cells. J Cell Physiol. 2013;228: 764-772.
35. Marcinkiewicz KM, Gudas LJ. Altered epigenetic regulation of homeobox genes in human oral squamous cell carcinoma cells. Exp Cell Res. 2014;320: 128-143.
36. Guo X, Knudsen BS, Peehl DM, et al. Retinol metabolism and lecithin:retinol acyltransferase levels are reduced in cultured human prostate cancer cells and tissue specimens. Cancer Res. 2002;62: 1654-1661.
37. Guo X, Gudas LJ. Metabolism of all-trans-retinol in normal human cell strains and squamous cell carcinoma (SCC) lines from the oral cavity and skin: reduced esterification of retinol in SCC lines. Cancer Res. 1998;58: 166-176.
38. Guo X, Nanus DM, Ruiz A, Rando RR, Bok D, Gudas LJ. Reduced levels of retinyl esters and vitamin A in human renal cancers. Cancer Res. 2001;61: 2774-2781.
39. Guo X, Ruiz A, Rando RR, Bok D, Gudas LJ. Esterification of all-trans-retinol in normal human epithelial cell strains and carcinoma lines from oral cavity, skin and breast: reduced expression of lecithin:retinol acyltransferase in carcinoma lines. Carcinogenesis. 2000;21: 1925-1933.
40. Xu XC, Ro JY, Lee JS, Shin DM, Hong WK, Lotan R. Differential expression of nuclear retinoid receptors in normal, premalignant, and malignant head and neck tissues. Cancer Res. 1994;54: 3580-3587.
41. Youssef EM, Lotan D, Issa JP, et al. Hypermethylation of the retinoic acid receptor-beta(2) gene in head and neck carcinogenesis. Clin Cancer Res. 2004;10: 1733-1742.
42. Hu L, Crowe DL, Rheinwald JG, Chambon P, Gudas LJ. Abnormal expression of retinoic acid receptors and keratin 19 by human oral and epidermal squamous cell carcinoma cell lines. Cancer Res. 1991;51: 3972-3981.

43. Yang Q, Wang R, Xiao W, Sun F, Yuan H, Pan Q. Cellular Retinoic Acid Binding Protein 2 Is Strikingly Downregulated in Human Esophageal Squamous Cell Carcinoma and Functions as a Tumor Suppressor. PLoS One. 2016;11: e0148381.
44. Osanai M, Lee GH. Increased expression of the retinoic acid-metabolizing enzyme CYP26A1 during the progression of cervical squamous neoplasia and head and neck cancer. BMC Res Notes. 2014;7: 697.
45. Klaassen I, Brakenhoff RH, Smeets SJ, Snow GB, Braakhuis BJ. Enhanced turnover of all-trans-retinoic acid and increased formation of polar metabolites in head and neck squamous cell carcinoma lines compared with normal oral keratinocytes. Clin Cancer Res. 2001;7: 1017-1025.
46. Lotan R. Roles of retinoids and their nuclear receptors in the development and prevention of upper aerodigestive tract cancers. Environ Health Perspect. 1997;105 Suppl 4: 985-988.
47. Xu XC. Tumor-suppressive activity of retinoic acid receptor-beta in cancer. Cancer Lett. 2007;253: 14-24.
48. Wolbach SB, Howe PR. TISSUE CHANGES FOLLOWING DEPRIVATION OF FAT-SOLUBLE A VITAMIN. J Exp Med. 1925;42: 753-777.
49. Clarke N, Germain P, Altucci L, Gronemeyer H. Retinoids: potential in cancer prevention and therapy. Expert Rev Mol Med. 2004;6: 1-23.
50. Lotan R. Retinoids in cancer chemoprevention. FASEB J. 1996;10: 1031-1039.
51. Lengfelder E, Saussele S, Weisser A, Büchner T, Hehlmann R. Treatment concepts of acute promyelocytic leukemia. Crit Rev Oncol Hematol. 2005;56: 261-274.
52. Uray IP, Dmitrovsky E, Brown PH. Retinoids and rexinoids in cancer prevention: from laboratory to clinic. Semin Oncol. 2016;43: 49-64.

53. Lo-Coco F, Avvisati G, Vignetti M, et al. Retinoic acid and arsenic trioxide for acute promyelocytic leukemia. N Engl J Med. 2013;369: 111-121.
54. Ablain J, de Thé H. Retinoic acid signaling in cancer: The parable of acute promyelocytic leukemia. Int J Cancer. 2014;135: 2262-2272.
55. Li M, Song S, Lippman SM, et al. Induction of retinoic acid receptor-beta suppresses cyclooxygenase-2 expression in esophageal cancer cells. Oncogene. 2002;21: 411-418.
56. Chen CF, Goyette P, Lohnes D. RARgamma acts as a tumor suppressor in mouse keratinocytes. Oncogene. 2004;23: 5350-5359.
57. Zou CP, Clifford JL, Xu XC, et al. Modulation by retinoic acid (RA) of squamous cell differentiation, cellular RA-binding proteins, and nuclear RA receptors in human head and neck squamous cell carcinoma cell lines. Cancer Res. 1994;54: 5479-5487.
58. Poddar S, Hong WK, Thacher SM, Lotan R. Retinoic acid suppression of squamous differentiation in human head-and-neck squamous carcinoma cells. Int J Cancer. 1991;48: 239-247.
59. Lim YC, Kang HJ, Kim YS, Choi EC. All-trans-retinoic acid inhibits growth of head and neck cancer stem cells by suppression of Wnt/β-catenin pathway. Eur J Cancer. 2012;48: 3310-3318.
60. Wang A, Zeng R, Huang H. Retinoic acid and sodium butyrate as cell cycle regulators in the treatment of oral squamous carcinoma cells. Oncol Res. 2008;17: 175-182.
61. Xu Q, Zhang Z, Zhang P, Chen W. Antisense oligonucleotides and all-trans retinoic acid have a synergistic anti-tumor effect on oral squamous cell carcinoma. BMC Cancer. 2008;8: 159.

62. Shalinsky DR, Bischoff ED, Gregory ML, et al. Enhanced antitumor efficacy of cisplatin in combination with ALRT1057 (9-cis retinoic acid) in human oral squamous carcinoma xenografts in nude mice. Clin Cancer Res. 1996;2: 511-520.
63. Tang XH, Knudsen B, Bemis D, Tickoo S, Gudas LJ. Oral cavity and esophageal carcinogenesis modeled in carcinogen-treated mice. Clin Cancer Res. 2004;10: 301-313.
64. Phillips DH. Smoking-related DNA and protein adducts in human tissues. Carcinogenesis. 2002;23: 1979-2004.
65. Tang XH, Albert M, Scognamiglio T, Gudas LJ. A DNA methyltransferase inhibitor and all-trans retinoic acid reduce oral cavity carcinogenesis induced by the carcinogen 4-nitroquinoline 1-oxide. Cancer Prev Res (Phila). 2009;2: 1100-1110.
66. Tang XH, Osei-Sarfo K, Urvalek AM, Zhang T, Scognamiglio T, Gudas LJ. Combination of bexarotene and the retinoid CD1530 reduces murine oral-cavity carcinogenesis induced by the carcinogen 4-nitroquinoline 1-oxide. Proc Natl Acad Sci U S A. 2014;111: 8907-8912.
67. Choi Y, Kim SY, Park K, et al. Chemopreventive efficacy of all-trans-retinoic acid in biodegradable microspheres against epithelial cancers: results in a 4-nitroquinoline 1-oxide-induced oral carcinogenesis model. Int J Pharm. 2006;320: 45-52.
68. Freemantle SJ, Dragnev KH, Dmitrovsky E. The retinoic acid paradox in cancer chemoprevention. J Natl Cancer Inst. 2006;98: 426-427.
69. Hong WK, Endicott J, Itri LM, et al. 13-cis-retinoic acid in the treatment of oral leukoplakia. N Engl J Med. 1986;315: 1501-1505.
70. Hong WK, Lippman SM, Itri LM, et al. Prevention of second primary tumors with isotretinoin in squamous-cell carcinoma of the head and neck. N Engl J Med. 1990;323: 795-801.

71. Lotan R, Xu XC, Lippman SM, et al. Suppression of retinoic acid receptor-beta in premalignant oral lesions and its up-regulation by isotretinoin. N Engl J Med. 1995;332: 1405-1410.

72. Khuri FR, Lee JJ, Lippman SM, et al. Randomized phase III trial of low-dose isotretinoin for prevention of second primary tumors in stage I and II head and neck cancer patients. J Natl Cancer Inst. 2006;98: 441-450.

73. Zhao D, McCaffery P, Ivins KJ, et al. Molecular identification of a major retinoic-acid-synthesizing enzyme, a retinaldehyde-specific dehydrogenase. Eur J Biochem. 1996;240: 15-22.

74. Duester G, Mic FA, Molotkov A. Cytosolic retinoid dehydrogenases govern ubiquitous metabolism of retinol to retinaldehyde followed by tissue-specific metabolism to retinoic acid. Chem Biol Interact. 2003;143-144: 201-210.

75. Niederreither K, Subbarayan V, Dollé P, Chambon P. Embryonic retinoic acid synthesis is essential for early mouse post-implantation development. Nat Genet. 1999;21: 444-448.

76. Niederreither K, Vermot J, Le Roux I, Schuhbaur B, Chambon P, Dollé P. The regional pattern of retinoic acid synthesis by RALDH2 is essential for the development of posterior pharyngeal arches and the enteric nervous system. Development. 2003;130: 2525-2534.

77. Mathew LK, Sengupta S, Franzosa JA, et al. Comparative expression profiling reveals an essential role for raldh2 in epimorphic regeneration. J Biol Chem. 2009;284: 33642-33653.

78. Kim H, Lapointe J, Kaygusuz G, et al. The retinoic acid synthesis gene ALDH1a2 is a candidate tumor suppressor in prostate cancer. Cancer Res. 2005;65: 8118-8124.

79. Touma SE, Perner S, Rubin MA, Nanus DM, Gudas LJ. Retinoid metabolism and ALDH1A2 (RALDH2) expression are altered in the transgenic adenocarcinoma mouse prostate model. Biochem Pharmacol. 2009;78: 1127-1138.
80. Williams SJ, Cvetkovic D, Hamilton TC. Vitamin A metabolism is impaired in human ovarian cancer. Gynecol Oncol. 2009;112: 637-645.
81. Wu S, Xue W, Huang X, et al. Distinct prognostic values of ALDH1 isoenzymes in breast cancer. Tumour Biol. 2015;36: 2421-2426.
82. Seidensaal K, Nollert A, Feige AH, et al. Impaired aldehyde dehydrogenase 1 subfamily member 2A-dependent retinoic acid signaling is related with a mesenchymal-like phenotype and an unfavorable prognosis of head and neck squamous cell carcinoma. Mol Cancer. 2015;14: 204.
83. Amory JK, Muller CH, Shimshoni JA, et al. Suppression of spermatogenesis by bisdichloroacetyldiamines is mediated by inhibition of testicular retinoic acid biosynthesis. J Androl. 2011;32: 111-119.

CHAPTER TWO

ALDEHYDE DEHYDROGENASE 1A2 IS REDUCED IN HEAD AND NECK SQUAMOUS CELL CARCINOMA AND IS A PUTATIVE TUMOR SUPPRESSOR

INTRODUCTION

Head and neck cancer, which includes cancers of the upper aerodigestive tract, represents one of the ten most common cancers worldwide and is characterized by high rates of morbidity and mortality[1]. In addition, outside of radiation and surgery, there are currently few therapeutic options of limited clinical efficacy available[1]. The vast majority of cases (~90%) are squamous cell carcinomas (HNSCCs), of which one of the primary etiological factors is long-term and excessive tobacco and/or alcohol use[2, 3]. Repeated exposure to these carcinogens results in multifocal lesion development in the epithelium of exposed tissues, such as the oral cavity and esophagus[4]. One of the current challenges in HNSCC research is to identify new drug targets and treatment strategies for more effective and less toxic therapies.

One pathway that has emerged as a potential target for chemotherapy/chemoprevention is the retinoid signaling pathway, which plays a critical role in regulating cellular differentiation, proliferation, and apoptosis[5]. Retinoids include vitamin A (retinol) and its natural and synthetic derivatives. In the endogenous signaling pathway retinol enters the cell and is converted into its most biologically-active metabolite, all-*trans* retinoic acid (RA), through a series of enzymatic steps occurring in the cytoplasm (Figure 1.2)[6]. A key step is catalyzed by aldehyde dehydrogenase 1a2 (ALDH1a2), which irreversibly oxidizes all-*trans* retinaldehyde to

synthesize RA[7]. RA is then shuttled to the nucleus by intracellular lipid binding proteins, whereupon it binds to and activates specific nuclear receptors – retinoic acid receptors (RARs) – to regulate the transcription of many diverse target genes[5].

Retinoid signaling is required for the normal growth, differentiation, and function of epithelial cells[8]. Thus, aberrations in retinoid signaling and metabolism contribute significantly to malignant dysregulation and are frequently observed in HNSCC and other cancers[9, 10]. Restoration of retinoid signaling through treatment with exogenous retinoids has exhibited efficacy in both preclinical and clinical trials[11]. Numerous studies have reported that retinoid treatment modulates cellular differentiation and inhibits proliferation of cultured human HNSCC cell lines[11-14].

The enzyme ALDH1a2 has recently emerged as a candidate tumor suppressor in several epithelial cancers[15-18]. Of note, researchers found that ALDH1a2 is expressed in normal but not cancerous prostate epithelium, and that its re-expression via transfection with exogenous ALDH1a2 inhibited the colony formation of prostate cancer cell lines[17]. Furthermore, decreased ALDH1a2 expression induced a mesenchymal-like phenotype and accelerated tumor growth in a xenograft model of HNSCC *in vivo*[18]. These results suggest an inverse correlation between ALDH1a2 expression and tumorigenesis in select cancers.

In the current study we investigated whether ALDH1a2 expression is reduced in HNSCC, and hypothesized that reinstatement of ALDH1a2 expression inhibits HNSCC cell growth by increasing cellular retinoic acid signaling. To address this question we used a viral vector to drive overexpression of ALDH1a2 in human HNSCC cell lines and assessed the resulting phenotype. Overall, our results provide evidence that ALDH1a2 functions as a tumor suppressor in HNSCC.

MATERIALS AND METHODS

Analysis of ALDH1a2 mRNA expression in human HNSCC patients

I analyzed ALDH1a2 mRNA levels in human HNSCC patients compared to matched normal tissue using Oncomine, a publicly available cancer microarray database (www.oncomine.org; Compendia Biocience)[19]. I examined transcript expression in ten available human HNSCC datasets from eight separate studies, some of which analyzed a specific tissue. All datasets utilized are detailed in Results Figure 2.1. We excluded datasets from pharyngeal tissue, as our interest lies in carcinomas of the oral cavity (OSCC).

Cell Culture

All cell lines used in this study were maintained as previously described[8, 20]. Briefly, the immortalized, non-transformed human oral keratinocyte cell line OKF4-TERT1 (OKF4) was generously provided by Dr. James G. Rheinwald, Harvard Medical School, and was cultured in Keratinocyte-SFM (Cat. No. 10744019; Gibco) supplemented with ~12 µg/mL bovine pituitary extract (BPE) (Cat. No. 13028-014; Gibco), penicillin (10,000 U/mL)/streptomycin (10,000 U/mL) (Cat. No. 10378-016; Gibco), 0.3 mM $CaCl_2$, and 0.2 ng/mL epidermal growth factor (EGF) (Cat. No. 10450-013; Gibco)[20]. Transformed human OSCC cell lines SCC-4, SCC-9, and SCC-25 were grown in Dulbecco's Modified Eagle Medium: Nutrient Mixture F-12 (DMEM/F-12) (Cat. No. 11320-033; Gibco) supplemented with 10% fetal bovine serum (FBS) and 400 ng/mL hydrocortisone[21]. All three SCC cell lines were generated by Dr. Rheinwald and obtained from the ATCC (Cat. No. CRL-1624, CRL-1629, and CRL-1628, respectively). HEK293T cells (ATCC) were cultured in DMEM (Gibco) supplemented

with 10% FBS. Each cell line was grown in a humidified atmosphere of 5% CO_2 at 37°C, and media was changed every 3 days.

Overexpression of ALDH1a2 by retroviral infection

To generate the retroviral vector driving constitutive ALDH1a2 overexpression, I inserted the AgeI fragment of pCMV-Sport6/ALDH1a2 (containing the *ALDH1a2* cDNA) into the AgeI site of the retroviral vector pQCXIP (Cat. No. 631516; Clontech Laboratories, Inc.). This generated pQC-ALDH1a2 (Supplemental Figure 2.1). Retroviral stocks were produced by transfecting HEK293T cells with pQC (empty vector control) or pQC-ALDH1a2 and collecting viral supernatant at 48 hours post-transfection, as described previously[22, 23]. Parental keratinocytes were transduced with viral supernatant in a 1:4 ratio with growth medium (DMEM + 10% FBS) overnight (12-16 hours). At this point, I replaced the media with normal growth medium with 0.5 μg/mL puromycin (Sigma) for selection, and changed it every 2-3 days for a total of 7-10 days, before harvesting or plating the cells for experiments.

RNA isolation and RT-PCR analysis

Total RNA was extracted using TRIzol reagent and isolated according to the manufacturer's protocol (Cat. No. 15596; Invitrogen). Total mRNA (1 μg) was reverse transcribed using qScript cDNA Supermix (Cat. No. 95048; Quanta Biosciences, Inc.) and diluted 1:10 with dH_2O[24]. Resulting cDNA (2 μL) was used as a template for semiquantitative RT-PCR using a Bio-Rad iCycler as previously described[25]. I utilized primers specific for housekeeping gene hypoxanthine phosphoribosyltransferase 1 (HPRT1) as a loading control, as previously described[8, 26]. Primer sequences are listed in Table 2.1.

Table 2.1: Primer sequences used for RT-PCR

Gene	Forward Primer (5'-3')	Reverse Primer (5'-3')	Product Size
ALDH1a2 TG	gacttgtagcagctgtcttcact	tcacccatttctctcccatttcc	160 bp
HPRT1	tgaggatttggaaagggtgt	aatccagcaggtcagcaaag	155 bp

Protein isolation and western blot analysis

Total protein from cultured cells was extracted in final sample buffer (0.5 M Tris–HCl, pH 6.8, 10% glycerol and 1% SDS), sonicated, boiled, and quantified using the *DC* Protein Assay (Cat. No. 500-0112; Bio-Rad). I separated 10 µg total protein on SDS-PAGE gels and transferred protein onto nitrocellulose membranes as previously described. Membranes were blocked in 5% skim milk in Tris-buffered saline containing 0.1% TWEEN 20 (Cat. No. P1379; Bio-Rad) (TBST) for 1 hour at room temperature before incubation with primary antibodies diluted in blocking solution, overnight at 4°C. Following two washes with TBST, membranes were then incubated with appropriate secondary antibodies for 1 hour at room temperature, washed with TBST, and developed using the Pierce ECL Substrate Kit (Cat. No. 32106; Pierce). I used a quantitative gel imaging station (Bio-Rad ChemiDoc System) and ImageLab software to record and analyze membrane chemiluminescence. Primary antibody details are provided in Table 2.2.

Table 2.2: Primary antibodies
PC = polyclonal antibody; MC = monoclonal antibody
ǂ A custom anti-ALDH1a2 antibody was generated for our lab by Alpha Diagnostics

Target	Company	Catalog #	Lot #	Source	Dilution
ALDH1a2	Alpha Diagnostics	N/A ǂ	Batch #4	Rabbit PC	1:100
β-Actin	Millipore	MAB1501	2665057	Mouse MC	1:80,000

Immunofluorescence staining

I performed immunofluorescence staining as previously described[27]. Briefly, cells were grown in monolayer on glass coverslips that had been pre-treated with FBS. Cells were then fixed with 4% (w/v) paraformaldehyde for 1 hour at room temperature, after which they were permeabilized using 0.3% (w/v) Triton X-100 for 3 minutes at room temperature. I then blocked with 2% BSA (in PBS) for 30 minutes before probing with primary antibody (Table 2.2) overnight at 4°C. Alexa Fluor 488 fluorescent secondary antibody (Invitrogen; 1:300) was used to probe for the protein of interest and Phalloidin-TRITC (Cat. No. FAK100; Millipore; 1:1000) was utilized for actin cytoskeleton counterstaining; both were applied for 1 hour at room temperature, with the plate wrapped in foil to prevent quenching of the fluorescent signal. Cell coverslips were mounted on slides using Vectashield mounting medium containing DAPI (Cat. No. H-1200; Vector Labs) to stain for cell nuclei. I imaged the slides using a Nikon TE2000-E microscope and CoolSnap HQ^2 camera (Roper Scientific).

Proliferation and colony formation assays

For proliferation assays, I plated cells in triplicate at a density of 10,000 cells/well in a 12-well plate at day -1. Cell numbers were counted at days 0, 3, 5 and 7, using a cell and particle counter (Coulter Z1, Beckman Coulter, Inc.). For colony formation assays, cells were plated at a density of 500 cells/well in a 6-well plate, and allowed to grow for approximately 14 days. Cells were then rinsed with PBS before fixation and staining using a mixture of paraformaldehyde (4%) and crystal violet (0.5% w/v) in PBS for 30 minutes at room temperature[28]. Crystal violet dye binds to proteins and DNA and is an effective means of visualizing viable adherent cells[28]. Cells were treated with 1 μM RA in DMSO (or vehicle control), starting at day 0. Throughout both

assays, growth medium was changed every 2 days. ImageJ Software (National Institutes of Health) was used to quantify the number and size of colonies.

Statistical analysis

All experiments include at least 3 independent biological replicates (n≥3). Statistical analyses were conducted using GraphPad Prism 6.0 software. The means ± S.E.M. were calculated before applying the Student's unpaired *t* test, or a one- or two-way ANOVA, as indicated in the figure legends. Differences of $p < 0.05$ were considered statistically significant.

RESULTS

ALDH1a2 expression is decreased in HNSCC

We first wanted to ascertain whether ALDH1a2 is aberrantly expressed in human OSCC. Using the online database Oncomine, we identified eight different studies of published microarray data from human OSCC patients[29-36]. In total, these studies include ten data sets which compared gene expression data from 229 carcinoma samples and 135 adjacent, non-tumor samples. We found that in the majority of the available data sets (70%, 7/10 data sets), ALDH1a2 was in the top 25% of genes with reduced transcript levels in cancer versus normal tissue (Figure 2.1). Strikingly, in four of these studies, ALDH1a2 was in the top 1-5% of underexpressed genes. This analysis reveals that ALDH1a2 mRNA levels are greatly reduced in human OSCC compared to normal oral tissue.

REFERENCE	CANCER LOCATION	SCC SAMPLES	NORMAL SAMPLES	p-VALUE	GENE RANK
Estilo et al., 2009	Tongue	31	26	7.04E-06	
Ginos et al., 2004	Head and Neck	41	13	5.31E-06	
Kuriakose et al., 2004	Tongue	3	22	2.00E-03	
Peng, et al., 2011	Oral Cavity	57	22	0.024	
	Floor of Mouth	5		8.40E-06	
Pyeon et al., 2007	Oral Cavity	4	10	1.00E-03	
	Tongue	15		6.00E-03	
Talbot el al., 2005	Tongue	31	26	1.67E-09	
Toruner et al., 2004	Oral Cavity	16	4	0.089	
Ye et al., 2008	Tongue	26	12	0.125	

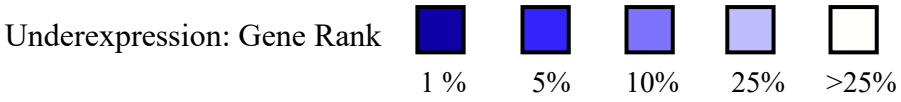

Figure 2.1: Summary of ALDH1a2 underexpression as observed in eight studies that collected microarray data from OSCC samples and adjacent healthy tissue. We examined every OSCC patient microarray data set available on Oncomine.com; this amounted to 10 data sets collected in 8 different studies. Together, these data sets represent 229 carcinoma samples and 135 adjacent, non-tumor samples from human patients. Shades of blue, as observed in 7 of 10 data sets, indicate ALDH1a2 is in the top 25% of underexpressed genes. Medium-dark blue, as seen in 4 of the data sets, means ALDH1a2 is in the top 1-5% of underexpressed genes. Gene overexpression, which would be represented by shades of red, was not observed in any of the data sets. Oncomine™ July 8, 2016.

We next examined ALDH1a2 protein levels in three transformed tongue SCC cell lines – SCC-4, SCC-9, and SCC-25 – and one normal, immortalized oral mucosal keratinocyte line, OKF4. Western blot analysis revealed that ALDH1a2 protein levels are decreased in all three SCC lines as compared to OKF4 (Figure 2.2). ALDH1a2

protein levels are reduced by approximately 86.4% (±6.6%; p=0.0002), 84.4% (±8.2%; p=0.0002) and 76.1% (±11.8%; p=0.004) in SCC-4, SCC-9, and SCC-25 cell lines, respectively, compared to the non-transformed OKF4 cells (Figure 2.2D). Together, these results from the patient microarray data and human SCC cell lines indicate that ALDH1a2 mRNA and protein levels are generally decreased in human OSCC.

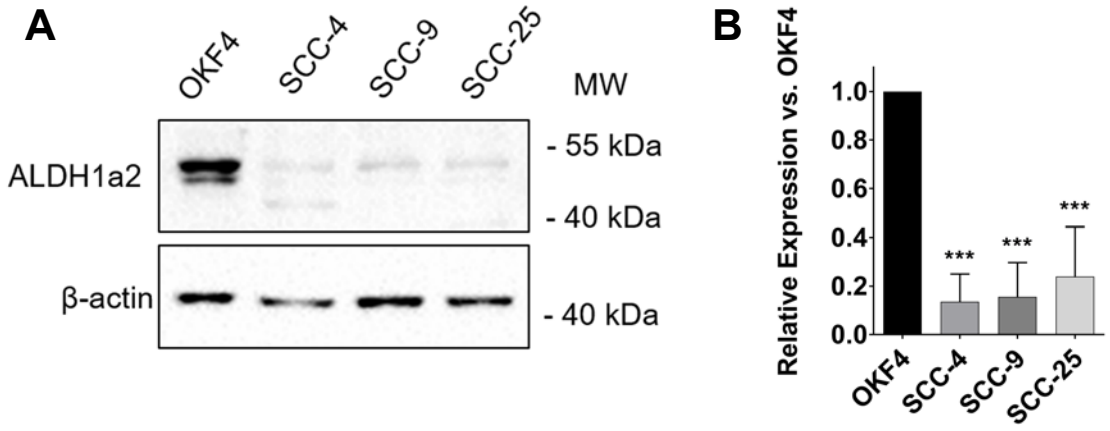

Figure 2.2: Endogenous ALDH1a2 expression is decreased in HNSCC cell lines. (A) Western blot analysis of OKF4, SCC-4, SCC-9, and SCC-25 keratinocyte lines. Membranes were probed with 1:100 ALDH1a2 antibody and 1:10,000 β-actin (loading control). Image shown is representative of analyses performed on distinct biological samples (n=3) with similar results. (B) Quantification of n=3 western blots such as shown in panel (A) using ImageLab Software (Bio-Rad). ALDH1a2 protein levels are normalized to β-actin protein levels and are represented relative to protein levels in OKF4 cells (set as 1). Bars represent mean± S.E.M. and data were analyzed using One-way ANOVA; ∗∗∗ indicates p<0.001.

ALDH1a2 overexpression suppresses proliferation and colony formation of SCC cells

To determine the functional role of ALDH1a2 in neoplastically transformed oral keratinocytes we generated a viral construct to drive the constitutive overexpression of ALDH1a2 (pQC-ALDH1a2; Supplemental Figure 2.1), and infected human squamous cell carcinoma cell lines SCC-4, SCC-9 and SCC-25. We used RT-PCR to confirm overexpression of transgenic (TG) ALDH1a2 mRNA in all three SCC lines (Figure 2.3A). No TG ALDH1a2 transcript was detected in cells infected with an empty control vector (pQC). Using immunofluorescence to detect total (endogenous + TG) ALDH1a2 protein, we verified that ALDH1a2 is overexpressed at the protein level in each pQC-ALDH1a2-infected SCC line (Figure 2.3B).

We then conducted phenotypic assays to determine the effect of ectopic ALDH1a2 expression on SCC cell growth. All three SCC cell lines infected with pQC-ALDH1a2 exhibited reduced proliferation over 7 days compared to empty vector-infected cells (Figure 2.4A-C). We also treated empty vector-infected cell lines with exogenous RA (1 μM). Since endogenous ALDH1a2 synthesizes intracellular RA, treatment with exogenous RA serves as a positive control for increased RA signaling. ALDH1a2 overexpression reduced SCC-4 and SCC-9 cell number by more than 40% (44% $p \leq 0.0001$, and 43% $p=0.0002$, respectively) and SCC-25 cell number by 23% ($p=0.0014$) (Figure 2.4A,B). In addition, RA treatment reduced the number of SCC-4, SCC-9, and SCC-25 cells by 26% ($p=0.0016$), 23% ($p=0.0092$), and 32% ($p=0.0002$), respectively.

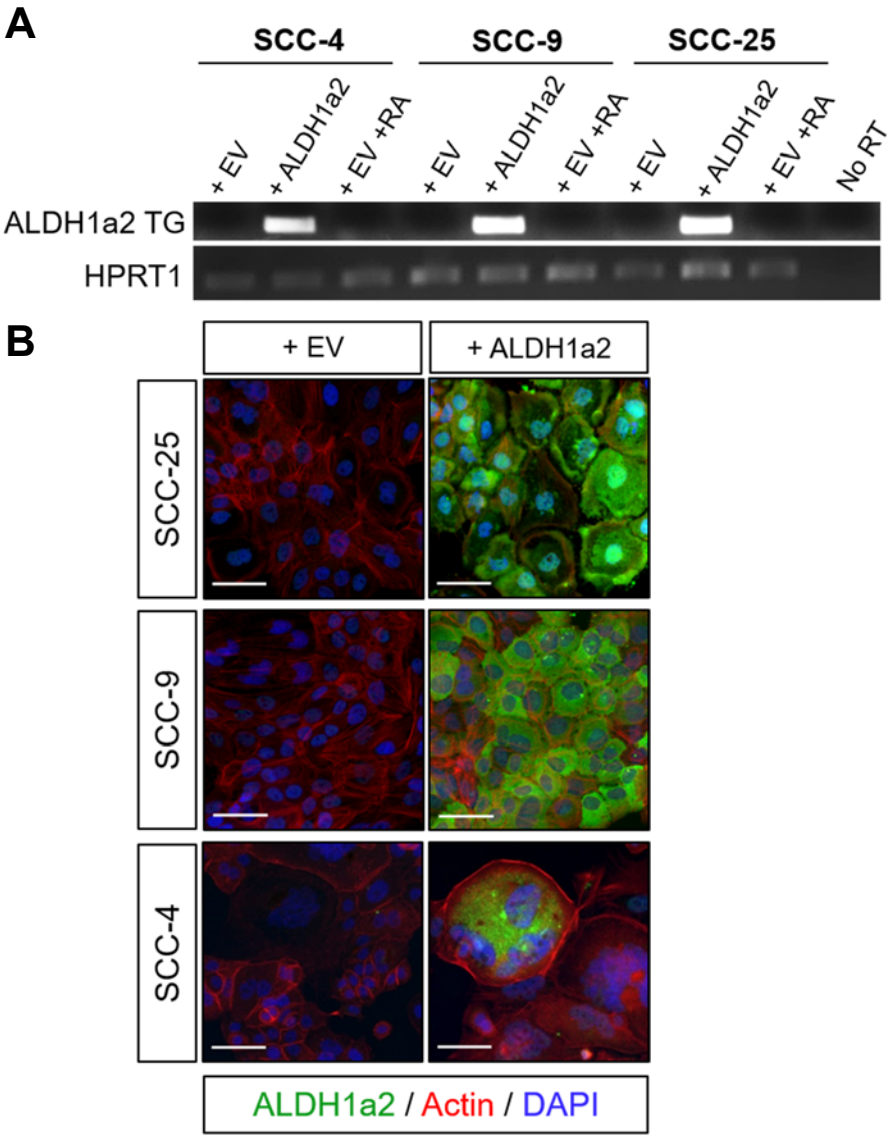

Figure 2.3: ALDH1a2 overexpression in human HNSCC cell lines. We infected SCC-4, SCC-9, and SCC-25 cells with either empty pQC vector (+EV) or a vector driving constitutive expression of ALDH1a2 (pQC-ALDH1a2; +ALDH1a2; Supplemental Figure 2.1) and selected 7-10 days with puromycin before harvesting the cells for analysis. (A) RT-PCR analysis of infected cell lines. One cohort of each EV-infected cell line was treated with 1 µM RA for 7 days as a positive control for the phenotypic assays shown in Figures 2.4 and 2.5 (+EV +RA). We used primers specific for the transgenic (TG) ALDH1a2 transcript as described in Table 2.1. HPRT1 was used as a loading control. (B) Immunofluorescence visualization of ALDH1a2 protein in EV- and ALDH1a2-infected cells. Cells were probed with ALDH1a2 primary antibody (Table 2.2) (green, 1:100) and stained with DAPI (blue, nuclei) and Phalloidin-TRITC (red, actin cytoskeleton). Images shown are representative of analysis performed on independent experiments (n=3) with similar results, and were taken at 200X. Scale bar represents 50 µm.

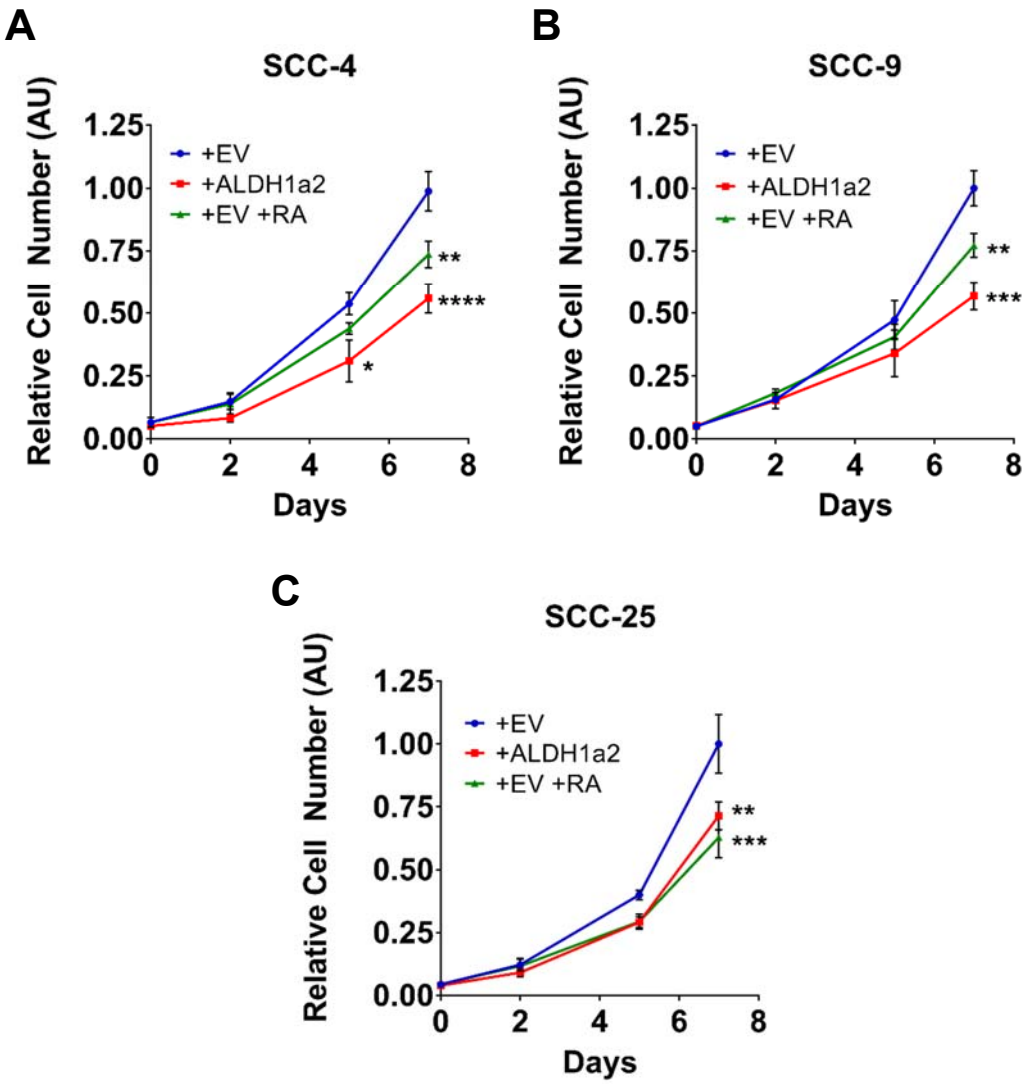

Figure 2.4: ALDH1a2 overexpression impairs proliferation in HNSCC cell lines. We infected SCC-4 (A), SCC-9 (B), and SCC-25 (C) cells overnight with empty vector (+EV) or a vector driving constitutive expression of ALDH1a2 (+ALDH1a2, Supplemental Figure 2.1) and selected 7-10 days with puromycin before plating for experiments. All cells were seeded at 10,000 cells/well, and allowed to attach for 24 hours before treatment and counting at Day 0. We treated one cohort of EV-infected cells with 1 μM RA. The remaining lines were treated with an equivalent volume of vehicle control (DMSO). Cells were counted on days 2, 5, and 7, and raw cell numbers were normalized to the cell count of the Day 7 EV-infected line (set as 1). We plated each independent experiment in triplicate. Each data point represents the mean of n≥3 separate experiments (biological repeats) ±SEM. The data was analyzed using two-way ANOVA; ∗ indicates $p<0.05$, ∗∗ indicates $p<0.01$, ∗∗∗ indicates $p<0.001$ and ∗∗∗∗ indicates $p<0.0001$.

To further verify the inhibitory effect of ALDH1a2 on SCC cell growth, we overexpressed ALDH1a2 in SCC cells and assayed for colony formation. When seeded at low density, ALDH1a2-infected SCC-4 and SCC-9 cells showed reduced colony-forming ability compared to cells infected with the empty vector control in terms of average colony size and number of colonies (Figure 2.5A,B). Colony number and size reflect cell survival and proliferation, respectively[37]. ALDH1a2 overexpression did not significantly affect the clonogenicity of SCC-25 cells (Figure 2.5A,B, bottom row). Treatment with exogenous RA inhibited colony formation in SCC-9 cells, but not SCC-4 or SCC-25. Consistent with our cell proliferation assays, these data confirm that ALDH1a2 expression suppresses SCC growth *in vitro*.

We also infected OKF4 cells with the pQC and pQC-ALDH1a2 viral vectors in order to determine the effect of ectopic ALDH1a2 on the growth of non-transformed keratinocytes. We observed no change in proliferation or colony formation in ALDH1a2-infected OKF4 cells as compared to empty vector-infected cells (Supplemental Figure 2.2B,C). In contrast, treatment with exogenous RA (1 μM) decreased cell number by 83% ($p<0.0001$) at Day 7 of our proliferation assays and prevented *in vitro* colony formation (Supplemental Figure 2.2B,C). These results suggest that ALDH1a2 overexpression does not significantly affect the growth of the non-transformed keratinocyte line OKF4.

DISCUSSION

The retinoid signaling pathway has been of interest in the context of HNSCC for some time; retinoids suppress the proliferation of HNSCC cells in culture, inhibit carcinogenesis in mouse models of OSCC, and have been used both alone and in combination in clinical trials to treat oral leukoplakia and squamous cell carcinoma[38-42]. Aberrations in this pathway, including reductions in RARβ, RARγ, cellular retinoic acid

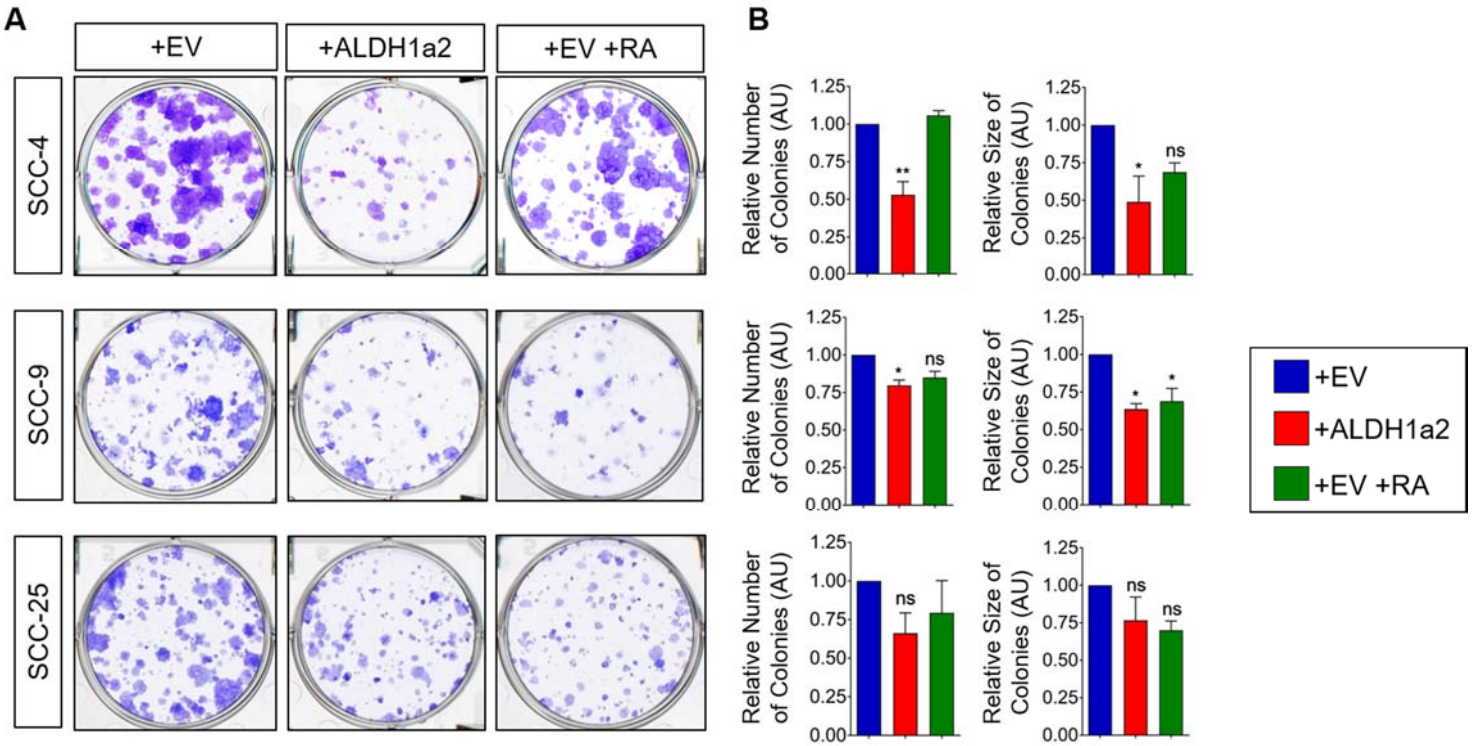

Figure 2.5: ALDH1a2 overexpression inhibits colony formation. We infected SCC-4, SCC-9, and SCC-25 cells overnight with empty vector (+EV) or a vector driving constitutive expression of ALDH1a2 (+ALDH1a2; Supplemental Figure 2.1) and selected 7-10 days with puromycin before plating for colony formation assays. All cells were seeded at 500 cells/well in a 6-well plate, and allowed to attach for 24 hours before treatment at Day 0. We treated one cohort of EV-infected cells with 1 μm RA (+EV +RA). The remaining lines were treated with an equivalent volume of vehicle control. (DMSO) After 14 days, cells were fixed and stained with crystal violet as described in the materials and methods. (A) Representative plates of n≥3 independent experiments performed with fresh cells. (B) Quantification of the mean colony number and size relative to the empty-vector-infected line. We quantified the colonies in each well using ImageJ software (National Institutes of Health). The data were analyzed using One-way ANOVA; ∗ indicates $p<0.05$, ∗∗ indicates $p<0.01$.

binding protein 2 (CRABP2), and lecithin:retinol acyltransferase (LRAT) mRNA and protein levels, as well as increases in cytochrome P450 26A1 (CYP26A1), the enzyme responsible for the first step of RA catabolism, are frequently observed in HNSCC[5, 10, 43-47].

Our work has identified another component of this pathway, ALDH1a2, that exhibits reduced expression in HNSCC. Endogenous ALDH1a2 catalyzes the intracellular synthesis of all-*trans* RA from all-*trans* retinaldehyde[7]. We observed reduced ALDH1a2 mRNA levels in human HNSCC patients through our examination of patient microarray data on Oncomine.com, and reductions in the protein levels of ALDH1a2 in cultured human HNSCC cell lines (Figures 2.1,2.2). These data are supported by a recent publication in which researchers reported that the ALDH1a2 promoter is often hypermethylated in HNSCC patients with non-HPV-driven tumors[48]. Interestingly, this group also found that there is a strong correlation between high ALDH1a2 protein expression and greater overall and progression-free patient survival (Figure 1.4)[48]. Taken together, these results indicate that a reduction in ALDH1a2 expression is a common event in HNSCC carcinogenesis. Because ALDH1a2 synthesizes RA, a known stimulator of growth arrest, apoptosis, and differentiation, there is a logical pathogenic connection between loss of ALDH1a2 and carcinogenesis[5].

In our phenotypic assays, we found that overexpression of TG ALDH1a2 and treatment with 1 μM RA had a similar effect on the growth of SCC-4, SCC-9, and SCC-25 cells. To date, a large body of research has been conducted to evaluate the effects of treatment with RA on the phenotype of cultured human HNSCC cell lines *in vitro*. Numerous studies have found that RA treatment inhibits the proliferation and colony formation of many HNSCC cell lines, to varying degrees depending on the cell line[12-14, 18, 49]. In addition, RA treatment has been observed to induce apoptosis and cell cycle

arrest in certain HNSCC cell lines; RA treatment induced apoptosis, as measured by DNA ladder formation, in human HNSCC lines UMSCC-17B, UMSCC-22A, UMSCC-38, and 1438, and induced cell cycle G1 arrest in HNSCC cell lines SCC-1, SCC-9, YCU-N861 and YCU-H891[50-52]. Treatment of HNSCC cell lines with RA also inhibits squamous cell differentiation, as indicated by decreased expression of cytokeratin 1 (K1), transglutaminase type 1, and involucrin following treatment with RA[12, 14, 49]. These three markers are frequently aberrantly overexpressed in HNSCC[49].

Previous work has also demonstrated the efficacy of restoring retinoid signaling to inhibit SCC growth. Overexpression of CRABP2 via transfection in an esophageal SCC line with low endogenous CRABP2 expression (EC109) inhibited cell growth and migration and promoted apoptosis[47]. Retroviral transduction of RARβ2 into a HNSCC line that does not express endogenous RARβ (SqCC/Y1) made the cells much more sensitive to growth suppression by RA[53, 54]. Consistent with these data, we found that overexpression of ectopic ALDH1a2 in human SCC cell lines reduced their proliferation rate and colony formation ability (Figures 2.4, 2.5). To our knowledge we are the first to study the effect of increased ALDH1a2 expression on the neoplastically transformed phenotype of cultured human HNSCC lines.

CONCLUSIONS

In the present study we have provided evidence that ALDH1a2 acts as a tumor suppressor in HNSCC. First, we have determined that reduced ALDH1a2 expression is a common event in HNSCC. Previous work has also identified a correlation between ALDH1a2 protein expression and improved patient clinical outcome[48]. Furthermore, we observed that overexpression of ectopic ALDH1a2 in SCC cell lines with low endogenous ALDH1a2 levels inhibits cell growth *in vitro*. In conclusion, this study indicates that enhanced ALDH1a2 has an inhibitory effect on HNSCC growth and

provides rationale for further research into the role of ALDH1a2 in HNSCC carcinogenesis *in vivo*.

SUPPLEMENTARY DATA

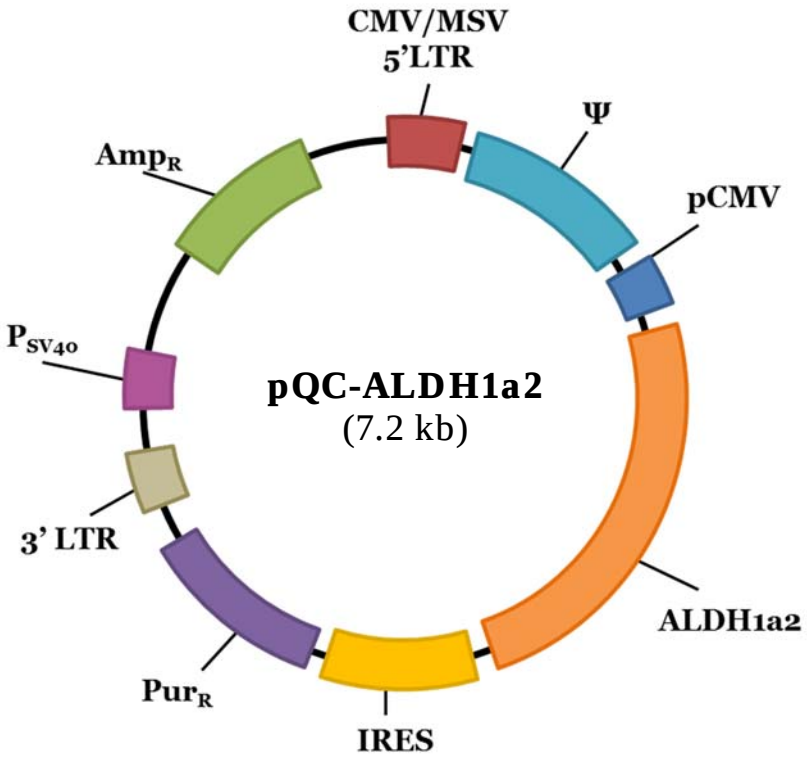

Supplemental Figure 2.1: Schematic of the pQC-ALDH1a2 retroviral vector used to drive constitutive overexpression of ALDH1a2. The vector was constructed by inserting the AgeI fragment of pCMV-Sport6/ALDH1a2 into pQCXIP (Clontech Laboratories, Inc.). We verified correct insertion by enzyme digest and sequencing at the Cornell CORE Facilities.

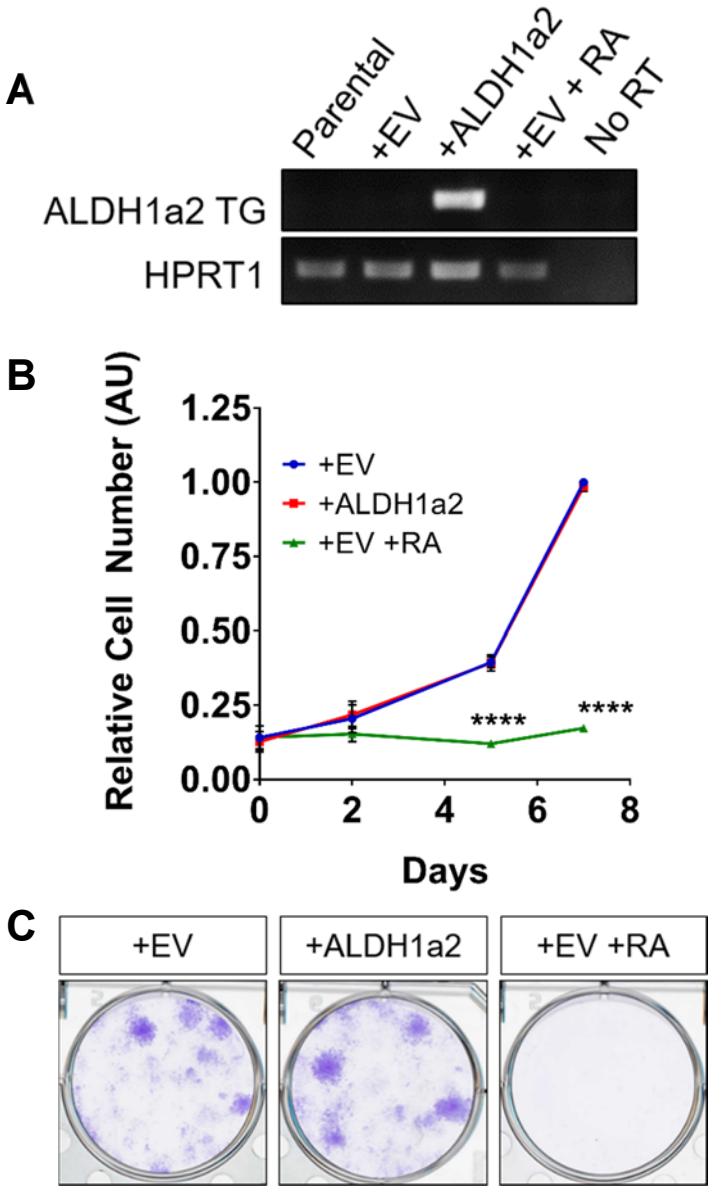

Supplemental Figure 2.2: ALDH1a2 overexpression in OKF4 cells. We infected OKF4 cells with either empty pQC vector (+EV) or a vector driving constitutive expression of ALDH1a2 (pQC-ALDH1a2; +ALDH1a2; Supplemental Figure 2.1) and selected 7-10 days with puromycin before plating cells for experiments. At Day 0, one cohort of EV-infected OKF4 cells was treated with 1 μM RA. The other lines were treated with an equivalent volume of vehicle control. (A) RT-PCR analysis of parental OKF4 cells and infected OKF4 cells. We used primers specific for the transgenic (TG) ALDH1a2 transcript. HPRT1 was used as a loading control. Primer sequences are listed in Table 2.1. (B) Cell proliferation assay of infected OKF4 cells. Each data point represents the mean of n≥3 separate experiments (biological repeats) ±SEM. The data were analyzed using two-way ANOVA (C) Colony formation assay of infected OKF4 cells.

REFERENCES

1. Rothenberg SM, Ellisen LW. The molecular pathogenesis of head and neck squamous cell carcinoma. J Clin Invest. 2012;122: 1951-1957.

2. Curado MP, Hashibe M. Recent changes in the epidemiology of head and neck cancer. Curr Opin Oncol. 2009;21: 194-200.

3. Osei-Sarfo K, Tang XH, Urvalek AM, Scognamiglio T, Gudas LJ. The molecular features of tongue epithelium treated with the carcinogen 4-nitroquinoline-1-oxide and alcohol as a model for HNSCC. Carcinogenesis. 2013;34: 2673-2681.

4. Leemans CR, Braakhuis BJ, Brakenhoff RH. The molecular biology of head and neck cancer. Nat Rev Cancer. 2011;11: 9-22.

5. Mongan NP, Gudas LJ. Diverse actions of retinoid receptors in cancer prevention and treatment. Differentiation. 2007;75: 853-870.

6. Bushue N, Wan YJ. Retinoid pathway and cancer therapeutics. Adv Drug Deliv Rev. 2010;62: 1285-1298.

7. Zhao D, McCaffery P, Ivins KJ, et al. Molecular identification of a major retinoic-acid-synthesizing enzyme, a retinaldehyde-specific dehydrogenase. Eur J Biochem. 1996;240: 15-22.

8. Marcinkiewicz KM, Gudas LJ. Altered epigenetic regulation of homeobox genes in human oral squamous cell carcinoma cells. Exp Cell Res. 2014;320: 128-143.

9. Tang XH, Gudas LJ. Retinoids, retinoic acid receptors, and cancer. Annu Rev Pathol. 2011;6: 345-364.

10. Hu L, Crowe DL, Rheinwald JG, Chambon P, Gudas LJ. Abnormal expression of retinoic acid receptors and keratin 19 by human oral and epidermal squamous cell carcinoma cell lines. Cancer Res. 1991;51: 3972-3981.

11. Lotan R. Roles of retinoids and their nuclear receptors in the development and prevention of upper aerodigestive tract cancers. Environ Health Perspect. 1997;105 Suppl 4: 985-988.
12. Poddar S, Hong WK, Thacher SM, Lotan R. Retinoic acid suppression of squamous differentiation in human head-and-neck squamous carcinoma cells. Int J Cancer. 1991;48: 239-247.
13. Zou CP, Clifford JL, Xu XC, et al. Modulation by retinoic acid (RA) of squamous cell differentiation, cellular RA-binding proteins, and nuclear RA receptors in human head and neck squamous cell carcinoma cell lines. Cancer Res. 1994;54: 5479-5487.
14. Jetten AM, Kim JS, Sacks PG, et al. Inhibition of growth and squamous-cell differentiation markers in cultured human head and neck squamous carcinoma cells by beta-all-trans retinoic acid. Int J Cancer. 1990;45: 195-202.
15. Williams SJ, Cvetkovic D, Hamilton TC. Vitamin A metabolism is impaired in human ovarian cancer. Gynecol Oncol. 2009;112: 637-645.
16. Wu S, Xue W, Huang X, et al. Distinct prognostic values of ALDH1 isoenzymes in breast cancer. Tumour Biol. 2015;36: 2421-2426.
17. Kim H, Lapointe J, Kaygusuz G, et al. The retinoic acid synthesis gene ALDH1a2 is a candidate tumor suppressor in prostate cancer. Cancer Res. 2005;65: 8118-8124.
18. Seidensaal K, Nollert A, Feige AH, et al. Impaired aldehyde dehydrogenase 1 subfamily member 2A-dependent retinoic acid signaling is related with a mesenchymal-like phenotype and an unfavorable prognosis of head and neck squamous cell carcinoma. Mol Cancer. 2015;14: 204.
19. Rhodes DR, Yu J, Shanker K, et al. ONCOMINE: a cancer microarray database and integrated data-mining platform. Neoplasia. 2004;6: 1-6.
20. Dickson MA, Hahn WC, Ino Y, et al. Human keratinocytes that express hTERT and also bypass a p16(INK4a)-enforced mechanism that limits life span become

immortal yet retain normal growth and differentiation characteristics. Mol Cell Biol. 2000;20: 1436-1447.

21. Rheinwald JG, Beckett MA. Tumorigenic keratinocyte lines requiring anchorage and fibroblast support cultured from human squamous cell carcinomas. Cancer Res. 1981;41: 1657-1663.

22. Kashyap V, Laursen KB, Brenet F, Viale AJ, Scandura JM, Gudas LJ. RARγ is essential for retinoic acid induced chromatin remodeling and transcriptional activation in embryonic stem cells. J Cell Sci. 2013;126: 999-1008.

23. Benoit YD, Lussier C, Ducharme PA, et al. Integrin alpha8beta1 regulates adhesion, migration and proliferation of human intestinal crypt cells via a predominant RhoA/ROCK-dependent mechanism. Biol Cell. 2009;101: 695-708.

24. Reynertson KA, Charlson ME, Gudas LJ. Induction of murine embryonic stem cell differentiation by medicinal plant extracts. Exp Cell Res. 2011;317: 82-93.

25. Laursen KB, Wong PM, Gudas LJ. Epigenetic regulation by RARα maintains ligand-independent transcriptional activity. Nucleic Acids Res. 2012;40: 102-115.

26. Raman JD, Mongan NP, Liu L, et al. Decreased expression of the human stem cell marker, Rex-1 (zfp-42), in renal cell carcinoma. Carcinogenesis. 2006;27: 499-507.

27. Benoit YD, Laursen KB, Witherspoon MS, Lipkin SM, Gudas LJ. Inhibition of PRC2 histone methyltransferase activity increases TRAIL-mediated apoptosis sensitivity in human colon cancer cells. J Cell Physiol. 2013;228: 764-772.

28. Franken NA, Rodermond HM, Stap J, Haveman J, van Bree C. Clonogenic assay of cells in vitro. Nat Protoc. 2006;1: 2315-2319.

29. Estilo CL, O-charoenrat P, Talbot S, et al. Oral tongue cancer gene expression profiling: Identification of novel potential prognosticators by oligonucleotide microarray analysis. BMC Cancer. 2009;9: 11.

30. Ginos MA, Page GP, Michalowicz BS, et al. Identification of a gene expression signature associated with recurrent disease in squamous cell carcinoma of the head and neck. Cancer Res. 2004;64: 55-63.
31. Kuriakose MA, Chen WT, He ZM, et al. Selection and validation of differentially expressed genes in head and neck cancer. Cell Mol Life Sci. 2004;61: 1372-1383.
32. Peng CH, Liao CT, Peng SC, et al. A novel molecular signature identified by systems genetics approach predicts prognosis in oral squamous cell carcinoma. PLoS One. 2011;6: e23452.
33. Pyeon D, Newton MA, Lambert PF, et al. Fundamental differences in cell cycle deregulation in human papillomavirus-positive and human papillomavirus-negative head/neck and cervical cancers. Cancer Res. 2007;67: 4605-4619.
34. Talbot SG, Estilo C, Maghami E, et al. Gene expression profiling allows distinction between primary and metastatic squamous cell carcinomas in the lung. Cancer Res. 2005;65: 3063-3071.
35. Toruner GA, Ulger C, Alkan M, et al. Association between gene expression profile and tumor invasion in oral squamous cell carcinoma. Cancer Genet Cytogenet. 2004;154: 27-35.
36. Ye H, Yu T, Temam S, et al. Transcriptomic dissection of tongue squamous cell carcinoma. BMC Genomics. 2008;9: 69.
37. Guzmán C, Bagga M, Kaur A, Westermarck J, Abankwa D. ColonyArea: an ImageJ plugin to automatically quantify colony formation in clonogenic assays. PLoS One. 2014;9: e92444.
38. Giannini F, Maestro R, Vukosavljevic T, Pomponi F, Boiocchi M. All-trans, 13-cis and 9-cis retinoic acids induce a fully reversible growth inhibition in HNSCC cell lines: implications for in vivo retinoic acid use. Int J Cancer. 1997;70: 194-200.

39. Tang XH, Albert M, Scognamiglio T, Gudas LJ. A DNA methyltransferase inhibitor and all-trans retinoic acid reduce oral cavity carcinogenesis induced by the carcinogen 4-nitroquinoline 1-oxide. Cancer Prev Res (Phila). 2009;2: 1100-1110.
40. Hong WK, Lippman SM, Itri LM, et al. Prevention of second primary tumors with isotretinoin in squamous-cell carcinoma of the head and neck. N Engl J Med. 1990;323: 795-801.
41. Hong WK, Endicott J, Itri LM, et al. 13-cis-retinoic acid in the treatment of oral leukoplakia. N Engl J Med. 1986;315: 1501-1505.
42. Uray IP, Dmitrovsky E, Brown PH. Retinoids and rexinoids in cancer prevention: from laboratory to clinic. Semin Oncol. 2016;43: 49-64.
43. Guo X, Gudas LJ. Metabolism of all-trans-retinol in normal human cell strains and squamous cell carcinoma (SCC) lines from the oral cavity and skin: reduced esterification of retinol in SCC lines. Cancer Res. 1998;58: 166-176.
44. Tang XH, Su D, Albert M, Scognamiglio T, Gudas LJ. Overexpression of lecithin:retinol acyltransferase in the epithelial basal layer makes mice more sensitive to oral cavity carcinogenesis induced by a carcinogen. Cancer Biol Ther. 2009;8: 1212-1213.
45. Xu XC, Ro JY, Lee JS, Shin DM, Hong WK, Lotan R. Differential expression of nuclear retinoid receptors in normal, premalignant, and malignant head and neck tissues. Cancer Res. 1994;54: 3580-3587.
46. Youssef EM, Lotan D, Issa JP, et al. Hypermethylation of the retinoic acid receptor-beta(2) gene in head and neck carcinogenesis. Clin Cancer Res. 2004;10: 1733-1742.
47. Yang Q, Wang R, Xiao W, Sun F, Yuan H, Pan Q. Cellular Retinoic Acid Binding Protein 2 Is Strikingly Downregulated in Human Esophageal Squamous Cell Carcinoma and Functions as a Tumor Suppressor. PLoS One. 2016;11: e0148381.

48. Kostareli E, Holzinger D, Bogatyrova O, et al. HPV-related methylation signature predicts survival in oropharyngeal squamous cell carcinomas. J Clin Invest. 2013;123: 2488-2501.

49. Lotan R. Suppression of squamous cell carcinoma growth and differentiation by retinoids. Cancer Res. 1994;54: 1987s-1990s.

50. Oridate N, Lotan D, Xu XC, Hong WK, Lotan R. Differential induction of apoptosis by all-trans-retinoic acid and N-(4-hydroxyphenyl)retinamide in human head and neck squamous cell carcinoma cell lines. Clin Cancer Res. 1996;2: 855-863.

51. Wang A, Zeng R, Huang H. Retinoic acid and sodium butyrate as cell cycle regulators in the treatment of oral squamous carcinoma cells. Oncol Res. 2008;17: 175-182.

52. Masuda M, Toh S, Koike K, et al. The roles of JNK1 and Stat3 in the response of head and neck cancer cell lines to combined treatment with all-trans-retinoic acid and 5-fluorouracil. Jpn J Cancer Res. 2002;93: 329-339.

53. Lotan R. Retinoids and their receptors in modulation of differentiation, development, and prevention of head and neck cancers. Anticancer Res. 1996;16: 2415-2419.

54. Wan H, Oridate N, Lotan D, Hong WK, Lotan R. Overexpression of retinoic acid receptor beta in head and neck squamous cell carcinoma cells increases their sensitivity to retinoid-induced suppression of squamous differentiation by retinoids. Cancer Res. 1999;59: 3518-3526.

CHAPTER THREE

GENERATION OF TRANSGENIC MICE WITH TETRACYCLINE-INDUCIBLE EXPRESSION OF ALDH1A2 IN THE ORAL CAVITY EPITHELIUM

INTRODUCTION

Vitamin A (all-*trans* retinol) and its derivatives, retinoids, play a critical regulatory role in differentiation and proliferation during both embryonic development and adult tissue homeostasis[1]. All-*trans* retinol is obtained from the diet, and is metabolized into its most biologically-active derivative, all-*trans* retinoic acid (RA), through the oxidization of retinaldehyde by aldehyde dehydrogenase 1a2 (ALDH1a2, formerly RALDH2). Intracellular lipid binding proteins such as cellular retinoic acid binding protein 2 (CRABP2) shuttle cytoplasmic RA to the nucleus[2, 3]. RA then signals by binding and activating specific nuclear receptors – retinoic acid receptors (RARs) and retinoid X receptors (RXRs) – thereby controlling the transcription of a wide assortment of target genes.[4]

Endogenous retinoid signaling is essential for proper epithelial differentiation and function[5]. As a result, altering this signaling pathway has a profound phenotypic effect upon epithelial tissues such as the oral mucosa; vitamin A deficiency in experimental animals induces hyperplasia and squamous metaplasia in the oral mucosa[6]. This phenotype is similar to the histology observed in human patients with head and neck squamous cell carcinoma (HNSCC), a disease characterized by abnormal cellular differentiation, growth, and morphology of cells in the basal and suprabasal layers of the squamous epithelium in the oral cavity[7]. While the squamous

epithelium is normally a highly-ordered structure consisting of stratified layers of cells in distinct differentiation states, this organization is lost during HNSCC carcinogenesis as cells accumulate DNA mutations and epigenetic changes in critical genes and become dysregulated[8, 9]. Tumors in patients with HNSCC frequently exhibit compromised retinoid signaling resulting from aberrant expression of key members of the retinoid signaling pathway[4, 7]. Reductions in RARγ, RARβ$_2$, CRABP2, and ALDH1a2 mRNA and protein levels have all been observed to be common events in HNSCC[10-14]. In addition, aberrant retinoid signaling has also been observed in psoriasis and melanoma, two disorders characterized by abnormal epithelial differentiation and hyperproliferation[15, 16].

Because endogenous retinoid signaling plays a critical role in preventing malignant dysregulation in the epithelium, restoring retinoid signaling through treatment with exogenous retinoids is a compelling therapeutic strategy[17]. Retinoids have proven effective at transiently suppressing oral premalignant lesions and second primary tumors (SPT) in HNSCC patients[18]. However, to date, pan-RAR retinoid therapies have not exhibited long-term efficacy in Phase III clinical trials of HNSCC[19]. Thus, further research into the proteins involved in endogenous retinoid synthesis and signaling could reveal new and more effective strategies for retinoid therapy.

To this end, we sought to characterize further the role of the enzyme ALDH1a2 in the stratified squamous epithelium. ALDH1a2 (Gene ID: 8854) catalyzes an irreversible step of RA synthesis – the oxidation of retinaldehyde to RA – thereby playing a critical role in endogenous retinoid signaling. In our previous work, detailed in Chapter 2, we showed that ALDH1a2 mRNA levels are decreased in human HNSCC compared to normal tissue, and that ALDH1a2 protein levels are lower in cultured human HNSCC cell lines compared to immortalized but non-transformed

keratinocytes, suggesting that expression of ALDH1a2 is reduced during HNSCC carcinogenesis (Figures 2.1, 2.2). In addition, overexpression of ectopic ALDH1a2 in these HNSCC cell lines decreased proliferation and colony formation (Figures 2.4, 2.5). These results indicate that ALDH1a2 inhibits the growth of neoplastically transformed HNSCC cells.

To test how ALDH1a2 affects carcinogenesis development *in vivo*, here we describe the development of a Tet-On transgenic mouse system for the inducible expression of ALDH1a2 exclusively in the basal layers of select, stratified squamous epithelial tissues including the tongue, skin, and esophagus. In this model, we detect ALDH1a2 induction only in the presence of doxycycline (dox), indicating that this is an effective system for tightly-regulated expression of ALDH1a2 in target tissues. This new transgenic mouse model is a valuable tool for studies on retinoid signaling in normal and disease states of the epithelium.

MATERIALS AND METHODS

Construction of the TRE-ALDH1a2 transgene

To generate the TRE-ALDH1a2 transgene, I released the mALDH1a2 cDNA from the pCMV-Sport6/ALDH1a2 vector (Clontech Laboratories, Inc.) by AgeI digest, and amplified it via PCR to generate BamHI and NotI restriction sites on the 5' and 3' ends, respectively. This fragment (1.5 kb) was then inserted into the BamHI/NotI sites of the pTRE2hyg expression vector (Cat. No. 631014; Clontech Laboratories, Inc.), placing ALDH1a2 downstream of the tetracycline response element (TRE) and CMV2 promoter, and upstream of a β-globin intron/poly(A) sequence (the full pTREhyg-ALDH1a2 construct is shown in Supplemental Figure 3.1). I confirmed correct insertion by restriction enzyme digest and sequencing through the Cornell University Core Laboratories Center. I verified the inducibility of

the transgenic ALDH1a2 in the human keratinocyte line SCC-9 (Supplemental Figure 3.2).

Generation and treatment of transgenic mice

We used two transgenic mouse lines, *TRE-ALDH1a2*, and *K14-rtTA*, in this Tet-On system. To create the *TRE-ALDH1a2* mice, I freed the TRE-ALDH1a2 expression cassette from the vector backbone by XhoI/SapI double partial digestion and purified it by gel electrophoresis using the QIAquick Gel Extraction Kit (Cat. No. 28704; QIAGEN). I then sequenced the resulting fragment (3.3 kb), diluted it to 50 ng/μL and submitted it to the Weill Cornell Medical College (WCMC) Transgenic Mouse Core Facility for microinjection into fertilized C57Bl/6 mouse eggs.

I identified potential *TRE-ALDH1a2* founder animals through Southern analyses. 10 μg of mouse tail genomic DNA was digested with EcoRI, separated on an agarose gel, and subjected to Southern blotting and hybridization using a Hybond-N membrane (Cat. No. 10600002; Amersham, GE Healthcare Life Sciences). Membranes were probed using the ^{32}P-labeled 662 bp AatII - BsaI fragment of pTRE-ALDH1a2 (for ALDH1a2), stripped, and re-probed using the ^{32}P-labeled 673 bp EcoRI - NotI fragment (for the β-globin intron). I detected signals using a phosphoimager. From this analysis I identified three positive founders: #9, 11, and 25. I confirmed the presence of the transgene by genotyping PCR, using primers specific for the transgenic ALDH1a2 (Table 3.1). Each of the verified *TRE-ALDH1a2* founder mice was then bred with C57Bl/6 wild-type mice to establish three independent *TRE-ALDH1a2* transgenic lines. I again confirmed positive progeny using both Southern blot and PCR, and all founders transmitted the transgene.

The *K14-rtTA* transgenic line was originally generated in the laboratory of Dr. Elaine Fuchs, Rockefeller University[20]. I obtained a *K14-rtTA* founder mouse from

The Jackson Laboratory (Cat. No. 008099) (FVB-Tg(KRT14-rtTA)F42Efu/J), and genotyped it via PCR as described previously (primers listed in Table 3.1).[21, 22] This *K14-rtTA*$^{+/-}$ mouse was crossed with *TRE-ALDH1a2*$^{+/-}$ females to generate bitransgenic *K14-rtTA/TRE-ALDH1a2* mice, which I then tested for both transgenes using PCR. The resulting mice, and all mice used for the experiments herein, were thus 50/50 C57Bl/6 and FVB in genetic background. In addition, all TG-positive mice described in the present study were single-allele positive for the transgene(s) (*K14-rtTA*$^{+/-}$, *TRE-ALDH1a2*$^{+/-}$, *K14-rtTA*$^{+/-}$*/TRE-ALDH1a2*$^{+/-}$).

Doxycycline (dox; Cat. No. D9891; Sigma) was diluted to 2 mg/mL in the drinking water. Mice had free access to the water, which was changed every 2-3 days. I maintained all mice in the WCMC Research Animal Resource Center, and I performed all studies according to a protocol approved by the Institutional Animal Care and Use Committee (IACUC).

Table 3.1: Primer sequences used for Genotyping PCR
ǂ Primer sequences provided by Jackson Labs

Gene	Forward Primer (5'-3')	Reverse Primer (5'-3')	Product Size
ALDH1a2	gacttgtagcagctgtcttcact	tcacccatttctctcccatttcc	160 bp
rtTA[ǂ]	cacgatacacctgactagctgggtg	catcacccacaggctagcgccaact	500 bp
MβCasein	gatgtgctccaggctaaagtt	agaaacggaatgttgtggagt	500 bp

Tissue dissection and immunostaining

After terminating treatment, I sacrificed mice by cervical dislocation and performed dissection immediately. I harvested tissue samples and then snap froze them in liquid nitrogen (for RNA or protein isolation), or fixed them in 4% paraformaldehyde in phosphate-buffered saline (PBS) at 4°C overnight before transfer

to 70% ethanol for tissue processing and paraffin embedding at the WCMC Electron Microscopy and Histology Core Facility. All tissue sections were cut to 7 μm. I deparaffinized the sections with Histo-Clear II (Cat. No. HS-202; National Diagnostics) and rehydrated them in a graded series of ethanol. Next, I performed heat-induced antigen retrieval using Antigen Unmasking Solution (Tris-based, Cat. No. H-3301, for ALDH1a2 primary antibody; citrate-based, Cat. No. H-3300, for all other antibodies; Vector Laboratories) in a pressure cooker for 3 minutes. I then treated the sections with 3% hydrogen peroxide diluted in methanol for 10 minutes, before blocking with 5% normal goat serum (Cat No. S-1000; Vector Laboratories) in PBS (for rabbit primary antibodies), 5% normal horse serum (Cat. No. S-2000; Vector Laboratories) in PBS (for goat primary antibodies), or mouse anti-IgG blocking reagent (Cat. No. MKB-2213; Vector Laboratories) (for mouse primary antibodies) for 30 minutes at room temperature. Sections were incubated with primary antibodies diluted in blocking solution overnight at 4°C. All primary antibodies used are described in Table 3.2. I then treated sections with secondary antibodies provided in the SuperPicture Polymer Detection Kit (Cat. No. 879263; Life Technologies) (for rabbit primary antibodies), ImmPRESS Reagent Kit (Cat. No. MP-7405; Vector Laboratories) (for goat primary antibodies), or Mouse on Mouse (MOM) Detection Kit (Cat. No. MKB-2213; Vector Laboratories) (for mouse primary antibodies).

I conducted immunohistochemical (IHC) staining for ALDH1a2 using a custom rabbit anti-mouse ALDH1A2 polyclonal antibody generated for our lab by Alpha Diagnostics International. Specificity for ALDH1a2 was confirmed as described previously[23]. Neighboring tissue sections were stained with antibodies as listed in Table 3.2.

Table 3.2: Primary antibodies
PC = polyclonal antibody; MC = monoclonal antibody
ǂ A custom anti-ALDH1a2 antibody was generated for our lab by Alpha Diagnostics

Target	Company	Catalog #	Lot #	Source	Dilution
ALDH1a2	Alpha Diagnostics	N/A ǂ	Batch #4	Rabbit PC	1:200
CRABP2	Santa Cruz	sc-10065	A2813	Goat PC	1:100
EZH2	Cell Signaling	5246S	7	Rabbit PC	1:200
K14	Novocastra Laboratories	NCL-002	N/A	Mouse MC	1:100

RNA isolation and RT-PCR analysis

I homogenized snap-frozen tissues in 1 mL TRIzol Reagent (Cat. No. 15596018; Ambion, Thermo Fisher Scientific Inc.), and extracted RNA according to manufacturer's protocol. I quantified RNA isolates using a NanoDrop 2000C (Thermo Fisher, Scientific, Inc.), and reverse transcribed 1 µg total RNA using the qScript cDNA Supermix (Cat. No. 95048; Quanta Biosciences). I diluted the resulting cDNA 1:10, and used 2 µL as template for semi-quantitative RT-PCR reactions as previously described[24]. All primers used for RT-PCR are listed in Table 3.3.

Table 3.3: Primer sequences used for RT-PCR
ǂ Primer complementary to transgenic β-globin poly-A sequence

Gene	Forward Primer (5'-3')	Reverse Primer (5'-3')	Product Size
ALDH1a2 total	gacttgtagcagctgtcttcact	tcacccatttctctcccatttcc	160 bp
ALDH1a2 TG	gacttgtagcagctgtcttcact	tgctcaaggggcttcatgatgtcc ǂ	467 bp
rtTA	tacactgggctgcgtattgg	ccgctttcgcactttagctg	198 bp
36B4	agaacaacccagctctggagaaa	acaccctcccagaaagcgagagt	448 bp

Statistical analysis of data

All experiments consist of at least 3 independent biological replicates (n≥3). Statistical analyses were conducted using GraphPad Prism 6.0 software. I determined the means ± S.E.M. and compared independent populations using the Student's *t*-test

or One-way ANOVA, as indicated. Differences with a $p < 0.05$ were considered statistically significant.

RESULTS

Generation of K14-rtTA/TRE- ALDH1a2 (KRT/ALDH) transgenic mice

We utilized two transgenic constructs to generate the *K14-rtTA/TRE-ALDH1a2* Tet-On bitransgenic mice. One construct contained the murine *Aldh1a2* inserted downstream from a minimal promoter and the tetracycline response element (TRE) (TRE-ALDH1a2), and the other contained the reverse tetracycline-controlled transactivator, rtTA2S-M2-VP16 (rtTA), under the control of the truncated human cytokeratin 14 (K14) promoter (K14-rtTA) (Figure 3.1). This K14 promoter is specifically active in the basal layer of some stratified squamous epithelia – such as the oral cavity and skin – thus driving the constitutive and tissue-specific expression of rtTA [25-28]. In this Tet-On system, the TRE allows expression of the transgenic *mALDH1a2* in the presence of doxycycline (dox)-activated rtTA (Figure 3.1).

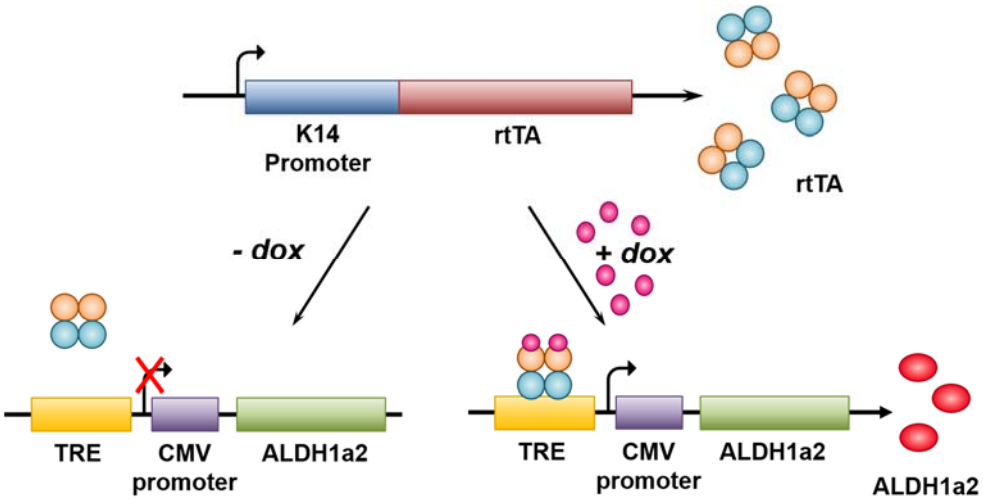

Figure 3.1: The Tet-On inducible system. A simplified schematic of the K14-rtTA and TRE-ALDH1a2 constructs utilized in this Tet-On inducible transgenic mouse system. The truncated K14 promoter drives rtTA expression in the basal layer of certain stratified squamous epithelia, and the TRE dictates that transgenic ALDH1a2 expression is induced in the presence of doxycycline (dox).

We identified a total of three positive *TRE-ALDH1a2* founder mice by Southern blot using a probe directed at the β-globin intron: mice #9, 11, and 25 (Figure 3.2A). We observed multiple bands in each positive founder, indicative of multiple copy insertion, and the presence of a band lower than expected (<2.2 kb) suggests that fragmentation occurred. Using primers specific for transgenic (TG) ALDH1a2, we confirmed the presence of the transgene by genotyping PCR (Figure 3.2B). In order to generate three genetically-distinct, independently-derived *TRE-ALDH1a2* lines, we crossed each of the three *TRE-ALDH1a2* founder mice with a WT C57Bl/6 mouse and again identified positive progeny by both Southern blot and PCR analysis (data not shown). We then crossed female F1 generation *TRE-ALDH1a2*$^{+/-}$ mice with a male *K14-rtTA*$^{+/-}$ mouse obtained from Jackson Labs to generate three independent *K14-rtTA*$^{+/-}$*/TRE-ALDH1a2*$^{+/-}$ *(KRT/ALDH)* lines. We used genotyping PCR to confirm the presence of the transgenes in each *KRT/ALDH* litter (Figure 3.2C).

Tissue-specific, dox-inducible ALDH1a2 expression in KRT/ALDH mouse lines

We treated 6-8 week-old bitransgenic *KRT/ALDH* mice from each line with 2 mg/mL dox or vehicle control (water) in the drinking water for 48 hours. Littermate mice that were negative for one or both transgenes were also treated. We detected rtTA transcripts in the esophagus, tongue, and skin of mice from all three *KRT/ALDH* lines by RT-PCR (Figure 3.3A). By quantification of the bands we observed that rtTA mRNA was approximately 4 to 30-fold higher in the tongue and 10 to 60-fold higher in the skin as compared to esophagus. This is consistent with previously reported data on the relative activity of the truncated K14 promoter in different squamous epithelial tissues[25]. Both the #11 and #25 *KRT/ALDH* lines exhibited expression of transgenic (TG) ALDH1a2 transcript in the esophagus, tongue, and skin during treatment with

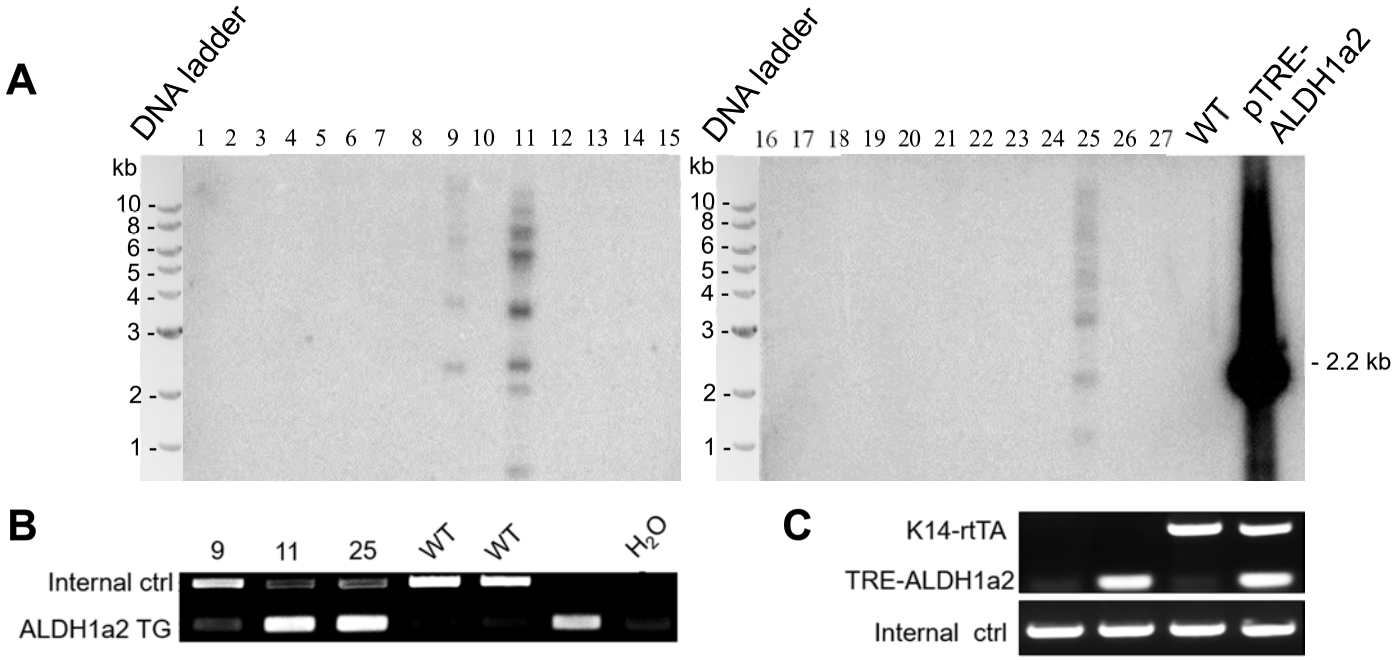

Figure 3.2: Generation of *TRE-ALDH1a2* and *K14-rtTA/TRE-ALDH1a2* mice. (A) Southern blot analysis of potential TRE-ALDH1a2 founder mice, using a probe directed against the β-globin intron. Tail genomic DNA was isolated from n=27 mice, and digested with EcoRI. DNA from a WT C57Bl/6 mouse was used as a negative control, and the original ALDH1a2 transgene-containing plasmid was used as a positive control. (B) Genotyping PCR of TRE-ALDH1a2 founder mice #9, 11, and 25, as well as two negative control mice (wild-type, WT). The ALDH1a2 TG band was noticeably fainter in the #9 line than the #11 and #25 lines. pTRE-ALDH1a2 plasmid was used as positive control. We used primers specific for the transgenic (TG) ALDH1a2. MβCasein was used as a loading (internal) control gene. (C) Genotyping PCR of 4 representative *K14-rtTA/TRE-ALDH1a2* mice, illustrating the passage of both transgenes and genotypes observed in each *K14-rtTA/TRE-ALDH1a2* litter. All primers used are listed in Table 3.1.

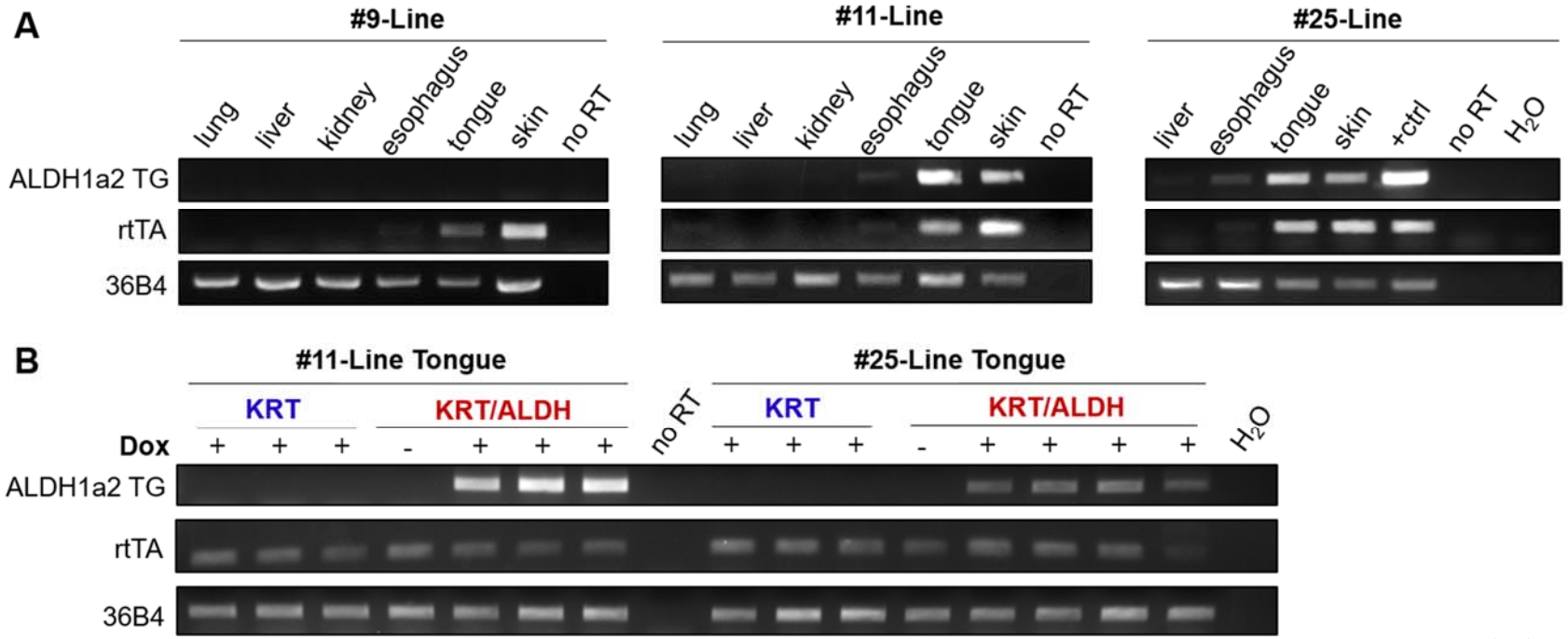

Figure 3.3: ALDH1a2 transcript induction in *KRT/ALDH* mice is tissue-specific and dox-dependent. (A) RT-PCR analysis of tissues from representative bitransgenic mice (positive for both transgenes) from each *KRT/ALDH (K14-rtTA*$^{+/-}$*/TRE-ALDH1a2*$^{+/-}$*)* line. Mice were treated with 2 mg/mL dox in the drinking water for 48 hours, before sacrifice and tissue harvest. All tissues were snap frozen in liquid nitrogen, before homogenization in TRIzol and RNA isolation according to standard protocol. RT-PCR was carried out with primers specific to the transgenic ALDH1a2 (ALDH1a2 TG, Row 1). Littermate control mice containing one, or neither transgene, or bitransgenic mice treated with vehicle control, exhibited no transgene induction (Supplemental Figure 3.3). Positive control lane in right panel represents a sample from a #11-line mouse tongue. (B) RT-PCR analysis of tongue tissue from n=7 or n=8 different mice from the #11 and #25 *KRT/ALDH* lines, respectively, after treatment with dox or vehicle control for 48 hours. Mice represented are either bitransgenic, or littermate controls positive for only the K14-rtTA transgene *(KRT)*. 36B4 (Row 3) was used as loading control in both (A) and (B). All primers used are listed in Table 3.3. RT-PCR analysis shown is representative of at least 3 mice per group (n≥3).

dox (Figure 3.3A, middle and right panels). Notably, we observed lower TG ALDH1a2 transcript levels in the esophagus compared to the tongue and skin, most likely attributable to the lower rtTA expression in this tissue. No TG ALDH1a2 or rtTA mRNA was detected in lung, liver, or kidney samples, illustrating the tissue-specificity of this expression system (Figure 3.3A). We could not detect any TG ALDH1a2 mRNA in the #9 *KRT/ALDH* line, in contrast to lines #11 and 25 (Figure 1A, left panel). We also did not detect any TG ALDH1a2 transcript expression in untreated mice and in dox-treated mice that did not carry both transgenes (data not shown). We found that the #11-line achieved greater average TG ALDH1a2 transcript expression (approximately 3-fold) after 48 hours of dox treatment compared to bitransgenic #25 line *KRT/ALDH* mice (Figure 3.3B). Together, our results show that this Tet-On expression system is both highly tissue-specific and dox-inducible. We performed additional experiments on the #11 *KRT/ALDH* line, as line #11 exhibited the greatest dox-induction of the TG ALDH1a2 transcript.

We utilized IHC analysis to examine total (endogenous + TG) ALDH1a2 protein levels following dox treatment, and to determine its localization within the target tissues. We detected ALDH1a2-positive cells in the epithelium of the tongue, skin, and esophagus of *KRT/ALDH* mice after 72 hours dox (brown stain, Figure 3.4A). Consistent with the RT-PCR results shown in Figure 3.3, we observed lower ALDH1a2 protein expression in the esophagus as compared to the tongue and skin (Figure 3.4B). We detected no changes in ALDH1a2 protein levels in the liver and in the tissue sections of dox-treated littermate *K14-rtTA*$^{+/-}$ *(KRT)* mice (Figure 3.4A, top row). The staining pattern and intensity of stain of endogenous ALDH1a2, as observed in the *KRT* mice (Figure 3.4A, left column), are consistent with previously reported data on ALDH1a2 protein expression in different human tissues (www.proteinatlas.org, accessed September 26, 2016).

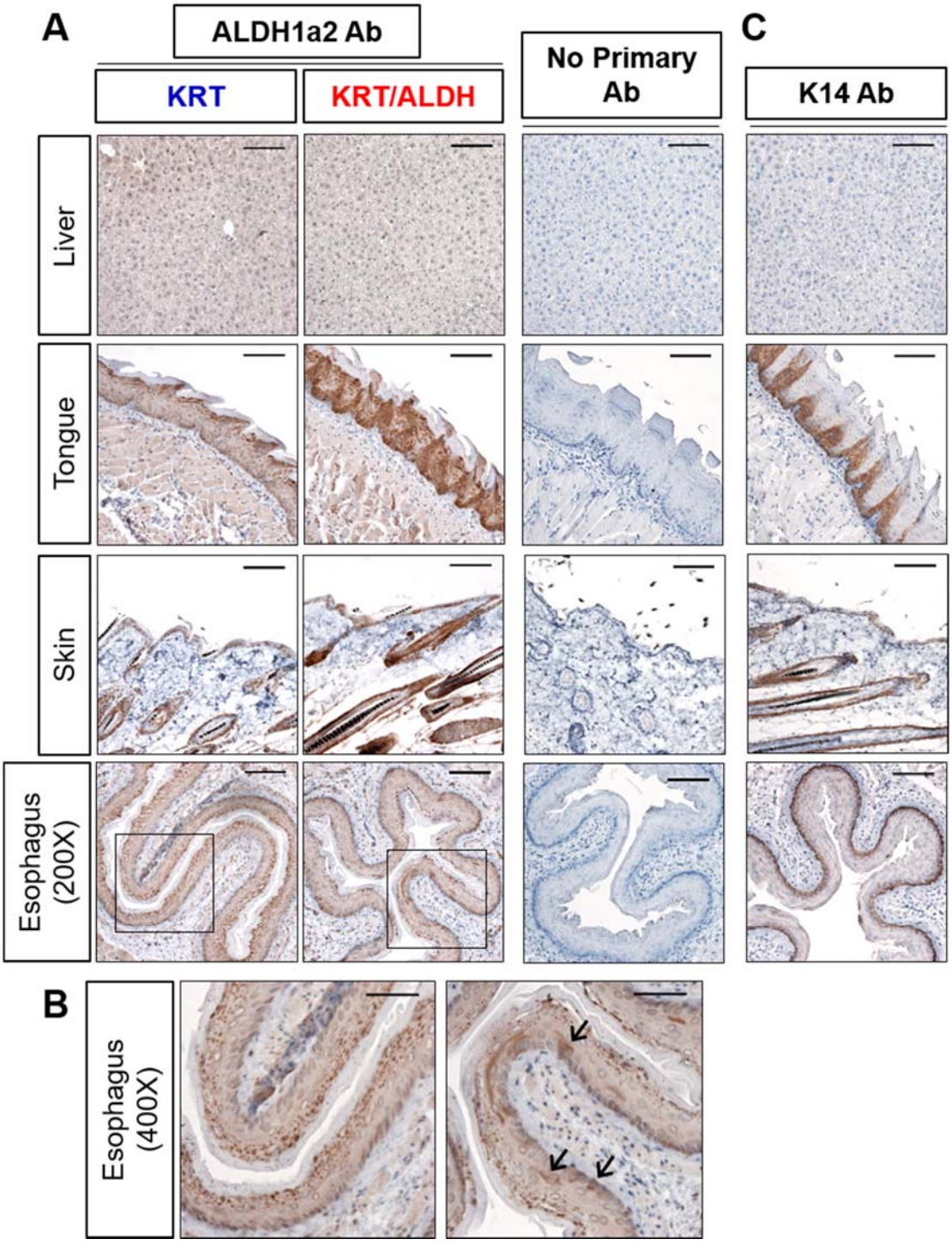
A
ALDH1a2 Ab
KRT
KRT/ALDH
No Primary Ab
C
K14 Ab
Liver
Tongue
Skin
Esophagus (200X)
B
Esophagus (400X)

Figure 3.4: ALDH1a2 protein is specifically induced in squamous epithelial tissues. 6-8 week-old *KRT* and *KRT/ALDH* mice were treated with dox (2 mg/mL) in the drinking water for 72 hours. (A,B) Paraffin-embedded tissue sections were stained with 1:200 ALDH1a2 antibody, except for no primary control sections. Fields shown are representative images from one of n≥3 mice of each genotype. Boxed regions in esophagus panels of (A) are displayed at higher magnification in (B). Black arrows indicate positively-stained cells in the esophageal epithelium. (C) Tissue sections were stained with 1:100 K14 antibody. Fields shown in (C) are representative images from one control mouse. Images in A,C taken at 200X, scale bar represents 100 μm. Images in B taken at 400X, scale bar represents 50 μm. All images shown are representative of ≥4 fields of each section. Primary antibody details are provided in Table 3.2.

In these transgenic mice rtTA expression is driven by a truncated K14 promoter. Therefore, in this model K14-expressing cells constitutively express rtTA and will express TG ALDH1a2 upon dox addition. IHC staining of endogenous K14 protein revealed high K14 expression specifically in the basal layers of the tongue and esophagus (Figure 3.4C). These data are consistent with previously reported expression patterns of K14 in these tissues[29]. In contrast, ALDH1a2 protein expression following dox treatment was not confined to the basal layer; while the majority of cells in the basal layer are ALDH1a2-positive following a 72 hr dox treatment (approx. 96.9% (± 2.0%)), some cells in the suprabasal layers also stained dark brown for ALDH1a2 (Figure 3.4A). This result suggests that TG ALDH1a2 expression persists even after the cells move upward through the epithelium and K14 expression decreases. Notably, we observed no change in K14 protein levels following TG ALDH1a2 induction by dox in #11 *KRT/ALDH* mice (data not shown).

Dox-inducible TG ALDH1a2 mRNA and protein over time

To characterize the dox-inducible expression of TG ALDH1a2 in the tongue epithelium further, we conducted time course experiments in which we treated bitransgenic #11 *KRT/ALDH* mice and singly-transgenic littermate *KRT* mice, used as negative controls, with dox for 24, 48, and 72 hours. We found that TG ALDH1a2 transcript levels in the tongue were maximal by 72 hours of dox treatment, while rtTA

mRNA levels remained constant (Figure 3.5A). We used different primer pairs to evaluate TG ALDH1a2 mRNA and total (endogenous + TG) ALDH1a2 mRNA levels, and observed that the TG ALDH1a2 transcript levels after dox treatment are representative of the total transcript levels of ALDH1a2 present in the tongue tissue. Upon removal of dox from the drinking water, ALDH1a2 transcript levels (TG and total) decreased steadily over a period of 2-3 days (Figure 3.5A).

We also observed ALDH1a2-postive cells in the basal layer of the tongue epithelium as early as at 48 hours of dox treatment using IHC (Figure 3.5B, second panel). By 72 hours, most of the basal layer cells (96.9% (± 2.0%)) and some cells in the suprabasal layers were positive for ALDH1a2 (Figure 3.5B, third panel). Adjacent tongue muscle tissue exhibited no changes in ALDH1a2 staining. After removal of dox, the percentage of ALDH1a2-positive cells in the basal layer decreased to 54.8% (± 5.3%) by 24 hrs and 19.5% (± 1.3%) by 48 hrs (Figure 3.5B, fourth and fifth panels). We also detected increased staining for ALDH1a2 in the suprabasal layers at these time points compared to earlier time points (down arrows, Figure 3.5B). Taken together with the data shown in Figure 3.4, these results indicate that the TG ALDH1a2 signal originates in K14-positive, basal layer progenitor cells, and that these cells maintain TG ALDH1a2 expression as they differentiate and move upward through the suprabasal layers[30]. Overall, these data demonstrate the inducibility, reversibility, and tissue specificity of TG ALDH1a2 expression in *KRT/ALDH* transgenic mice.

CRABP2 protein level is increased in tongue epithelia following ALDH1a2 induction

To determine whether TG ALDH1a2 enhances endogenous intracellular RA signaling, we utilized LC-MS to directly measure retinoid levels in the tongues of *KRT* and *KRT/ALDH* mice following dox treatment. Ultimately, this analysis was

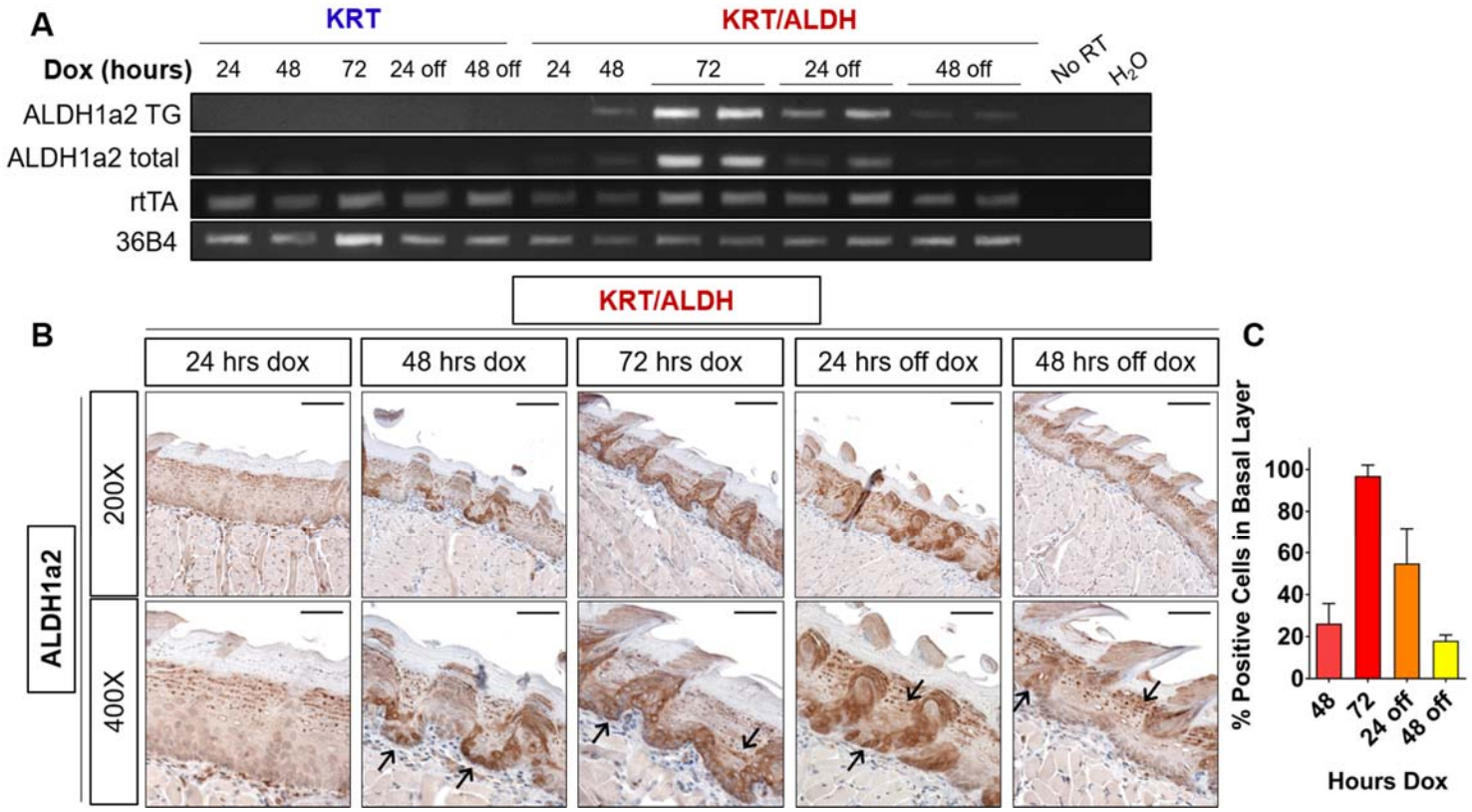

Figure 3.5: ALDH1a2 inducibility in tongue with respect to length of doxycycline treatment. (A) RT-PCR analysis of tongues from *KRT (K14-rtTA$^{+/-}$)* and *KRT/ALDH (K14-rtTA$^{+/-}$/TRE-ALDH1a2$^{+/-}$)* mice from the #11 line treated with 2 mg/mL dox in the drinking water for 24, 48, or 72 hours, or 72 hours followed by 24 or 48 hours of normal drinking water (n≥3, ea. treatment). Primers used are specific to the transgenic (TG) ALDH1a2, total ALDH1a2 (TG and endogenous), rtTA, and 36B4 (loading control). (B) IHC analysis of tongue sections from #11 line *KRT/ALDH* mice shown in (A). Tissues were incubated with 1:200 anti-ALDH1a2. Shown are representative images of ≥4 fields analyzed from each section (200X, scale bar represents 100 µm; 400X, scale bar represents 50 µm). Brown color indicates positively stained cells, blue color represents hematoxylin-stained nuclei. Arrows indicate positively-stained cells in the basal and surprabasal layers. Primers and primary antibodies used are listed in Tables 3.2 and 3.3. (C) Quantification of the percent cells in the basal layer stained dark brown for ALDH1a2 protein.

inconclusive, as discussed in detail in the Appendix (Figures A.2, A.3). In addition, our LC-MS experiments can not delineate the effects of ALDH1a2 induction specifically in loci of interest, such as the tongue epithelium, because we analyzed whole tongues by LC-MS. We therefore used IHC to stain for CRABP2; the function of endogenous CRABP2 is to facilitate retinoid signaling by binding free cytoplasmic RA and shuttling it to the nucleus for binding and activation of RAR/RXR receptors[31, 32]. CRABP2 is downstream of ALDH1a2 in the classical retinoid metabolism and signaling pathway (Figure 1.2). In addition, CRABP2 expression is increased by RA[33, 34]. We treated #11 *KRT/ALDH* mice and *KRT* mice with dox for 7 days (1 week) and stained for CRABP2 protein (Figure 3.6). We found that the tongue epithelia of *KRT/ALDH* mice showed greater CRABP2 protein expression than those of *KRT* mice in terms of mean stain intensity (1.35-fold change ± 0.12, p=0.0442; Figure 3.6B). As CRABP2 is an integral member of the RA signaling pathway and is induced by RA, these data provide strong, though indirect evidence for increased RA synthesis and signaling after TG ALDH1a2 induction by dox in #11 *KRT/ALDH* TG mice.

Exogenous ALDH1a2 reduces EZH2 protein levels in the tongue epithelium

Enhancer of zeste homolog 2 (EZH2) is an epigenetic regulatory protein that functions as a transcriptional repressor as a core component of the polycomb repressive complex 2 (PRC2)[35]. EZH2 is overexpressed in numerous malignancies, including HNSCC, in which it has been proposed as a potential drug target[36]. Previous research in our lab has demonstrated that RA signaling decreases the activity of PRC2 (and EZH2) by stimulating the dissociation of PRC2 from the promoters of target genes[35, 37, 38]. In addition, experiments in mouse embryonic stem cells (CCE) revealed that EZH2 mRNA and protein levels are decreased following treatment with RA[39]. We therefore investigated whether TG ALDH1a2 overexpression in the tongue epithelia of

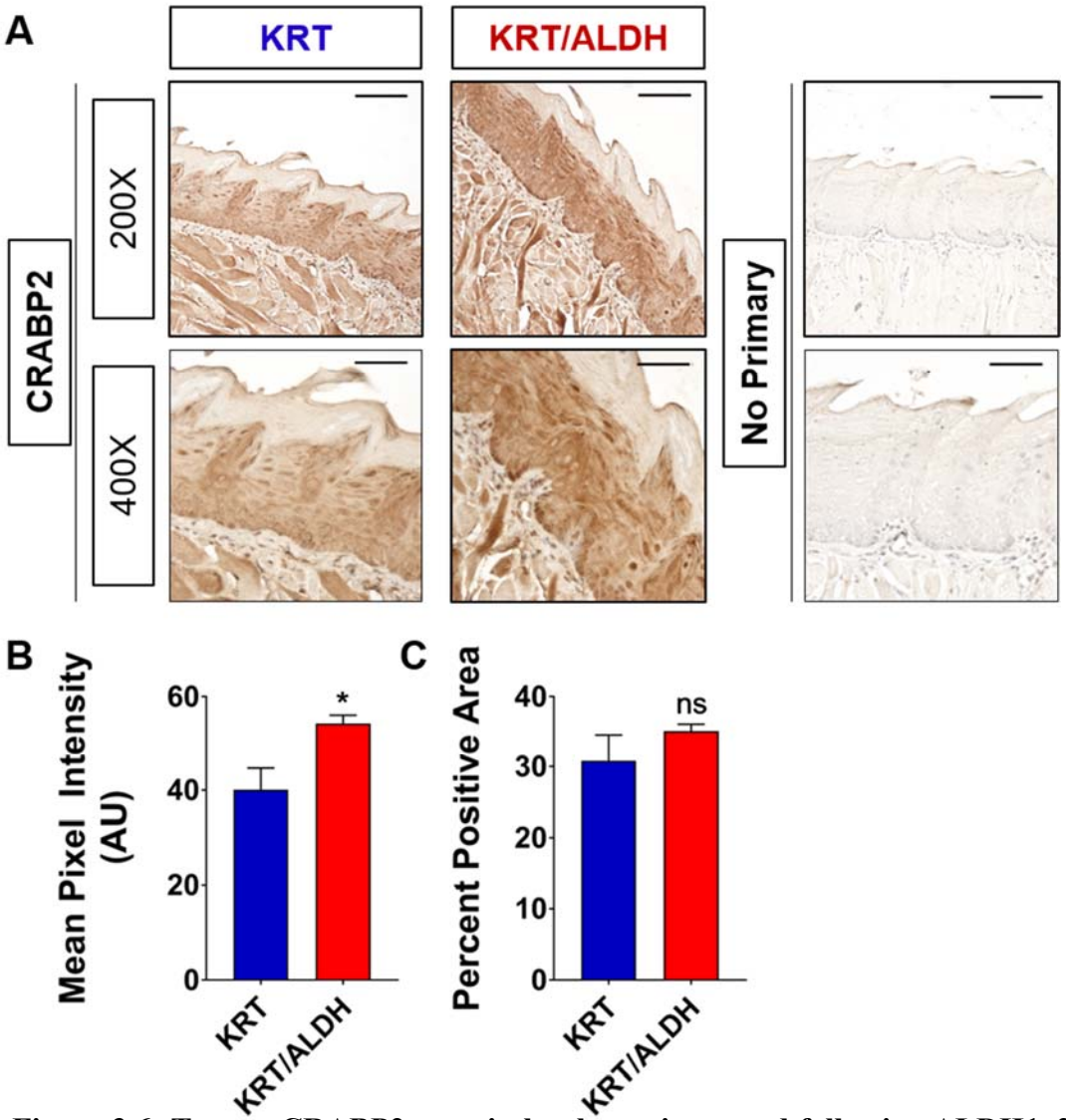

Figure 3.6: Tongue CRABP2 protein levels are increased following ALDH1a2 overexpression. IHC analysis of tongue sections from *KRT (K14-rtTA$^{+/-}$)* and *KRT/ALDH (K14-rtTA$^{+/-}$/TRE-ALDH1a2$^{+/-}$)* mice treated with dox (2 mg/mL) or vehicle control (water) for 1 week (7 days). All mice shown in this figure are from the #11 KRT/ALDH line. Sections were incubated with 1:100 anti-CRABP2 (Table 3.2). Sections incubated without primary antibodies were used as negative controls. (A) Images shown are representative of at least 4 fields from each of n≥3 mice from each group. Brown color indicates positively stained cells. Images were taken at 200X and 400X, as indicated. Scale bars represents 100 µm and 50 µm, respectively. (B,C) Quantification of CRABP2 staining in tongues using Image J software. We analyzed n=4 fields of a stained tongue section from each mouse. Bars represent mean ±S.E.M. of n=3 mice from each group. (B) Each field was analyzed for the mean pixel intensity (AU). (C) Quantification of the percent area of the tongue epithelium that stained positive for CRABP2 protein. The data were analyzed using a Student's *t*-test; ∗ indicates $p<0.05$.

KRT/ALDH mice affects EZH2 expression. We treated line #11 *KRT* and *KRT/ALDH* mice with dox for 1 and 4 weeks and stained for EZH2 protein using IHC. Staining for EZH2 was greatest in basal layer cells (brown stain, Figure 3.7). We used ImageJ software to quantify the mean intensity of the stain and the percent of the epithelium in each field that stained positively for EZH2. We did not observe a significant change in EZH2 protein levels after 1 week of dox treatment. However, we observed decreased staining for EZH2 protein in the tongue epithelia of *KRT/ALDH* mice compared to *KRT* mice after 4 weeks of dox treatment: mean stain intensity was decreased by 1.47-fold (p=0.0164) and the percent positive epithelial area was decreased by 1.38-fold (p=0.007) (Figure 3.7). These results suggest that ectopic, TG ALDH1a2 leads to a reduction in EZH2 in the tongue epithelium. This is an interesting observation that is explored further in Chapter 4.

DISCUSSION

In this chapter we describe the generation of a novel bitransgenic mouse system that allows for the inducible expression of ALDH1a2 specifically in certain stratified squamous epithelial tissues: the tongue, skin, and esophagus. This tissue-specificity is accomplished through the use of a truncated human K14 promoter, first generated and utilized by Fuchs *et al*[28]. This truncated K14 promoter has been used by our lab and others to express various transgenes in the basal cells[21, 26, 27, 40-42]. Endogenous K14 is expressed exclusively in the basal layer of the normal epithelium, which is the innermost epithelial layer and adjoins the basement membrane (Figure 1.2). The basal layer contains a stem cell population that is long-lived, highly proliferative, and responsible for repopulating the regenerating epithelium[43]. In addition, these cells are the site of origin of squamous cell carcinomas of the skin and

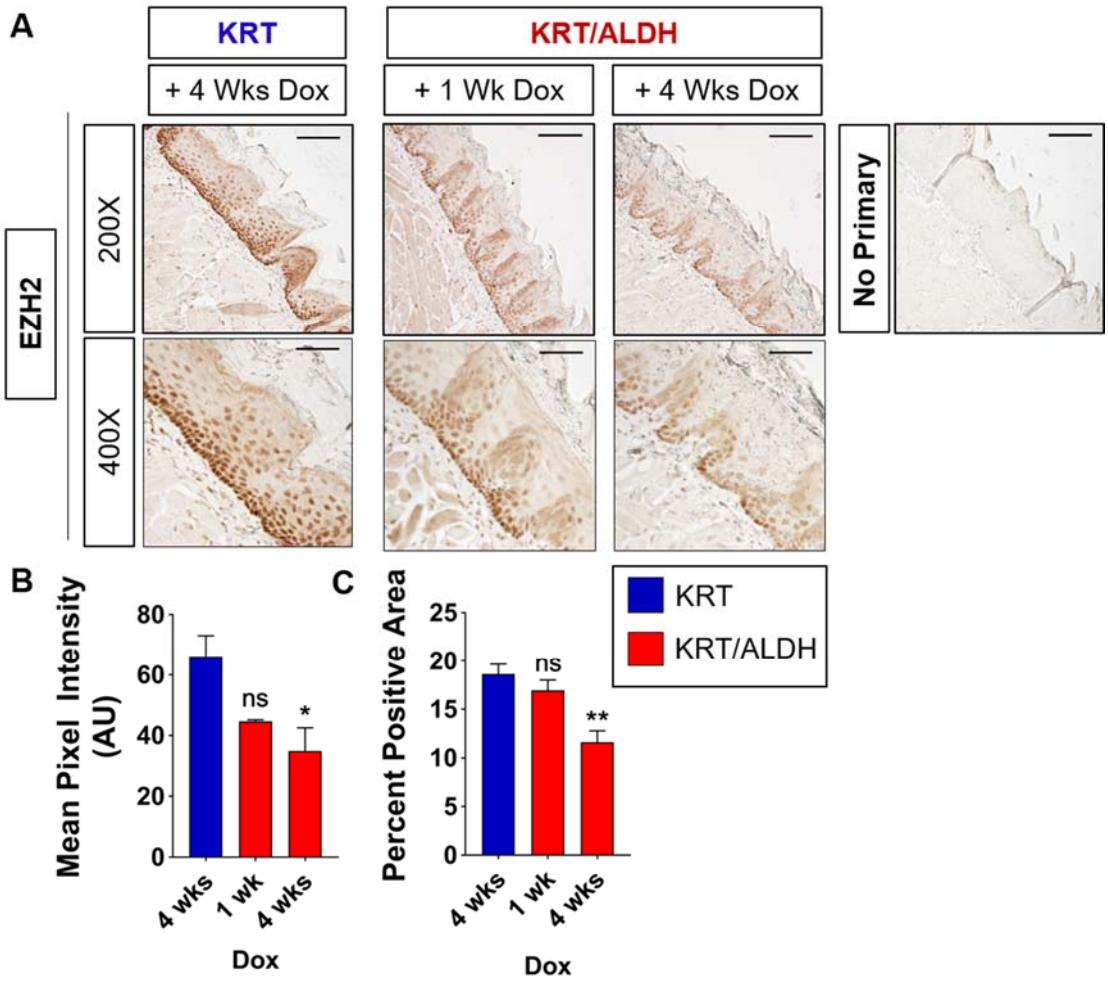

Figure 3.7: Tongue EZH2 protein levels are decreased following ALDH1a2 overexpression. IHC analysis of tongue sections from line #11 *KRT (K14-rtTA$^{+/-}$)* and *KRT/ALDH (K14-rtTA$^{+/-}$/TRE-ALDH1a2$^{+/-}$)* mice treated with dox (2 mg/mL) or vehicle control (water) for 1 or 4 weeks, as indicated. Tissue sections were incubated with 1:200 anti-EZH2 primary antibody. Primary antibody information is provided in Table 3.2. (A) Images shown are representative of at least 6 fields from each of n≥3 mice from each treatment group. Brown color indicates positively stained cells. All mice shown in this figure are from the #11 KRT/ALDH line. Images were taken at 200X and 400X, as indicated. . Scale bars represents 100 µm and 50 µm, respectively. (B,C) Quantification of EZH2 staining in tongues using Image J software. We analyzed n=3 fields of stained tongue section from each mouse. Bars represent mean ±S.E.M. of n=3 mice from each group. (B) Each field was analyzed for the mean pixel intensity (AU). We set the Y-axis minimum to the minimum detectable stain intensity (y=94). (C) Quantification of the percent area of the tongue epithelium that stained positive for EZH2 protein. The data were analyzed using One-way ANOVA; ∗ indicates $p<0.05$, ∗∗ indicates $p<0.01$.

oral cavity[30, 43, 44]. These characteristics make K14-postive cells of particular interest for study in the context of epithelial malignancies.

Our bitransgenic mouse system utilizes a modified Tet-On expression system. To date, the Tet-On system has proven a powerful and elegant experimental tool for inducible and reversible transgene expression[45]. This temporal control allows us to rapidly induce and terminate TG ALDH1a2 transcript and protein expression through administration and removal of dox, respectively. Using this expression system, we were able to detect TG ALDH1a2 transcript and protein induction in the tongue epithelium by 48 hours of dox treatment (Figures 3.2, 3.4). By 72 hours of dox administration, ALDH1a2 induction was maximal and most of the epithelial basal layer cells stained positive for ALDH1a2 protein (Figures 3.3, 3.4). Li, *et al*. generated bitransgenic mice containing the *K14-rtTA* cassette to drive dox-inducible GFP in the tongue epithelium, and found that GFP was distributed throughout the dorsal surface of the tongue after 72 hours of dox administration via the drinking water[46].

We observed increased CRABP2 protein levels in tongue epithelia following induction of ALDH1a2 (Figure 3.5). CRABP2 is an intracellular lipid binding protein that binds and translocates free RA, and is known to exhibit increased expression in response to RA[31, 33]. CRABP2 is considered to be an indicator of RA activity in epithelial tissues such as the epidermis[47, 48]. Therefore, our results suggest that the dox-inducible expression of TG ALDH1a2 increases intracellular RA. This result is of particular clinical interest, as loss of CRABP2 expression is observed in squamous cell carcinomas and has been found to promote carcinogenesis[13, 49]. For this reason, restoration of CRABP2 signaling has been proposed as a therapeutic strategy in treating squamous cell carcinomas[49].

An interesting finding of our study is that ectopic TG ALDH1a2 decreases EZH2 protein levels in tongue epithelia (Figure 3.6). EZH2, a H3K27 methyltransferase, is a Polycomb group protein[35]. This group of proteins plays a critical role in controlling stem cell activity and differentiation in normal epidermal keratinocytes[50]. Previous research in mouse embryonic stem cells showed that EZH2 mRNA and protein levels are reduced by RA; therefore the reduction in EZH2 protein levels we observe in dox-treated *KRT/ALDH* mice suggests that TG ALDH1a2 increases intracellular RA signaling[39]. In addition, EZH2 is frequently overexpressed in several human epithelial cancer types, including HNSCC[51]. Zhou et. al. analyzed HNSCC patient RNAseq data available from the Cancer Genome Atlas (TCGA), and found that high EZH2 mRNA was associated with worse overall patient survival and advanced tumor grade[36]. In cell cultures, EZH2 overexpression promotes tumor cell proliferation, epithelial-mesenchymal transition (EMT), invasion and migration[36, 51-54]. Conversely, inhibition or depletion of EZH2 induces apoptosis and inhibits cell proliferation, colony formation, migration, and invasion in tongue squamous cell carcinoma cells[55, 56]. To date, EZH2 has been proposed as a critical biomarker for diagnosis, a prognostic indicator, and a novel drug target in HNSCC[55].

CONCLUSIONS

Taken together, our data show that the *K14-rtTA/TRE-ALDH1a2* mouse line (#11) is an effective system for the tissue-specific induction of exogenous ALDH1a2. This mouse line is a powerful experimental tool for *in vivo* studies on RA synthesis in the context of the stratified squamous epithelium. In addition, our findings that ectopic TG ALDH1a2 expression in the tongue epithelium increases CRABP2 expression and decreases EZH2 expression evidence a role for ALDH1a2 in intracellular RA signaling. The effects of ALDH1a2 induction on CRABP2 and EZH2 are particularly

interesting in the context of HNSCC, and support our subsequent work in which we utilized our *KRT/ALDH* mice in a murine model of oral cavity squamous cell carcinoma (OSCC), as described in Chapter 4.

SUPPLEMENTAL DATA

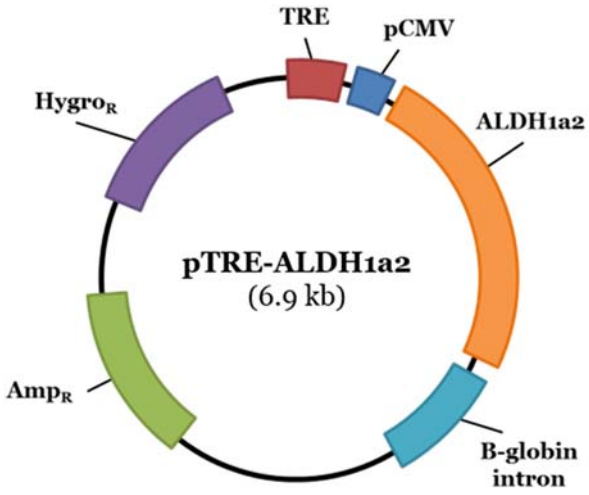

Supplemental Figure 3.1: Schematic of the pTRE-ALDH1a2 construct used to drive inducible expression of ALDH1a2. The vector was constructed by digesting pCMV-Sport6/ALDH1a2 with AgeI, and amplifying the resulting fragment to generate BamHI/NotI restriction sites for insertion into the BamHI/NotI sites of pTRE2hyg (Clontech Laboratories, Inc.). The resulting plasmid was verified by enzyme digest, and by sequencing at the Cornell CORE Facility.

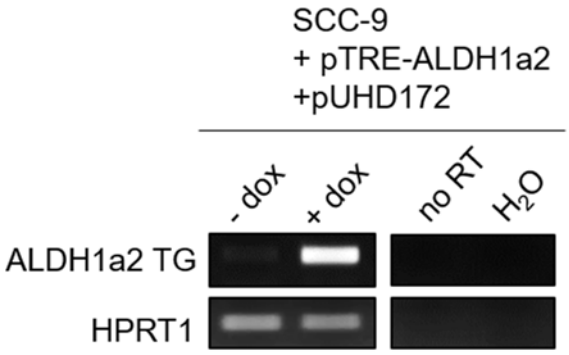

Supplemental Figure 3.2: Verification of inducibility of pTRE2-ALDH1a2 in keratinocyte line SCC-9 via RT-PCR. SCC-9 cells were first stably transfected with pUHD172-1neo, which drives constitutive expression of rtTA. Six stable clones were then generated after transfection with pTRE-ALDH1a2. These clones were treated with dox (1 mg/mL) for 48 hrs, before harvest and RNA isolation as previously described. Primers used for TG ALDH1a2 are specific to the transgenic (not endogenous, TG) transcript. HPRT1 was used as a loading control. Data shown is from one representative clone. Primers used are listed in Table 3.2.

REFERENCES

1. Means AL, Gudas LJ. The roles of retinoids in vertebrate development. Annu Rev Biochem. 1995;64: 201-233.

2. Delva L, Bastie JN, Rochette-Egly C, et al. Physical and functional interactions between cellular retinoic acid binding protein II and the retinoic acid-dependent nuclear complex. Mol Cell Biol. 1999;19: 7158-7167.

3. Noy N. Retinoid-binding proteins: mediators of retinoid action. Biochem J. 2000;348 Pt 3: 481-495.

4. Mongan NP, Gudas LJ. Diverse actions of retinoid receptors in cancer prevention and treatment. Differentiation. 2007;75: 853-870.

5. Darmon M. Retinoic acid in skin and epithelia. Seminars in Developmental Biology. 1991 2: 219-228.

6. Wolbach SB, Howe PR. TISSUE CHANGES FOLLOWING DEPRIVATION OF FAT-SOLUBLE A VITAMIN. J Exp Med. 1925;42: 753-777.

7. Lotan R. Roles of retinoids and their nuclear receptors in the development and prevention of upper aerodigestive tract cancers. Environ Health Perspect. 1997;105 Suppl 4: 985-988.

8. Leemans CR, Braakhuis BJ, Brakenhoff RH. The molecular biology of head and neck cancer. Nat Rev Cancer. 2011;11: 9-22.

9. Squier CA, Kremer MJ. Biology of oral mucosa and esophagus. J Natl Cancer Inst Monogr. 2001: 7-15.

10. Xu XC, Ro JY, Lee JS, Shin DM, Hong WK, Lotan R. Differential expression of nuclear retinoid receptors in normal, premalignant, and malignant head and neck tissues. Cancer Res. 1994;54: 3580-3587.

11. Youssef EM, Lotan D, Issa JP, et al. Hypermethylation of the retinoic acid receptor-beta(2) gene in head and neck carcinogenesis. Clin Cancer Res. 2004;10: 1733-1742.
12. Hu L, Crowe DL, Rheinwald JG, Chambon P, Gudas LJ. Abnormal expression of retinoic acid receptors and keratin 19 by human oral and epidermal squamous cell carcinoma cell lines. Cancer Res. 1991;51: 3972-3981.
13. Yang Q, Wang R, Xiao W, Sun F, Yuan H, Pan Q. Cellular Retinoic Acid Binding Protein 2 Is Strikingly Downregulated in Human Esophageal Squamous Cell Carcinoma and Functions as a Tumor Suppressor. PLoS One. 2016;11: e0148381.
14. Kostareli E, Holzinger D, Bogatyrova O, et al. HPV-related methylation signature predicts survival in oropharyngeal squamous cell carcinomas. J Clin Invest. 2013;123: 2488-2501.
15. Amann PM, Luo C, Owen RW, et al. Vitamin A metabolism in benign and malignant melanocytic skin cells: importance of lecithin/retinol acyltransferase and RPE65. J Cell Physiol. 2012;227: 718-728.
16. Elder JT, Aström A, Pettersson U, et al. Differential regulation of retinoic acid receptors and binding proteins in human skin. J Invest Dermatol. 1992;98: 673-679.
17. Lotan R. Retinoids in cancer chemoprevention. FASEB J. 1996;10: 1031-1039.
18. Lee JJ, Wu X, Hildebrandt MA, et al. Global assessment of genetic variation influencing response to retinoid chemoprevention in head and neck cancer patients. Cancer Prev Res (Phila). 2011;4: 185-193.
19. Freemantle SJ, Dragnev KH, Dmitrovsky E. The retinoic acid paradox in cancer chemoprevention. J Natl Cancer Inst. 2006;98: 426-427.
20. Nguyen H, Rendl M, Fuchs E. Tcf3 governs stem cell features and represses cell fate determination in skin. Cell. 2006;127: 171-183.

21. Xie W, Chow LT, Paterson AJ, Chin E, Kudlow JE. Conditional expression of the ErbB2 oncogene elicits reversible hyperplasia in stratified epithelia and up-regulation of TGFalpha expression in transgenic mice. Oncogene. 1999;18: 3593-3607.
22. Jay FF, Schneider MR. A reporter mouse line with doxycyclin-inducible expression of β-glucosidase. Histochem Cell Biol. 2014;142: 721-724.
23. Touma SE, Perner S, Rubin MA, Nanus DM, Gudas LJ. Retinoid metabolism and ALDH1A2 (RALDH2) expression are altered in the transgenic adenocarcinoma mouse prostate model. Biochem Pharmacol. 2009;78: 1127-1138.
24. Laursen KB, Wong PM, Gudas LJ. Epigenetic regulation by RARα maintains ligand-independent transcriptional activity. Nucleic Acids Res. 2012;40: 102-115.
25. Vassar R, Rosenberg M, Ross S, Tyner A, Fuchs E. Tissue-specific and differentiation-specific expression of a human K14 keratin gene in transgenic mice. Proc Natl Acad Sci U S A. 1989;86: 1563-1567.
26. Tang XH, Vivero M, Gudas LJ. Overexpression of CRABPI in suprabasal keratinocytes enhances the proliferation of epidermal basal keratinocytes in mouse skin topically treated with all-trans retinoic acid. Exp Cell Res. 2008;314: 38-51.
27. Tang XH, Su D, Albert M, Scognamiglio T, Gudas LJ. Overexpression of lecithin:retinol acyltransferase in the epithelial basal layer makes mice more sensitive to oral cavity carcinogenesis induced by a carcinogen. Cancer Biol Ther. 2009;8: 1212-1213.
28. Vassar R, Rosenberg M, Ross S, Tyner A, Fuchs E. Tissue-specific and differentiation-specific expression of a human K14 keratin gene in transgenic mice. Proc Natl Acad Sci U S A. 1989;86: 1563-1567.
29. Tang XH, Knudsen B, Bemis D, Tickoo S, Gudas LJ. Oral cavity and esophageal carcinogenesis modeled in carcinogen-treated mice. Clin Cancer Res. 2004;10: 301-313.

30. Tang XH, Scognamiglio T, Gudas LJ. Basal stem cells contribute to squamous cell carcinomas in the oral cavity. Carcinogenesis. 2013;34: 1158-1164.
31. Napoli JL, Boerman MH, Chai X, Zhai Y, Fiorella PD. Enzymes and binding proteins affecting retinoic acid concentrations. J Steroid Biochem Mol Biol. 1995;53: 497-502.
32. Wolf G. Cellular retinoic acid-binding protein II: a coactivator of the transactivation by the retinoic acid receptor complex RAR.RXR. Nutr Rev. 2000;58: 151-153.
33. Balmer JE, Blomhoff R. Gene expression regulation by retinoic acid. J Lipid Res. 2002;43: 1773-1808.
34. Durand B, Saunders M, Leroy P, Leid M, Chambon P. All-trans and 9-cis retinoic acid induction of CRABPII transcription is mediated by RAR-RXR heterodimers bound to DR1 and DR2 repeated motifs. Cell. 1992;71: 73-85.
35. Benoit YD, Laursen KB, Witherspoon MS, Lipkin SM, Gudas LJ. Inhibition of PRC2 histone methyltransferase activity increases TRAIL-mediated apoptosis sensitivity in human colon cancer cells. J Cell Physiol. 2013;228: 764-772.
36. Zhou X, Ren Y, Kong L, et al. Targeting EZH2 regulates tumor growth and apoptosis through modulating mitochondria dependent cell-death pathway in HNSCC. Oncotarget. 2015;6: 33720-33732.
37. Kashyap V, Gudas LJ, Brenet F, Funk P, Viale A, Scandura JM. Epigenomic reorganization of the clustered Hox genes in embryonic stem cells induced by retinoic acid. J Biol Chem. 2011;286: 3250-3260.
38. Gillespie RF, Gudas LJ. Retinoid regulated association of transcriptional co-regulators and the polycomb group protein SUZ12 with the retinoic acid response elements of Hoxa1, RARbeta(2), and Cyp26A1 in F9 embryonal carcinoma cells. J Mol Biol. 2007;372: 298-316.

39. Lee ER, Murdoch FE, Fritsch MK. High histone acetylation and decreased polycomb repressive complex 2 member levels regulate gene specific transcriptional changes during early embryonic stem cell differentiation induced by retinoic acid. Stem Cells. 2007;25: 2191-2199.
40. Arnold I, Watt FM. c-Myc activation in transgenic mouse epidermis results in mobilization of stem cells and differentiation of their progeny. Curr Biol. 2001;11: 558-568.
41. Ballarò C, Ceccarelli S, Tiveron C, et al. Targeted expression of RALT in mouse skin inhibits epidermal growth factor receptor signalling and generates a Waved-like phenotype. EMBO Rep. 2005;6: 755-761.
42. Feith DJ, Bol DK, Carboni JM, et al. Induction of ornithine decarboxylase activity is a necessary step for mitogen-activated protein kinase kinase-induced skin tumorigenesis. Cancer Res. 2005;65: 572-578.
43. Okubo T, Clark C, Hogan BL. Cell lineage mapping of taste bud cells and keratinocytes in the mouse tongue and soft palate. Stem Cells. 2009;27: 442-450.
44. Lapouge G, Youssef KK, Vokaer B, et al. Identifying the cellular origin of squamous skin tumors. Proc Natl Acad Sci U S A. 2011;108: 7431-7436.
45. Albanese C, Hulit J, Sakamaki T, Pestell RG. Recent advances in inducible expression in transgenic mice. Semin Cell Dev Biol. 2002;13: 129-141.
46. Li F, Zhou M. Local microenvironment provides important cues for cell differentiation in lingual epithelia. PLoS One. 2012;7: e35362.
47. Chapellier B, Mark M, Messaddeq N, et al. Physiological and retinoid-induced proliferations of epidermis basal keratinocytes are differently controlled. EMBO J. 2002;21: 3402-3413.
48. Fisher GJ, Voorhees JJ. Molecular mechanisms of retinoid actions in skin. FASEB J. 1996;10: 1002-1013.

49. Passeri D, Doldo E, Tarquini C, et al. Loss of CRABP-II Characterizes Human Skin Poorly Differentiated Squamous Cell Carcinomas and Favors DMBA/TPA-Induced Carcinogenesis. J Invest Dermatol. 2016;136: 1255-1266.
50. Botchkarev VA, Mardaryev AN. Repressing the Keratinocyte Genome: How the Polycomb Complex Subunits Operate in Concert to Control Skin and Hair Follicle Development. J Invest Dermatol. 2016;136: 1538-1540.
51. Cao W, Feng Z, Cui Z, et al. Up-regulation of enhancer of zeste homolog 2 is associated positively with cyclin D1 overexpression and poor clinical outcome in head and neck squamous cell carcinoma. Cancer. 2012;118: 2858-2871.
52. Zheng M, Jiang YP, Chen W, et al. Snail and Slug collaborate on EMT and tumor metastasis through miR-101-mediated EZH2 axis in oral tongue squamous cell carcinoma. Oncotarget. 2015;6: 6797-6810.
53. Chase A, Cross NC. Aberrations of EZH2 in cancer. Clin Cancer Res. 2011;17: 2613-2618.
54. Wang C, Liu X, Chen Z, et al. Polycomb group protein EZH2-mediated E-cadherin repression promotes metastasis of oral tongue squamous cell carcinoma. Mol Carcinog. 2013;52: 229-236.
55. Li Z, Wang Y, Qiu J, et al. The polycomb group protein EZH2 is a novel therapeutic target in tongue cancer. Oncotarget. 2013;4: 2532-2549.
56. Chang JW, Gwak SY, Shim GA, et al. EZH2 is associated with poor prognosis in head-and-neck squamous cell carcinoma via regulating the epithelial-to-mesenchymal transition and chemosensitivity. Oral Oncol. 2016;52: 66-74.

CHAPTER FOUR

OVEREXPRESSION OF ALDH1A2 IN THE TONGUE BASAL EPITHELIAL LAYER DURING ORAL SQUAMOUS CELL CARCINOMA CARCINOGENESIS

INTRODUCTION

Head and neck squamous cell carcinoma (HNSCC) is one of the most common human neoplasms worldwide, with an estimated 550,000 new cases and 300,000 deaths globally each year[1]. While treatment of primary tumors with radiation and/or surgery is often successful, high rates of second primary tumor (SPT) development and recurrence complicate treatment and contribute to an overall 5-year survival rate of ~55%[2]. In addition, despite recent advances in biology and medicine, there are currently few chemotherapeutic options of limited clinical efficacy available for the treatment of HNSCC[3]. It is therefore imperative that we further our understanding of HNSCC carcinogenesis at the molecular level in order to develop new and more efficacious strategies for prevention and therapy.

One of the major subtypes of HNSCC is oral cavity squamous cell carcinoma (OSCC), for which the primary etiological factors are long-term and excessive tobacco and/or alcohol use[4]. Repeated exposure to these carcinogens results in genetic, epigenetic, and metabolic changes to the epithelium of the oral cavity[5]. As these changes accumulate, the epithelium develops oral premalignant lesions and eventually, squamous cell carcinoma and metastatic cancer[2]. Another subtype of HNSCC is driven by human papilloma virus (HPV) infection; this subtype is comprised primarily of oropharyngeal cancers[4]. We are focused on non-HPV-related OSCC.

To date, retinoids – a group which includes the natural and synthetic derivatives of vitamin A (retinol) – are some of the best-studied agents in the treatment and prevention of SPT and recurrence in HNSCC[6]. The chemopreventive functions of retinoids are mediated through their binding to and subsequent activation of specific nuclear receptors, including the retinoic acid receptors (RARs) and retinoid X receptors (RXRs)[6]. Activation of RAR/RXRs by retinoids causes the dissociation of corepressors and the initiation of transcription of a wide assortment of target genes that control many critical cellular processes such as cellular proliferation, differentiation, and apoptosis[7]. Numerous studies have found that retinoids modulate cell differentiation and decrease proliferation of human HNSCC cells *in vitro*, and inhibit carcinogenesis in mouse models of OSCC [6, 8-10]. When tested in humans, retinoids were efficacious in suppressing oral premalignant lesions and SPTs in both HNSCC and lung cancer patients[6]. However, despite their considerable chemopreventive and chemotherapeutic success in preclinical and clinical trials, retinoids do not exhibit long-term efficacy in preventing oral cavity cancer when given orally as a single drug in Phase III clinical trials [11]. This paradoxical lack of clinical efficacy calls for greater research into the molecular mechanisms and pharmacology of retinoids in HNSCC, and investigation into novel retinoid therapy options[12, 13].

The most biologically-active derivative of retinol, all-*trans* retinoic acid (RA), is synthesized intracellularly primarily by aldehyde dehydrogenase 1a2 (ALDH1a2)[14-16]. Decreased ALDH1a2 expression has been observed in numerous cancers, including prostate cancer, ovarian cancer, and HNSCC[17-20]. Researchers found that restoration of ALDH1a2 expression via transfection in human prostate cancer cells impaired colony formation[18]. Conversely, in a xenograft model of HNSCC, ALDH1a2 knockdown resulted in accelerated tumor growth[21]. Clinically, high ALDH1a2 mRNA and protein expression correlated with better overall survival in breast cancer and HNSCC

patients[20, 22]. In our previous work, described in Chapter 2, we also found that overexpression of ALDH1a2 inhibited the proliferation and colony formation of several SCC cell lines (Figures 2.5, 2.6). Taken together, these data suggest that ALDH1a2 is a candidate tumor suppressor in the pathogenesis of several cancers, including HNSCC. However, the role of ALDH1a2 in HNSCC carcinogenesis has yet to be elucidated.

In this study we investigated the effects of ectopic ALDH1a2 expression on the development and progression of HNSCC *in vivo* during carcinogenesis. To this end, we generated a bitransgenic mouse (*K14-rtTA/TRE-ALDH1a2*) for the inducible and tissue-specific overexpression of ALDH1a2 in the basal layer of the tongue epithelium, as detailed in Chapter 3. Researchers in our lab have previously developed a murine model of OSCC in which the carcinogen 4-nitroquinoline 1-oxide (4-NQO) in drinking water is administered to mice over a period of 10 weeks[23]. The oral SCCs observed in this murine model are molecularly, histologically, and morphologically very similar to human SCCs[23]. Furthermore, research in our lab has shown that carcinogenesis in the 4-NQO model of OSCC is inhibited by treatment with exogenous retinoids[24, 25]. Therefore, this mouse carcinogenesis model is an ideal system in which to test the function of the RA-synthesizing enzyme ALDH1a2 during carcinogenesis. Herein, we describe the molecular and phenotypic effects of ectopic ALDH1a2 overexpression on 4-NQO-induced OSCC carcinogenesis.

MATERIALS AND METHODS

Animals and treatments

I used 8-12 week-old female mice in this experiment: 20 *K14-rtTA*$^{+/-}$*/TRE-ALDH1a2*$^{+/-}$ (*KRT/ALDH*) bitransgenic mice, and 20 littermate control mice positive for the *K14-rtTA*$^{+/-}$ (*KRT*) transgene only. Genotypes of all mice were determined by

PCR as previously described (Chapter 3). I maintained all mice under controlled conditions, with a daily 12 hour light/dark cycle and access to normal chow (Lab-diet with constant nutrition, Lab-Diet Co.). I treated 10 mice of each genotype (20 total) with 100 μg/mL 4-NQO (Sigma, St. Louis, MO, USA) and 2 mg/mL doxycycline (dox) in their drinking water for 10 weeks (4N+Dox). I treated the remaining 20 mice with 2 mg/mL dox and propylene glycol vehicle control (VC) for 10 weeks (VC+Dox). I prepared 4-NQO and dox fresh each week throughout the entire treatment, and changed the drinking water weekly. Following 10 weeks of 4-NQO treatment, all mice were switched to drinking water containing 2 mg/mL dox alone and monitored for cancerous lesion development and weight loss. Eleven weeks after the termination of the 4-NQO treatment, two 4N+Dox-treated mice had died, and many of the remaining mice exhibited weight loss and large, visible lesions on their tongues. Therefore, mice were sacrificed at this time. This end point (21 weeks) is 4 weeks earlier than our standard protocol because these mice exhibited an accelerated rate of 4-NQO-induced carcinogenesis compared to the mice in our previous studies[23, 26]. This difference in response to 4-NQO is likely due to the genetic background of the *KRT* and *KRT/ALDH* mice (50/50 C57Bl/6/FVB). A simplified schematic of the treatment protocol is shown in Figure 4.1A. All studies were carried out according to a protocol approved by the WCMC Institutional Animal Care and Use Committee (IACUC).

Tissue dissection, grading, and pathology

I sacrificed the mice by cervical dislocation, and tissues were dissected immediately. I photographed whole tongues and esophagi, counted gross visible lesions, and graded the lesions 0-5 in a blinded manner as previously described (0 indicating no lesions, and 5 being the most severe)[23, 26]. Tongues and esophagi were

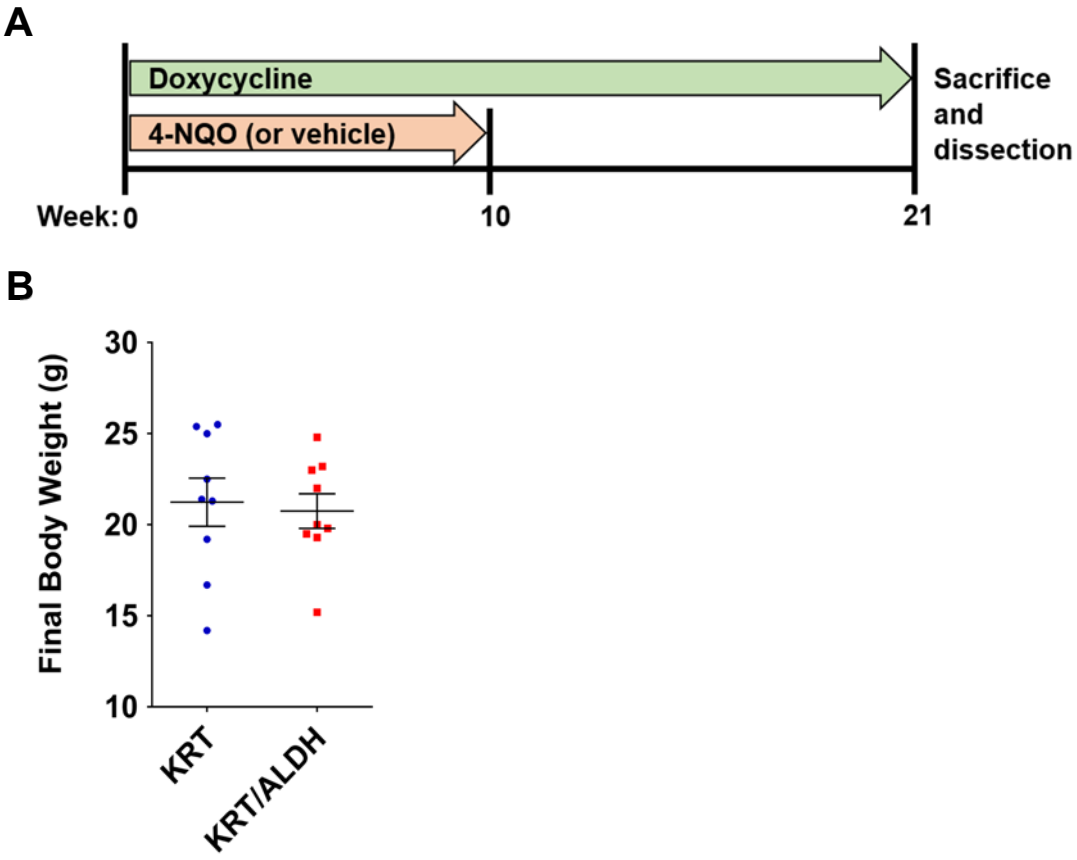

Figure 4.1: Experimental design of the 4-NQO treatment experiment. (A) A simplified diagram of the treatment protocol. A total of 40 mice were treated with doxycycline (dox; 2 mg/mL) plus 4-NQO (100 µg/mL) (4N+Dox) or dox plus vehicle control (VC+Dox) for 10 weeks. All mice were then switched to dox alone (2 mg/mL) until sacrifice at 21 weeks. At this point lesions were counted and graded, and tissues were harvested as described. (B) Final body weights of the 18 surviving 4N+Dox mice at the time of sacrifice. Error bars represent mean ±SEM. Analyses revealed no significant difference in final body weights between 4N+Dox *KRT* and *KRT/ALDH* mice.

cut in thirds longitudinally, and the middle third fixed in freshly-made 4% paraformaldehyde (in PBS) overnight at 4°C before tissue processing and paraffin embedding at the WCMC Electron Microscopy and Histology Core Facility. Sectioned tissue samples (cut to 7 µm) were stained with hematoxylin and eosin (H&E), and examined by pathologist Dr. Theresa Scognamiglio for squamous neoplasia. The lesions observed were classified as epithelial hyperplasia, dysplasia (mild, moderate,

or severe), carcinoma in situ, and squamous cell carcinoma, as previously described[23, 26]. The remaining two thirds of each tongue were snap-frozen in liquid nitrogen and stored at -80°C for long-term storage.

Immunohistochemistry

I analyzed protein expression by immunohistochemistry (IHC) as previously described[26, 27]. Paraffin-embedded sections were deparaffinized with Histo-Clear II (National Diagnostics, Atlanta, Georgia, USA), rehydrated using a graded series of ethanol, and antigen retrieval was performed using Antigen Unmasking Solution (Tris-based, Cat. No. H-3301, for ALDH1a2 primary antibody; citrate-based, Cat. No. H-3300, for all other antibodies; Vector Laboratories, Burlingame, CA) in a pressure cooker for 3 minutes. I then quenched endogenous peroxidase activity with 3% hydrogen peroxide diluted in methanol for 10 minutes, before blocking with 5% normal goat serum (Cat No. S-1000; Vector Laboratories) in PBS (for rabbit primary antibodies), 5% normal horse serum (Cat. No. S-2000; Vector Laboratories) in PBS (for goat primary antibodies), or mouse anti-IgG blocking reagent (Cat. No. MKB-2213; Vector Laboratories) (for mouse primary antibodies) for 30 minutes at room temperature. Sections were incubated with primary antibodies diluted in blocking solution overnight at 4°C (primary antibodies are described in Table 4.1). I used sections incubated without primary antibodies as negative controls. I utilized the secondary antibodies and staining reagents and protocols of the SuperPicture Polymer Detection Kit (Cat. No. 879263; Life Technologies) (for rabbit primary antibodies), ImmPRESS Reagent Kit (Cat. No. MP-7405; Vector Laboratories) (for goat primary antibodies), or Mouse on Mouse (MOM) Detection Kit (Cat. No. MKB-2213; Vector Laboratories) (for mouse primary antibodies).

To quantify IHC staining, I utilized ImageJ software (National Institutes of Health) to detect positive area (brown stain). I used a protocol adapted from "Basic Intensity Quantification with ImageJ" (University of Chicago; available online at: https://www.unige.ch/medecine/bioimaging/files/1914/1208/6000/Quantification.pdf). Mean pixel intensity was normalized to the minimum detectable staining intensity of each stained set of slides.

Table 4.1: Primary antibodies
PC = polyclonal antibody; MC = monoclonal antibody
ǂ A custom anti-ALDH1a2 antibody was generated for our lab by Alpha Diagnostics

Target	Company	Catalog #	Lot #	Source	Dilution
ALDH1a2	Alpha Diagnostics	N/A ǂ	Batch #4	Rabbit PC	1:200
β-Actin	Millipore	MAB1501	2665057	Mouse MC	1:80,000
CRABP2	Santa Cruz	sc-10065	A2813	Goat PC	1:100
EZH2	Cell Signaling	5246S	7	Rabbit PC	1:200
K14	Novocastra Laboratories	NCL-002	N/A	Mouse MC	1:100
Vimentin	Santa Cruz	sc-7557	H1514	Goat PC	1:200

RNA isolation and RT-PCR analysis

Snap-frozen tissue was homogenized in 1 mL TRIzol Reagent (Cat. No. 15596018; Ambion, Thermo Fisher Scientific Inc.) for RNA extraction following the manufacturer's protocol. Total RNA was quantified using a NanoDrop 2000C (Thermo Fisher, Scientific, Inc.), and 1 µg RNA was reverse transcribed using the qScript cDNA Supermix (Cat. No. 95048; Quanta Biosciences). Resulting cDNA was diluted 1:10, and 2 µL used as template for semi-quantitative RT-PCR (SQ-PCR) as previously described[28]. All primers used are listed in Table 4.2. I detected transgenic ALDH1a2 transcript using the ALDH1a2 forward primer and a reverse primer specific to the β-globin poly-A region of the transgenic cassette (Table 4.2).

Table 4.2: Primer sequences used for RT-PCR
ǂ Primer complementary to transgenic β-globin poly-A sequence

Gene	Forward Primer (5'-3')	Reverse Primer (5'-3')	Product Size
ALDH1a2	gacttgtagcagctgtcttcact	tcacccatttctctcccatttcc	160 bp
ALDH1a2 TG	gacttgtagcagctgtcttcact	tgctcaaggggcttcatgatgtcc[ǂ]	467 bp
rtTA	tacactgggctgcgtattgg	ccgctttcgcactttagctg	198 bp
36B4	agaacaacccagctctggagaaa	acaccctcccagaaagcgagagt	448 bp

Western blot analysis

I homogenized snap-frozen tissues in final sample buffer (0.5 M Tris–HCl, pH 6.8, 10% glycerol and 1% SDS) containing protease inhibitors (cOmplete Mini Protease Inhibitor Cocktail Tablets, Cat. No. 11836153001; Roche). Samples were boiled before quantification of total protein using the *DC* Protein Assay (Cat. No. 500-0112; Bio-Rad). I separated 25 µg total protein on SDS-PAGE gels and transferred protein onto nitrocellulose membranes as previously described[27]. After blocking membranes in 5% skim milk in Tris-buffered saline containing 0.1% TWEEN 20 (Cat. No. P1379; Bio-Rad) (TBST) for 1 hour at room temperature, I incubated with primary antibodies overnight at 4ºC. Primary antibodies are described in Table 4.1. I then washed the membranes with TBST and incubated with appropriate secondary antibody for 1 hour at room temperature. Following a TBST wash, I developed membranes using the Pierce ECL Substrate Kit (Cat. No. 32106; Pierce) and a quantitative gel imaging station (Bio-Rad ChemiDoc System). I utilized ImageLab software to record and analyze membrane chemiluminescence.

Statistical analysis of the data

I used GraphPad Prism 6.0 software for statistical analyses of the results. To compare two independent groups, I determined the means ± S.E.M. or ± S.D. (as

indicated) and utilized the Student's *t*-test. Differences with a $p < 0.05$ were considered statistically significant.

RESULTS

Oral cavity carcinogenesis after 4-NQO treatment

All mice survived the 10-week 4-NQO treatment, consistent with our previous studies[23, 24, 26]. To confirm that transgenic (TG) ALDH1a2 was being induced during this phase of treatment, we took ear snips from each 4N+Dox mouse at the 10-week time point, isolated RNA, and performed RT-PCR analysis for TG ALDH1a2 transcripts. We detected TG ALDH1a2 transcripts in *KRT/ALDH* mice, indicating that co-treatment with 4-NQO did not interfere with our dox-inducible system in this tissue (Supplemental Figure 4.1). No TG ALDH1a2 was detected in 4N+Dox *KRT* mice (Supplemental Figure 4.1).

We elected to use dox-treated *KRT* mice as the control group in our experiments rather than untreated *KRT/ALDH* mice for several reasons. First, this strategy controls for any off-target effects of long term low-dose doxycycline (2 mg/mL for 21 weeks). In addition, unlike untreated *KRT/ALDH* mice, there is no risk of ectopic ALDH1a2 expression in *KRT* mice due to the inherent leakiness of Tet-On systems. The use of dox-treated *KRT* mice as a control in Tet-On transgenic mouse experiments is well-documented and this strategy was employed in the original research on *KRT* mice conducted by Nguyen, *et al*[29].

We observed the development of multifocal precancerous and cancerous lesions, primarily on the dorsal side of the tongue, in both *KRT* and *KRT/ALDH* mice during the weeks following 4N+Dox treatment. By 11 weeks post-treatment, 10% of the 4N+Dox-treated mice had died (2/20; n=1 *KRT* and n=1 *KRT/ALDH*), and many

mice had large visible tongue lesions, so the mice were sacrificed at this time (Figure 4.1A). The body weights of the surviving 4N+Dox-treated *KRT* and *KRT/ALDH* mice did not differ from each other at the time of sacrifice (Figure 4.1B).

RESULTS PART I: MOLECULAR CHANGES

Endogenous ALDH1a2 expression is decreased in 4-NQO-treated mice

ALDH1a2 expression is reduced in HNSCC patients and in human HNSCC cell lines (as discussed in Chapter 2 (Figures 2.1, 2.2)). We therefore investigated whether endogenous ALDH1a2 expression is also reduced in the 4-NQO murine model of OSCC carcinogenesis following carcinogen treatment. By western blot analysis of *KRT* mice we observed a ~2.4-fold decrease in ALDH1a2 protein levels in 4N+Dox mice as compared to VC (vehicle control)+Dox mice (Figure 4.2A). This result is in accord with our previous data on ALDH1a2 mRNA levels published in Tang *et al*., 2014; Tang *et al.* assessed genome-wide transcript levels in normal mouse tongues and tongue SCCs induced by 4-NQO using Next-Generation Sequencing (RNA-Seq) analysis[25]. These data are now freely accessible in the Gene Expression Omnibus (GEO) database (accession no. GSE54246). These data show that endogenous ALDH1a2 transcript levels are decreased by approximately 62% in tongue SCCs induced by 4-NQO as compared to normal mouse tongue samples (Figure 4.2B). We therefore conclude that endogenous ALDH1a2 mRNA and protein expression is decreased during carcinogenesis in the 4-NQO mouse model of OSCC.

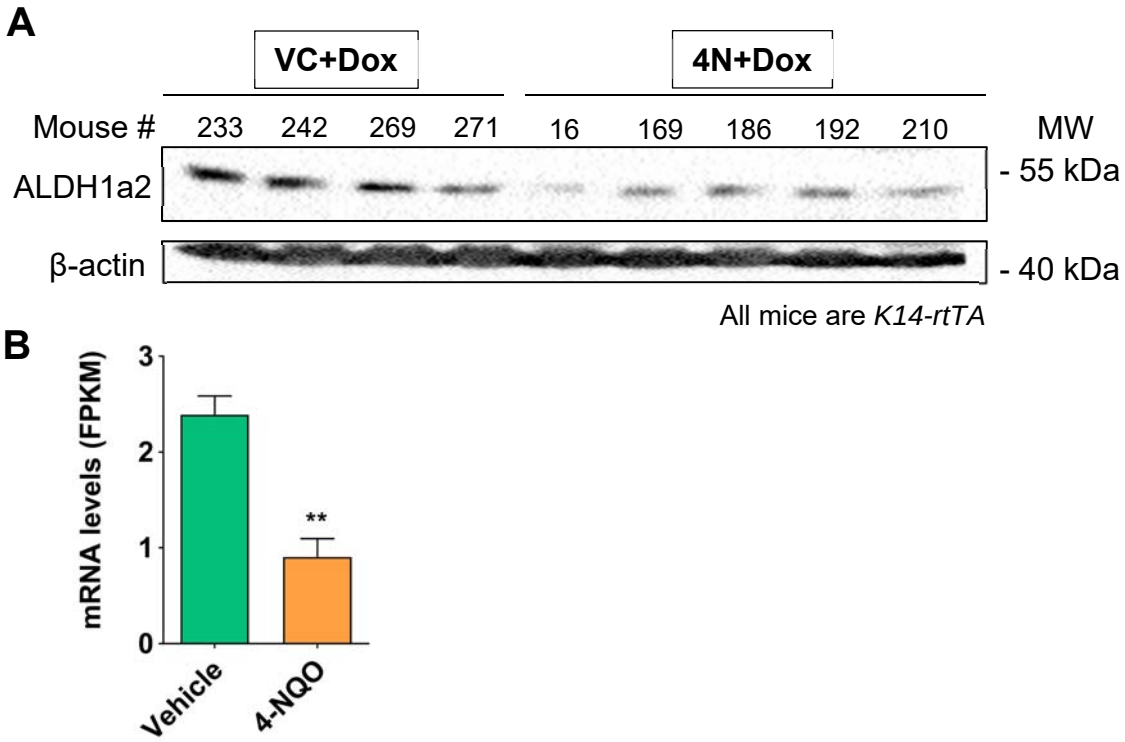

Figure 4.2: Endogenous ALDH1a2 expression is decreased in mouse tongues during carcinogenesis in the 4-NQO murine model of OSCC. (A) Western blot analysis of tongues of *KRT* mice treated with VC+Dox (n=4 shown) or 4N+Dox (n=5 shown). We treated mice as described (Figure 4.1). Tongues were snap frozen in liquid nitrogen before homogenization in final sample buffer. We incubated membranes with 1:100 ALDH1a2 primary antibody and 1:80,000 β-actin (loading control) (primary antibodies are detailed in Table 4.1). (B) Quantitative analysis of ALDH1a2 transcripts from RNA-Seq data obtained by Tang *et al*., 2014. These data are freely accessible in the Gene Expression Omnibus (GEO) database (accession no. GSE54246). FPKM, fragments per kilobase of exon model per million mapped reads. The data was analyzed using a Student's *t*-test; ∗∗ indicates $p<0.01$

Transgenic ALDH1a2 transcript expression in KRT/ALDH mice following treatment with VC+Dox or 4N+Dox

We utilized RT-PCR to verify the transcript expression of TG ALDH1a2 in tongues from *KRT/ALDH* mice following treatment. We detected TG ALDH1a2 transcripts in both VC+Dox and 4N+Dox *KRT/ALDH* mice, but not in littermate *KRT* mice (Figure 4.3A,B). Interestingly, while we were able to detect TG ALDH1a2 transcripts in all of the *KRT/ALDH* mice, the level of transcript expression was

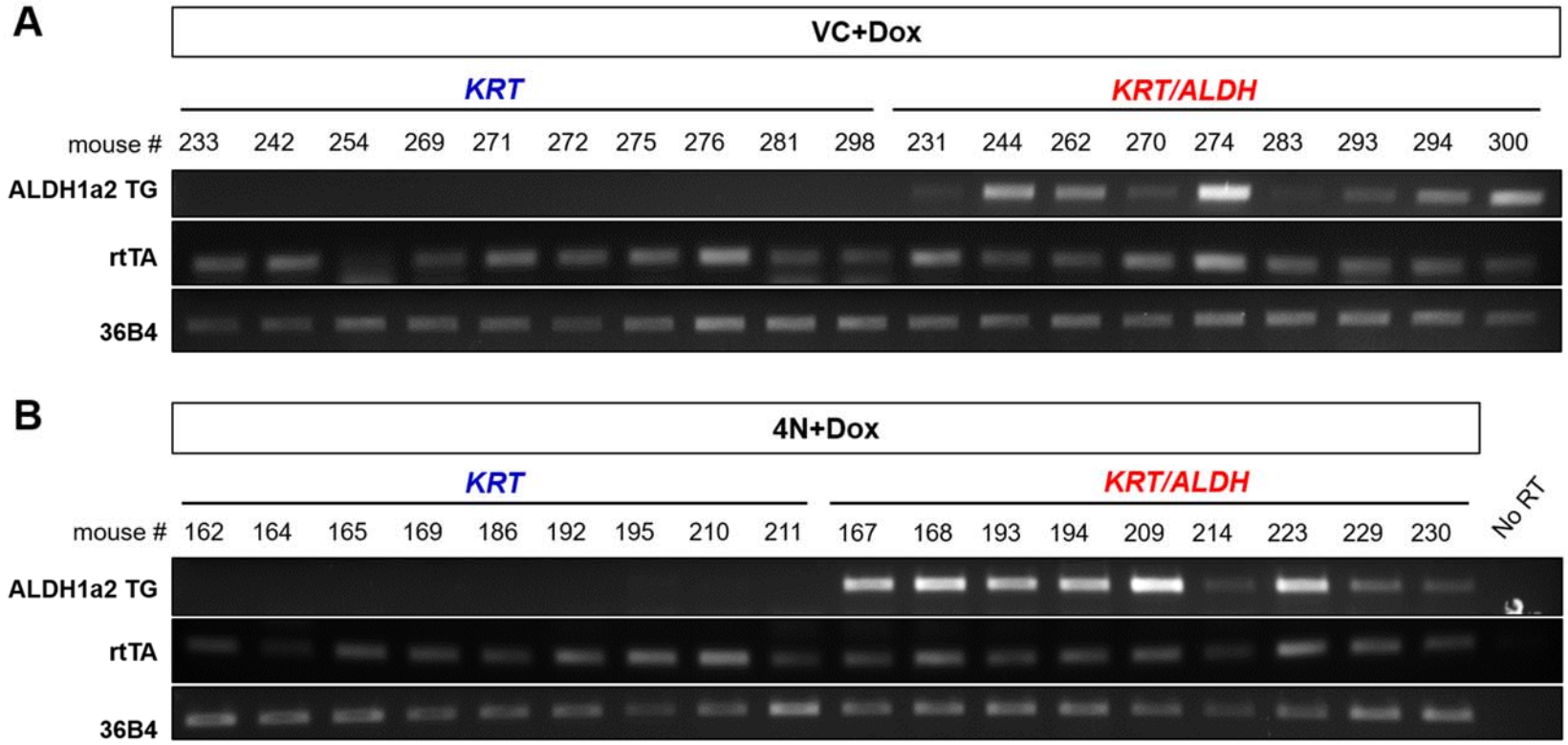

Figure 4.3: Analysis of exogenous, transgenic ALDH1a2 transcript induction in the tongues of *KRT* and *KRT/ALDH* mice at 21 weeks (see Figure 4.1). *KRT* and *KRT/ALDH* mice were treated with dox (2 mg/mL) plus vehicle control (VC+Dox) or dox plus 4-NQO (100 µg/ml) (4N+Dox) as described. Tongue samples were dissected immediately following sacrifice, and snap frozen before RNA isolation. We analyzed levels of transgenic ALDH1a2 (ALDH1a2 TG) and rtTA using primers as described in Table 4.2. 36B4 was used as a loading control. (A) RT-PCR analysis of n=10 *KRT* and n=9 *KRT/ALDH* mice treated with VC+Dox. (B) RT-PCR analysis of n=9 *KRT* and n=9 *KRT/ALDH* mice treated with 4N+Dox. All primer sequences are provided in Table 4.1.

variable; some *KRT/ALDH* mice exhibited low expression of TG ALDH1a2 transcript (ALDH1a2^{low}; n=7 total, n=4 VC+Dox and n=3 4N+Dox), while some exhibited high expression of TG ALDH1a2 (ALDH1a2^{high}; n=11 total, n=5 VC+Dox and n=6 4N+Dox) (Table 4.3). We quantitated the RT-PCR bands and showed that TG ALDH1a2 transcript levels are on average approximately 4.4-fold higher in ALDH1a2^{high} mice than in ALDH1a2^{low} mice (Supplemental Figure 4.2). In contrast, rtTA transcript levels were relatively constant across the entire cohort of mice, independent of treatment or genotype (Figure 4.3A, second row). We also observed variations in TG ALDH1a2 transcript expression in ear samples taken from 4N+Dox *KRT/ALDH* mice after 10 weeks of 4-NQO treatment, suggesting that this effect is not confined to tongues or to the 24-week end point (Supplemental Figure 4.1).

Table 4.3: Relative ALDH1a2 expression in *KRT/ALDH* mice.

	KRT/ALDH	
	ALDH1a2^{low}	**ALDH1a2^{high}**
VC+Dox	231, 283, 293	244, 262, 270, 274, 294, 300
4N+Dox	214, 229, 230	167, 168, 193, 194, 209, 223

Note: ALDH1a2^{low} and ALDH1a2^{high} designations applied to each *KRT/ALDH* mouse based on the data shown in Figures 4.3, 4.4.

ALDH1a2 protein levels after treatment with VC+Dox or 4N+Dox

We used immunohistochemistry (IHC) to evaluate total (endogenous + TG) ALDH1a2 protein levels in the tongue epithelia at 21 weeks (see Figure 4.1A). We detected dark brown staining for ALDH1a2 protein in the tongue epithelia of VC+Dox and 4N+Dox *KRT/ALDH* mice but not in the epithelia of VC+Dox and 4N+Dox *KRT* mice (Figure 4.4A-C). Consistent with the RT-PCR data in Figure 4.3A, we observed variations in the levels of total ALDH1a2 protein in VC+Dox and 4N+Dox

KRT/ALDH mice, and these staining results were used to confirm the ALDH1a2^{high} and ALDH1a2^{low} designations applied to each *KRT/ALDH* mouse in Table 4.3. ALDH1a2^{high} *KRT/ALDH* mice exhibited large regions of dark brown staining for ALDH1a2 protein, while ALDH1a2^{low} mice showed scattered ALDH1a2-positive cells (Figure 4.4B,C) (additional images of ALDH1a2 protein expression in ALDH1a2^{high} *KRT/ALDH* tongue epithelia are shown in Figure 4.5 and Supplemental Figure 4.3). Both the VC+Dox and 4N+Dox groups of *KRT/ALDH* mice exhibited variations in the levels of ALDH1a2 mRNA and protein expression; therefore, this variation is independent of 4-NQO treatment.

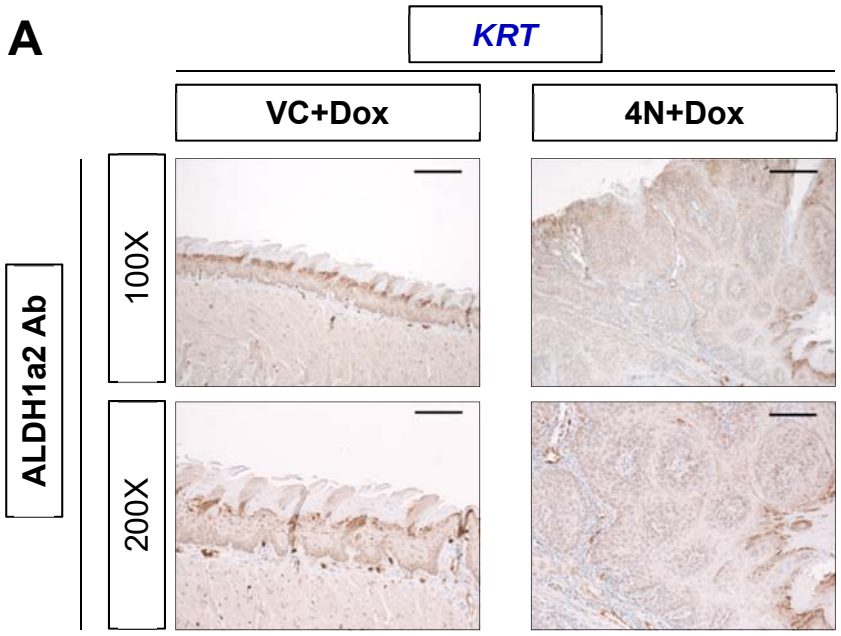

Figure 4.4: Expression of endogenous ALDH1a2 protein in tongues of *KRT* mice and endogenous plus exogenous (TG) ALDH1a2 protein in tongues of *KRT/ALDH* mice treated with VC+Dox or 4N+Dox. Tongues were fixed, embedded, sectioned, and stained with anti-ALDH1a2 (1:200; antibody details provided in Table 4.1). (A) ALDH1a2 staining of VC+Dox and 4N+Dox *KRT* control mice. Images were taken at 100X and 200X, scale bar represents 200µm and 100µm, respectively. We analyzed one tongue section per mouse (n=19 *KRT*). The fields shown are representative of n ≥6 fields taken of each section. Left column: mouse #254; right column: mouse #195. (B,C) Pictured on the following page.

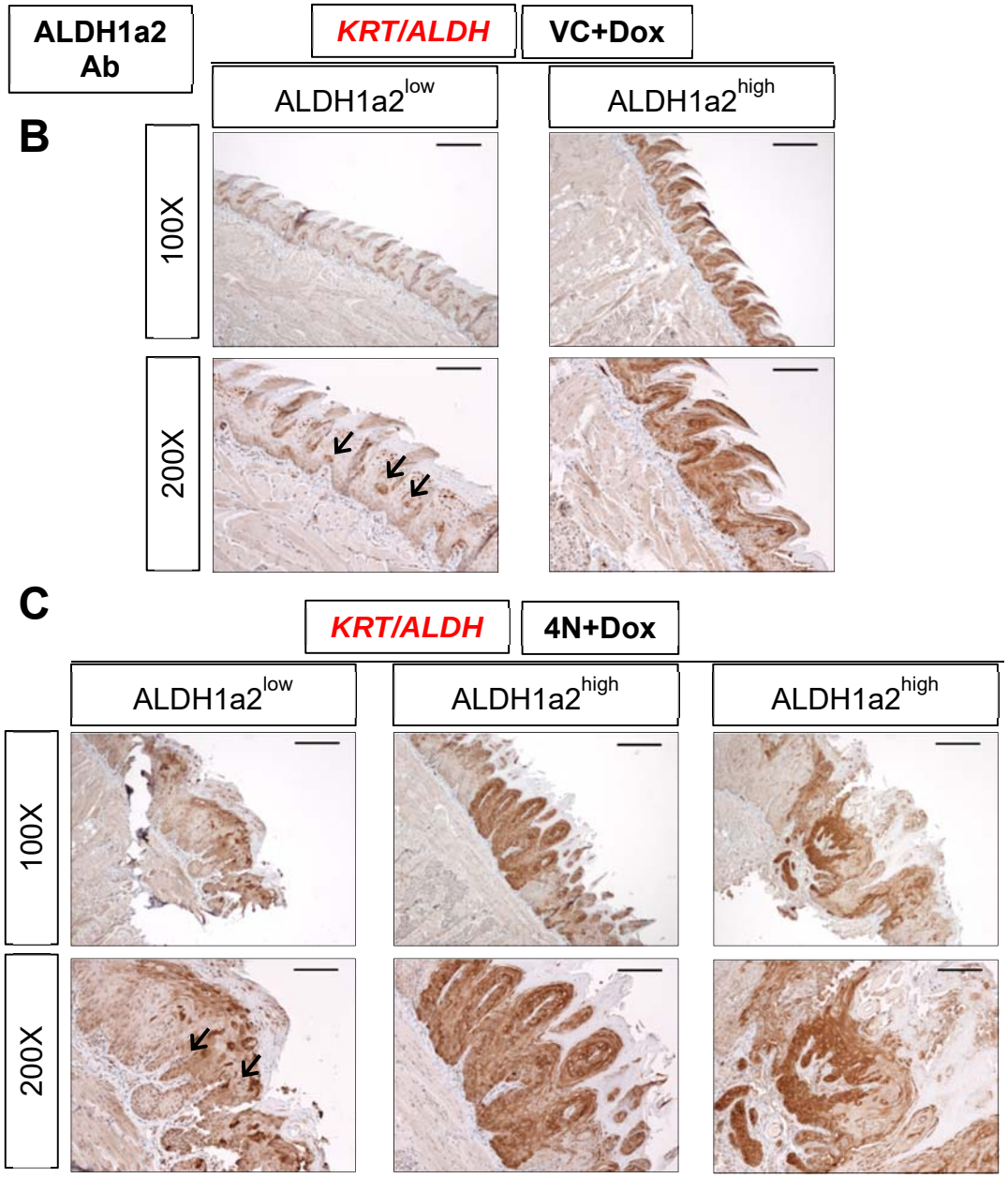

Figure 4.4 (continued): (B) ALDH1a2 staining of VC+Dox *KRT/ALDH* mice. Left column: mouse #231; right column: mouse #274. (C) ALDH1a2 staining of 4N+Dox *KRT/ALDH* mice. Two different 4N+Dox ALDH1a2^{high} *KRT/ALDH* mice are shown to convey some of the different staining patterns we observed. Left column: mouse #214; middle column: mouse #167; right column: mouse #223. Images were taken at 100X and 200X, scale bar represents 200µm and 100µm, respectively. We analyzed one tongue section per mouse (n=18 total *KRT/ALDH*). The fields shown are representative of n ≥6 fields taken of each section. *KRT/ALDH* mice were sorted into ALDH1a2^{high} and ALDH1a2^{low} groups based on the results in (B) and (C) in conjunction with RT-PCR results as shown in Figure 4.3A (Table 4.3).

ALDH1a2 protein in tongue epithelia of VC+Dox and 4N+Dox ALDH1a2^{high} *KRT/ALDH* mice was not homogeneous in its distribution. Regions of dark brown staining directly adjoin regions of no detectable staining in both treatment groups (Figure 4.4B,C). This effect is more pronounced in 4N+Dox ALDH1a2^{high} *KRT/ALDH* mice; at 200X magnification, it is possible to find fields in the tongue epithelia of some 4N+Dox ALDH1a2^{high} *KRT/ALDH* mice with no dark brown staining for ALDH1a2. We did not observe any 200X fields of VC+Dox ALDH1a2^{high} *KRT/ALDH* tongue epithelia without any dark brown staining for ALDH1a2. In total, these data on ALDH1a2 mRNA and protein levels illustrate that there is notable variation in ALDH1a2 expression between *KRT/ALDH* mice in each treatment group, as well as within each ALDH1a2-positive tongue epithelium.

Endogenous K14 Expression in VC+Dox and 4N+Dox KRT and KRT/ALDH mice

Endogenous cytokeratin 14 (K14) is a type II intermediate filament protein normally expressed in the basal layer of the squamous epithelium[30]. Numerous studies have found that the expression of K14 and other keratins is altered upon malignant transformation of human epithelial cells[31, 32]. Chu *et al*. observed high K14 expression throughout the epithelium in the vast majority (>90%) of cases of human SCC, regardless of the grade of differentiation or site of origin[33]. Previous research conducted in our lab by Tang *et al*. revealed that K14 exhibits altered expression in the tongue epithelia of 4-NQO-treated mice[23]. While K14 is normally expressed only in the basal epithelial layer, he observed that K14 is expressed in the suprabasal layers in addition to the basal layer of the tongue after 4-NQO treatment[23].

We used IHC to stain for endogenous K14 protein in tongue sections of VC+Dox and 4N+Dox *KRT* and *KRT/ALDH* mice. In our Tet-On transgenic mouse system, rtTA expression is driven by a truncated human K14 promoter (Figure 3.1).

Therefore the expression pattern of endogenous K14 would inform us as to the probable localization of rtTA in the tongue epithelia of *KRT* and *KRT/ALDH* transgenic mice. We observed that K14 is expressed only in the epithelial basal layer in the tongues of VC+Dox mice (Figure 4.5A(i), A(v)). In the tongue epithelia of 4N+Dox mice with dysplasia and SCC, we observed K14 expression in the suprabasal layers in addition to the basal layer of the tongue epithelium (Figure 4.5A(ii-iv), A(vi-viii)). In addition, some adjacent, quasi-normal fields of tongues from 4N+Dox mice did exhibit basal layer-only expression of K14 (Figure 4.5A(ii), data not shown). We did not observe any difference in K14 staining between *KRT* and *KRT/ALDH* mice. In total, these results are consistent with the K14 staining patterns in 4-NQO-treated mice previously reported by Tang *et al*.

We compared the expression pattern of K14 protein to the expression pattern of ALDH1a2 protein in *KRT/ALDH* mice by staining adjacent tongue sections for ALDH1a2 (Figure 4.5B). Consistent with the results presented in Figure 4.4C, we observed regions with high and low total ALDH1a2 protein expression within the tongue epithelia of 4N+Dox *KRT/ALDH* mice (presence or absence of dark brown stain; Figure 4.5B). However, in adjacent sections stained for K14, there were no fields of the tongue epithelium without brown staining for K14 (Figure 4.5A(vi-viii)). This result suggests that endogenous K14 and exogenous (TG) ALDH1a2 are differentially expressed in bitransgenic *KRT/ALDH* mice.

Effect of exogenous TG ALDH1a2 expression on the extent of EZH2 expression in tongue epithelia after treatment with VC+Dox or 4N+Dox

In the experiments presented in Chapter 3 we observed that inducing ectopic ALDH1a2 reduced EZH2 protein levels in the tongue epithelium (Figure 3.7). EZH2 is a methyltransferase that carries out the trimethylation of lysine 27 and lysine 9 of

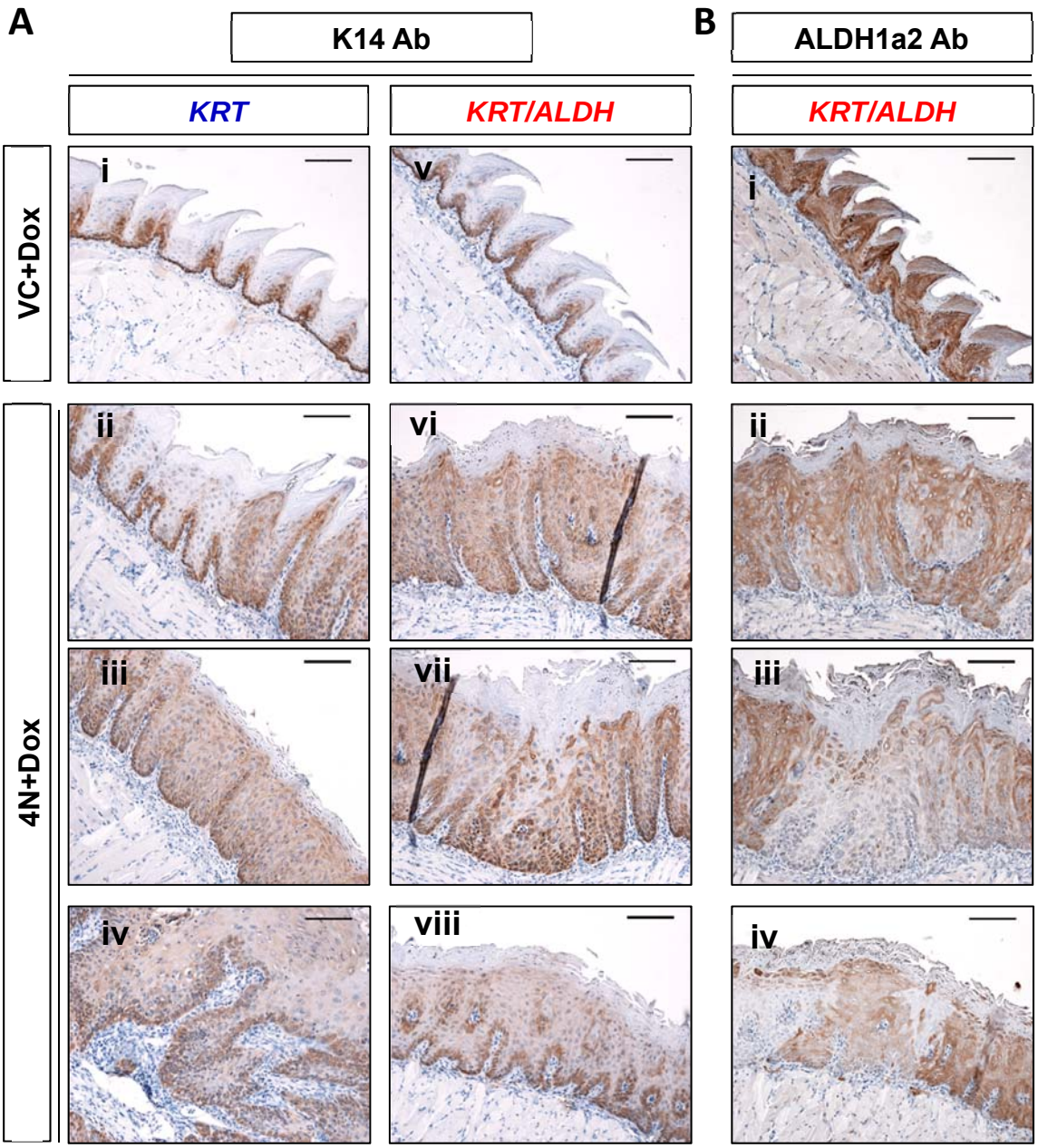

Figure 4.5: Cytokeratin 14 (K14) protein expression in VC+Dox and 4N+Dox *KRT* and *KRT/ALDH* mice. Mice were treated with dox (2 mg/mL) plus 4-NQO (100 µg/ml) (4N+Dox) or dox plus vehicle control (VC+Dox) as described. Tongues were fixed, embedded, sectioned, and stained with 1:100 anti-K14 or 1:200 anti-ALDH1a2 (primary antibody details provided in Table 4.2). (A) K14 staining in tongues from *KRT* mice (i-iv) and *KRT/ALDH* mice (v-viii). (B) ALDH1a2 staining in matched, adjacent sections of tongues from the *KRT/ALDH* mice shown in A(v-viii). Mouse number and pathology are as follows: A(i) #275, normal; A(ii,iii) #169, moderate to severe dysplasia; A(iv) #210, invasive SCC; A(v) & B(i) #262, normal; A(vi,vii) & B(ii,iii) #194, moderate to severe dysplasia; A(viii) & B(iv) #193, superficially invasive SCC. All fields are representative of n≥8 fields analyzed per tongue section. We analyzed n=4 mice per group.

histone 3 (H3K27me3, H3K9me3) and functions as a transcriptional regulator as a part of the Polycomb repressive complex 2 (PRC2)[34]. EZH2 is overexpressed in numerous cancers, including HNSCC, and has emerged as a potential therapeutic target[35, 36]. We used IHC to stain for EZH2-positive cells in the tongue epithelia of VC+Dox and 4N+Dox *KRT* and *KRT/ALDH* mice. We then used ImageJ software (National Institutes of Health) to quantify the percent of the basal and suprabasal layers of the tongue epithelium that stained positive for EZH2. Compared to the VC+Dox mice, the 4N+Dox mice exhibited more cells that stained for EZH2 protein in the tongue epithelia (in terms of percent positive area; Figure 4.6A,B,C). There was a trend towards increased EZH2 staining as the histopathology becomes more severe (Figure 4.6B). In addition, total EZH2 staining was decreased by approximately 13% in 4N+Dox ALDH1a2^{high} *KRT/ALDH* mice compared to 4N+Dox *KRT* mice (p=0.0408; Figure 4.6C). This result suggests that exogenous ALDH1a2 expression during 4-NQO-induced oral cavity carcinogenesis reduces the number of EZH2-positive cells in the tongue epithelium.

TG ALDH1a2^{high} inversely correlates with vimentin expression in 4-NQO-treated mice

Vimentin is a type III intermediate filament protein expressed by mesenchymal cells, and is well-characterized as a marker of epithelial-mesenchymal transition (EMT)[37]. Numerous studies of human epithelial carcinomas (including breast cancer, prostate cancer, and HNSCC) have found that vimentin expression correlates with tumor invasion and poor prognosis[38]. In studies of HNSCC, decreased ALDH1a2 activity or expression was correlated with increased expression of vimentin both in tumor cells *in vitro*, and in tumors in xenograft experiments *in vivo*[21]. We therefore investigated whether this inverse relationship is observed when TG ALDH1a2 is overexpressed in 4N+Dox *KRT/ALDH* mice. Using IHC, we evaluated vimentin

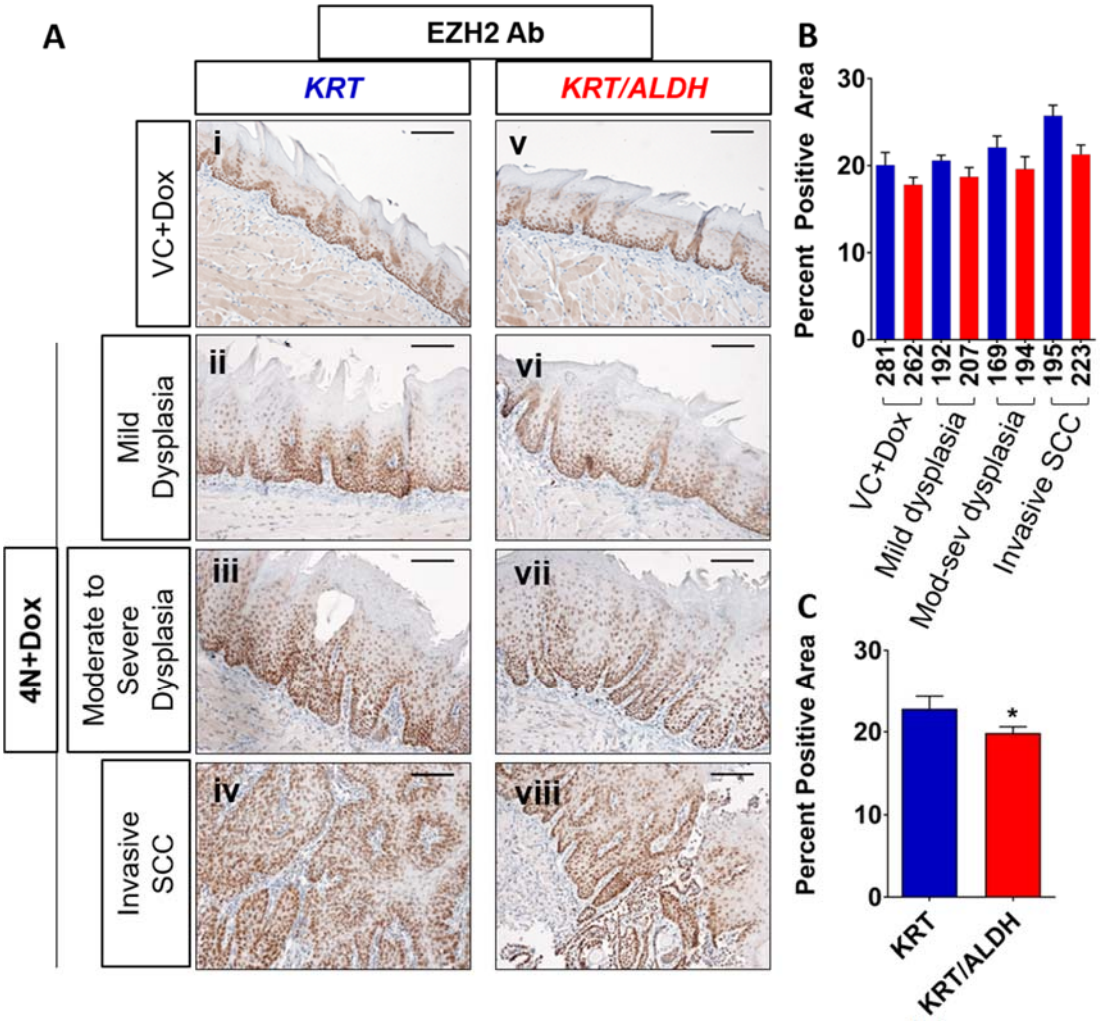

Figure 4.6: EZH2 protein in tongue epithelia of *KRT* and ALDH1a2^{high} *KRT/ALDH* mice following treatment. Mice were treated with dox plus 4-NQO (4N+Dox) or dox plus vehicle control (VC+Dox) in the drinking water as described. Tongues were fixed, embedded, sectioned, and stained with anti-EZH2 (1:200; antibody details provided in Table 4.2). We stained one section per mouse, and images shown are representative of n≥10 fields imaged per section (A). In total, we stained sections from n=8 *KRT* mice and n=9 *KRT/ALDH* mice. (i-iv) EZH2 staining of n=4 *KRT* mouse tongues. (v-viii) EZH2 staining of n=4 *KRT/ALDH* mouse tongues. Mice were treated as indicated. Each row of images represents two mice of an equivalent pathologic grade and treatment. Mouse number and pathology are as follows: (i,v) #281, 262, normal; (ii,vi) #192, 207, mild dysplasia; (iii,vii) #169, 194, moderate to severe dysplasia; (iv,viii) #195, 223, invasive SCC. All of the *KRT/ALDH* mice pictured are ALDH1a2^{high}. All images taken at 200X, scale bar represents 100 µm. (B,C) Quantification of the percent area of the tongue epithelium that stained positive for EZH2 protein. Positive area was quantified using ImageJ software (National Institutes of Health) and plotted as a percentage of the total tongue epithelium area present in each field. (B) Mean percent positive area of each 4N+Dox mouse pictured in (A). Bars represent the mean±SEM of 4 separate fields analyzed per mouse. (C) Mean percent positive area of 4N+Dox *KRT* and *KRT/ALDH* mice represented in (ii-iv) and (vi-viii). Bars represent the mean±SEM of 4 separate fields analyzed per mouse, n=3 mice analyzed per group.

protein expression in tongues of 4N+Dox *KRT* and ALDH1a2^{high} *KRT/ALDH* mice of various histopathologic grades (Figure 4.7A). Because vimentin expression is low in the normal squamous epithelium and is increased in SCC (especially invasive SCC), we stained the tongue sections from the mice of each group that presented with the most advanced histopathology and grade (n=4 *KRT*, n=4 *KRT/ALDH*: n=1 *KRT/ALDH* ALDH1a2^{low} and n=3 *KRT/ALDH* ALDH1a2^{high})[38]. We then used ImageJ software to analyze the intensity of the stain and the percent of each field that stained positively for vimentin. We found that 4N+Dox *KRT* tongues had more staining for vimentin protein (approx. 2.5-fold more positive area, p=0.0073; approx. 1.14-fold greater average stain intensity, p=0.0223) compared to those from 4N+Dox ALDH1a2^{high} *KRT/ALDH* mice (Figure 4.7B,C,D,E). We also observed that the n=1 ALDH1a2^{low} *KRT/ALDH* mouse had higher vimentin protein expression than the n=3 ALDH1a2^{high} *KRT/ALDH* mice (both area and intensity of stain; Figure 4.7A,B,C). These data indicate that higher TG ALDH1a2 in 4N+Dox-treated mice results in reduced vimentin expression, and support an inverse relationship between ALDH1a2 and vimentin in HNSCC.

DISCUSSION PART I: MOLECULAR CHANGES

Aberrant expression of key members of the RA signaling pathway is frequently observed during HNSCC carcinogenesis[7, 39]. ALDH1a2, an enzyme that synthesizes intracellular RA, is decreased at both the mRNA and protein levels in human HNSCC patients and cell lines (Chapter 2, Figures 2.1, 2.2)[20]. In addition, we found that endogenous ALDH1a2 mRNA and protein levels are reduced in 4-NQO-treated mice compared to mice treated with vehicle control (Figure 4.2). Other members of the RA signaling pathway that exhibit reduced mRNA and protein levels in HNSCC include lecithin:retinol acyltransferase (LRAT), CRABP2, RARβ, and RARγ[40-44]. Conversely,

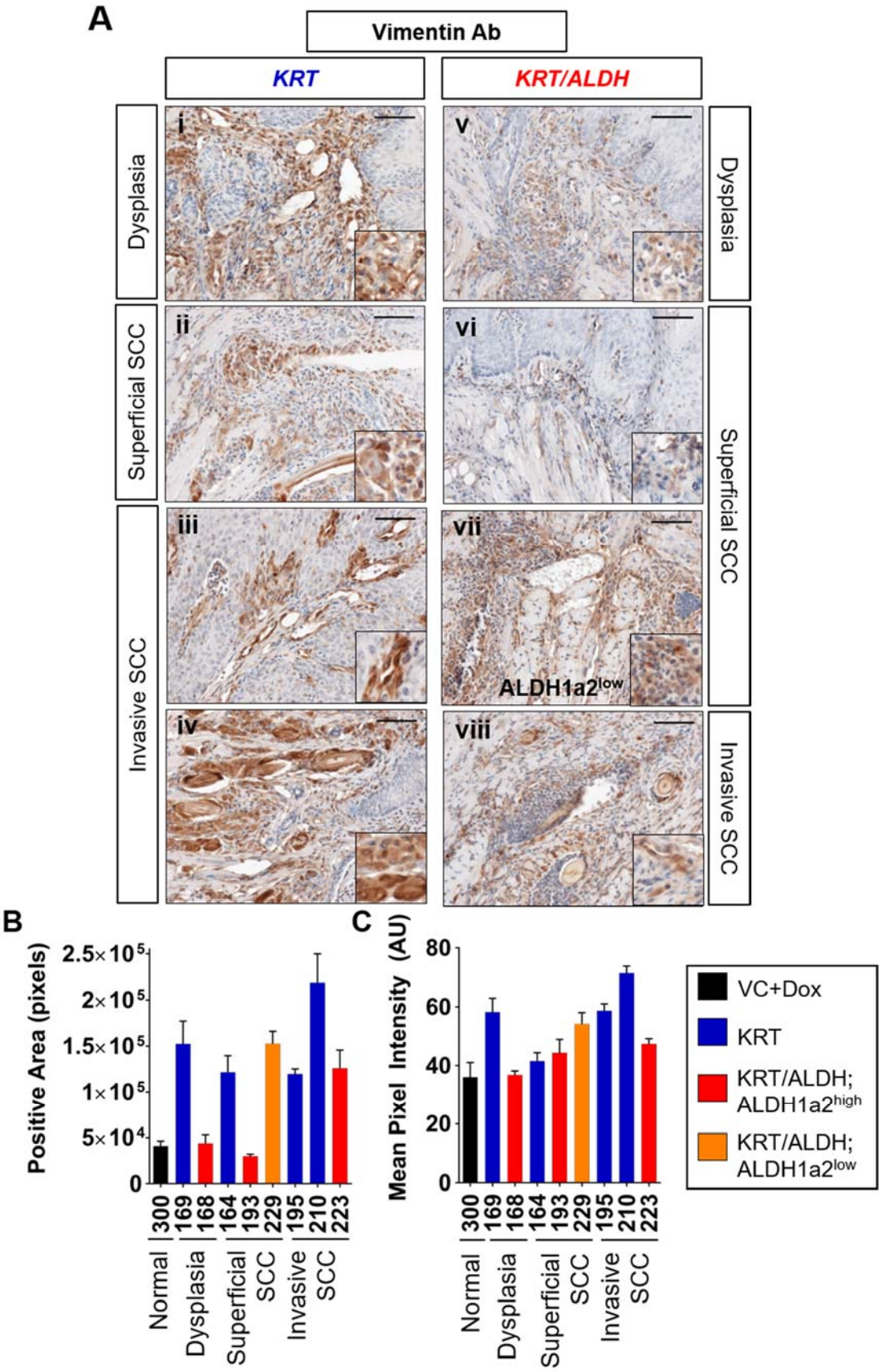
A
Vimentin Ab
KRT
KRT/ALDH
Dysplasia
Superficial SCC
Invasive SCC
i
ii
iii
iv
v
vi
vii
viii
ALDH1a2low
B
Positive Area (pixels)
2.5×10^5
2×10^5
1.5×10^5
1×10^5
5×10^4
0
300 169 168 164 193 229 195 210 223
Normal
Dysplasia
Superficial SCC
Invasive SCC
C
Mean Pixel Intensity (AU)
80
60
40
20
0
VC+Dox
KRT
KRT/ALDH; ALDH1a2high
KRT/ALDH; ALDH1a2low

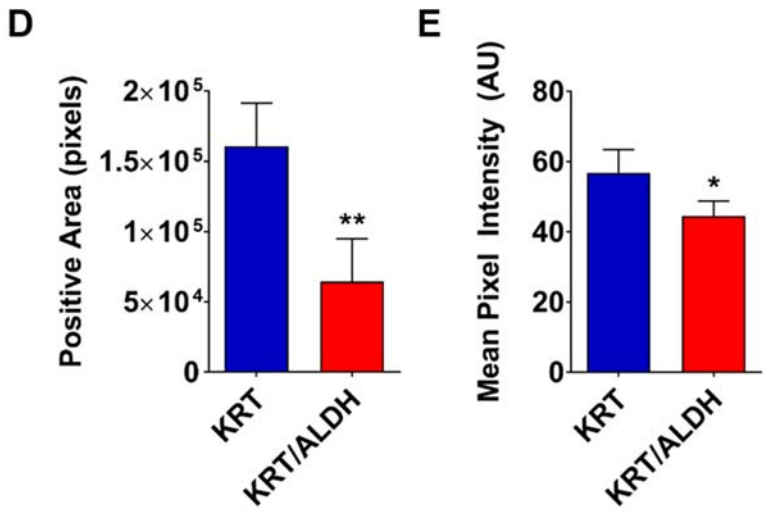

Figure 4.7: Vimentin expression is decreased in 4N+Dox ALDH1a2^{high} *KRT/ALDH* mice. *KRT* and *KRT/ALDH* mice were treated with dox (2 mg/mL) and 4-NQO (100 μg/ml) (4N+Dox) in drinking water for 10 weeks and then maintained on dox alone before sacrifice at 21 weeks (Figure 4.1A). Tongues were fixed, embedded, sectioned, and stained with anti-Vimentin (1:200; antibody details provided in Table 4.2). We stained tongue sections from the n=8 mice that presented with the most severe pathologies. We stained one section per mouse, and images shown are representative of n≥10 fields imaged per section (A). (a-d) Vimentin staining of n=4 4-NQO-treated *KRT* mouse tongues. (e-h) Vimentin staining of n=4 4-NQO-treated *KRT/ALDH* mouse tongues. Each mouse is pictured next to to n≥1 mice from the other group of the same treatment and pathology. Mouse number and pathology are as follows: (a) #169, moderate to severe dysplasia, (e) #168, severe dysplasia; (b) #164, SCC *in situ* with superficial invasion, (f) #193, superficially invasive SCC, (g) #229, superficially-invasive SCC, SCC *in situ*; (c,d) #195 and #210, invasive SCC, (h) #223, invasive SCC. All of the *KRT/ALDH* mice pictured are ALDH1a2^{high} with the exception of #229 shown in (g), which is ALDH1a2^{low}. All images taken at 200X, scale bar represents 100 μm. The inset in each picture is approximately 2.5X the digital magnification of a region of interest. (B,C) Quantification of vimentin staining in tongues from mice shown in (A) using Image J software. We analyzed n≥5 fields of a stained tongue section from each mouse. Each field was analyzed for total positively-stained area (in pixels) (B), and for the mean pixel intensity (arbitrary units) (C). Mouse #300 is a representative VC+Dox for reference. The other 8 mice were all treated with 4N+Dox. The results are presented as mean ±SEM. (D,E) Compilation of quantification of vimentin staining in tongues of 4N+Dox *KRT* and *KRT/ALDH* mice shown in (B,C). These results are representative of data from n=5 fields per mouse, and are graphed as mean ±SEM. All statistical analysis was conducted using GraphPad Prism 6.0 software. The results are presented as mean ±SEM. The data were analyzed using a Student's *t*-test, and differences with a $p < 0.05$ were considered statistically significant (marked with an asterisk).

cytochrome P450 26A1 (CYP26A1), which catalyzes the first step of RA degradation, is increased in HNSCC[45, 46]. These changes illustrate that RA signaling is often reduced in HNSCC, which is thought to greatly contribute to tumor development[7]. A better understanding of the roles of these proteins in HNSCC carcinogenesis could provide valuable information for future prevention and treatment of HNSCC and other human cancers.

To study the role of ALDH1a2 in HNSCC carcinogenesis we utilized transgenic mice with inducible TG ALDH1a2 expression in the tongue epithelium (*K14-rtTA/TRE-ALDH1a2; KRT/ALDH*) (Chapter 3, Figures 3.2-3.4). At the end of the 21-week treatment we observed that within the tongue epithelia of 4N+Dox ALDH1a2^{high} *KRT/ALDH* mice there is notable variation in ALDH1a2 protein expression: populations of cells with dark brown staining for ALDH1a2 directly adjoin regions in which there is no observable increase in staining compared to control tongues from *KRT* mice (Figure 4.4C).

We hypothesize that this result can be partly explained by recent research conducted in our laboratory by Tang *et al.*[47]. Tang *et al.* used a cell lineage tracing approach in K14-CreER^{TAM}/ROSA26 mice to identify and track K14+ epithelial stem cells in the normal tongue and in tongues undergoing 4-NQO treatment. By observing X-Gal(+) clonal cell populations the authors concluded that in the normal tongue, K14+ basal epithelial cells are long-lived and undergo asymmetric division to generate differentiated progeny and maintain homeostasis (Supplemental Figure 4.3). However, following treatment with 4-NQO, there were fewer X-Gal(+) clonal cell populations, and the X-Gal(+) clonal cell populations were larger than those in control tongues (Supplemental Figure 4.3A-C). In addition, 4-NQO treatment resulted in increased apoptosis and proliferation of basal cells, as measured using a TUNEL assay and Ki67

labeling, respectively (data not shown)[47]. These data indicate that 4-NQO treatment causes some basal stem cells to die and that the surviving neighboring stem cells compensate for this through symmetric division, resulting in the disappearance of some X-Gal(+) clonal cell populations and the expansion of others (Supplemental 4.3E). In the present study, some of the ALDH1a2-positive regions in 4N+Dox ALDH1a2^{high} *KRT/ALDH* mice display characteristics similar to the horizontally-expanded X-Gal(+) clonal populations observed by Dr. Tang (Figure 4.4C, middle and right columns; Supplemental Figure 4.3D)[47]. This suggests that these regions of high or low ALDH1a2 expression originate from one or more basal layer progenitor cells and expand laterally to replace regions of basal cells killed by 4-NQO.

In addition, we observed that VC+Dox and 4N+Dox *KRT/ALDH* mice varied significantly in the degree of ALDH1a2 mRNA and protein levels (ALDH1a2^{high} vs. ALDH1a2^{low} groups; Figures 4.3, 4.4). We do not yet have an explanation for this variance; possibilities range from differences in mouse water intake to differences in epigenetic regulation at the sites of the genetic copies of the ALDH1a2 transgene in the genomes of the individual mice.

As epithelial cells undergo EMT, they lose their adhesion and polarization properties and become more prone to invasion and migration[48]. EMT is believed to play a key role in cancer metastasis, as it enables the cells to leave the primary tumor site and initiate metastases in distant sites[49, 50]. Many proteins and signaling networks contribute to the process of EMT. One such protein is EZH2, which regulates gene expression as a central component of the PRC2; recent research has found that overexpression of EZH2 is a frequent event in HNSCC and correlates with advanced clinical stage, tumor size, poor prognosis, and lymph node metastases[51, 52]. EZH2 has therefore been proposed as a novel biomarker as well as a molecular target for future

targeted therapies in HNSCC patients[53]. In HNSCC, EZH2 negatively regulates E-cadherin, an epithelial marker, and positively regulates vimentin, a mesenchymal marker; loss of E-cadherin expression and gain of vimentin expression are key factors in EMT[52]. In HNSCC patients, reduced E-cadherin expression and enhanced vimentin expression correlate with higher incidence of metastasis[50]. In HNSCC cell lines, knockdown of EZH2 using siRNA induced E-cadherin expression, reduced vimentin expression, and inhibited cell migration and invasion[51, 52].

In the present study, we found that the expression of TG ALDH1a2 during 4-NQO-induced carcinogenesis reduced the expression of EZH2 and vimentin in mouse tongues (Figures 4.6, 4.7). Numerous previous studies have found that RA negatively regulates PRC2 activity, and treatment of nasopharyngeal carcinoma cells with RA decreases EZH2 expression[34, 54]. Because ALDH1a2 catalyzes the intracellular synthesis of RA, we hypothesize that ALDH1a2 expression reduces EZH2 expression by increasing RA synthesis and signaling; in turn, it is plausible that reduced EZH2 expression then decreases vimentin expression. However, the underlying molecular mechanisms of the downregulation of EZH2 and vimentin by ALDH1a2 remain to be elucidated. Our results are in agreement with recent work by Siedensaal *et al*., which showed that inhibition of ALDH1a2-RAR signaling in HNSCC cell lines *in vitro* and knockdown of ALDH1a2 in xenograft experiments *in vivo* promoted a mesenchymal-like phenotype characterized by increased vimentin expression, enhanced migration *in vitro* and accelerated tumor growth *in vivo*[21]. However, our current study is the first to provide a link between ALDH1a2 and EZH2, and taken together, these results indicate that ALDH1a2 may inhibit tumor cell EMT, invasion, and metastasis during HNSCC carcinogenesis.

RESULTS PART II: PHENOTYPIC CHANGES

Lesion severity and multiplicity in 4N+Dox KRT and KRT/ALDH mice

All of the surviving 4N+Dox mice (n=18 total, n=9 *KRT* and n=9 *KRT/ALDH*) exhibited observable gross lesions on the tongue (grade ≥1, Figure 4.8A). In contrast, mice treated with VC+Dox (n=19 total, n=10 *KRT* and n=9 *KRT/ALDH*) exhibited no visible gross lesions (grade 0, data not shown). We analyzed the severity (grade) and numbers (multiplicity) of gross lesions of 4N+Dox mice in a blinded manner. We found no statistical difference in the average lesion grade or average lesion multiplicity between *KRT* mice and *KRT/ALDH* mice (Figure 4.8B,E). The scatter plots in Figure 4.8C,F illustrate the distribution of lesion severity and multiplicity within each group. After 4N+Dox treatment, approximately 22% of *KRT* mice presented with low-grade lesions (grade <2; n=2), ~56% with medium-grade lesions (grade 2-3; n=5), and ~22% with high grade lesions (grade 4-5; n=2) (Figure 4.8D). Approximately 44% of *KRT/ALDH* mice exhibited low-grade lesions (grade <2; n=4), ~22% exhibited medium-grade lesions (grade 2-3; n=2), and ~33% exhibited high-grade lesions (grade 4-5; n=3) (Figure 4.8D). Therefore, following 4-NQO treatment, *KRT/ALDH* mice had greater incidence of low-grade lesions (grade <2) and lower incidence of medium-grade lesions (grade 2-3) compared to *KRT* mice. The rate of high grade lesions was comparable between the two groups (n=2 *KRT* vs. n=3 *KRT/ALDH*), however the only grade 5 lesion observed was on the tongue of a *KRT* mouse. See Supp. Fig. 4.1 for the grade and multiplicity of each 4N+Dox mouse.

Because we observed notable variation in the degree of ALDH1a2 mRNA and protein expression in *KRT/ALDH* mice (Figures 4.3, 4.4), we analyzed lesion severity and multiplicity relative to ALDH1a2 expression (Figure 4.9). By separating the 4N+Dox *KRT/ALDH* group into ALDH1a2^{high} and ALDH1a2^{low} subgroups, we

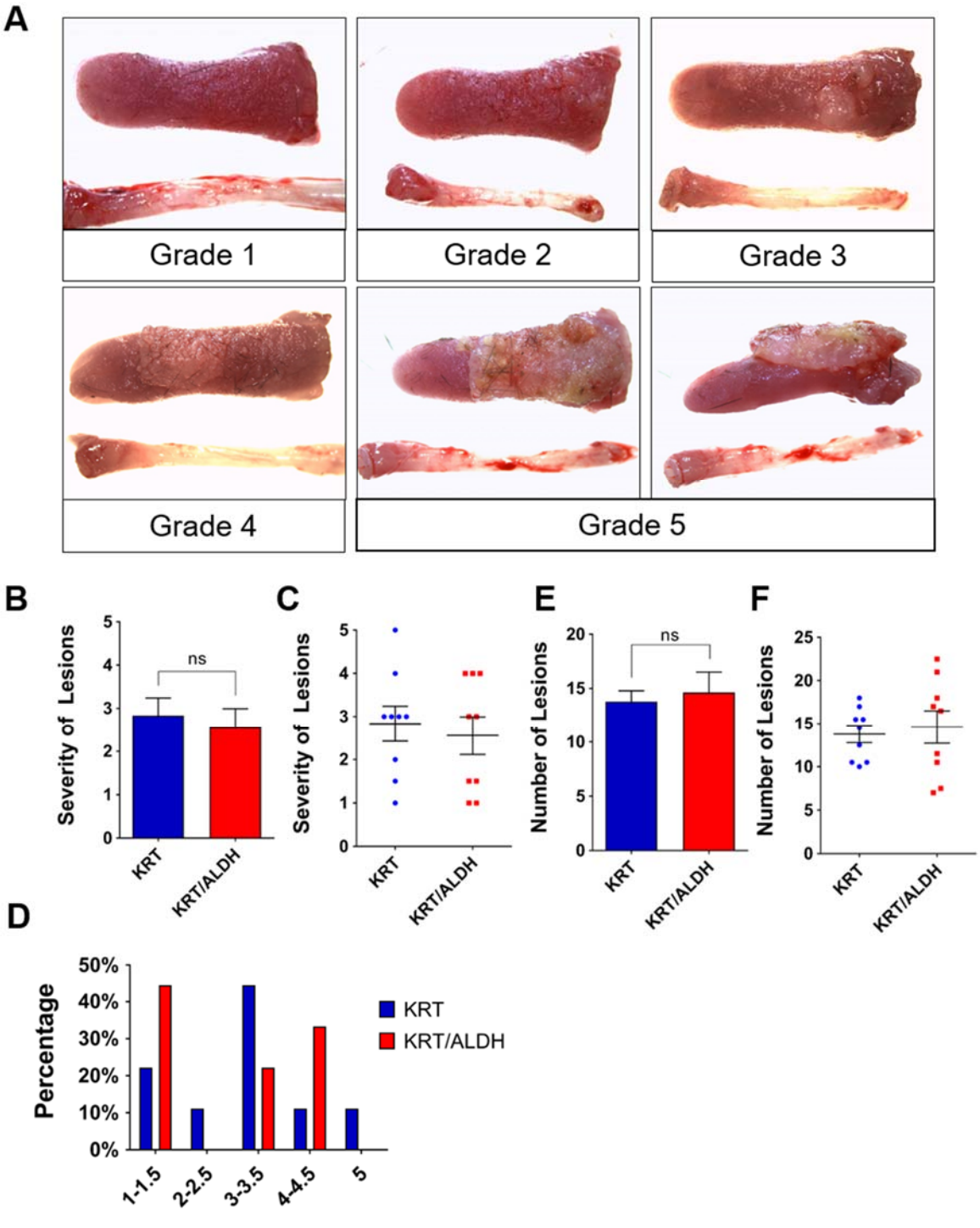
A
Grade 1
Grade 2
Grade 3
Grade 4
Grade 5
B
Severity of Lesions
ns
KRT
KRT/ALDH
C
Severity of Lesions
KRT
KRT/ALDH
E
Number of Lesions
ns
KRT
KRT/ALDH
F
Number of Lesions
KRT
KRT/ALDH
D
Percentage
50%
40%
30%
20%
10%
0%
KRT
KRT/ALDH
1-1.5
2-2.5
3-3.5
4-4.5
5

Figure 4.8: Lesion development following 4-NQO treatment. *KRT* and *KRT/ALDH* mice (n=10, each group) were treated with dox (2 mg/mL), and 4-NQO (100 μg/mL) for 10 weeks (4N+Dox). All mice were then switched to dox alone (2 mg/mL) until sacrifice at 21 weeks. (A) Representative images of gross tongue morphology observed at the time of sacrifice (images taken at 10X). All mice were graded in a blinded manner on a scale of 1-5 (5 being the most severe) depending on the observable gross lesion severity on the tongue surface. Pictured is a tongue representative of each grade. There was only one tongue that received a grade of 5, which is shown twice to better illustrate the size of the lesion (bottom right panels). Esophagi were also photographed at this time. (B-D) Grading of observable tongue lesions of *KRT* and *KRT/ALDH* mice treated with 4N+Dox. (D) Graphical representation of the percentage of each group of mice (*KRT* or *KRT/ALDH*) that presented with each lesion grade. Graph represents n=9 total surviving mice per group. (E,F) Counting of gross observable lesions on the tongues of 4N+Dox *KRT* and *KRT/ALDH* mice. In all panels, error bars represent mean±SEM. Statistical analysis conducted using GraphPad Prism 6.0 software.

observed an interesting pattern among the n=6 ALDH1a2^{high} mice. 50% of the ALDH1a2^{high} mice presented with low lesion grade and lower multiplicity (grade <2, lesion number <12; n=3 mice), 50% with high grade and higher multiplicity (grade 4-5, lesion number ≥18; n=3), and none with medium grade or multiplicity (grade 2-3, lesion number 12-17) (Figure 4.9A-C). This suggests that high expression of ALDH1a2 during 4-NQO-induced carcinogenesis can have two disparate effects: overexpression of ectopic ALDH1a2 can result in either a less severe phenotype or a more severe phenotype.

Histopathological analysis of tongues from mice subjected to the 4-NQO murine model of carcinogenesis

In order to evaluate the histopathology of the tongue epithelia of 4N+Dox mice, a blinded board-certified pathologist analyzed one H&E-stained tongue section from each 4N+Dox mouse. Each tongue section was characterized according to the observed stage of oral carcinogenesis; these stages include normal, hyperplasia, dysplasia (mild, moderate, severe), and carcinoma (carcinoma *in situ*/superficial SCC

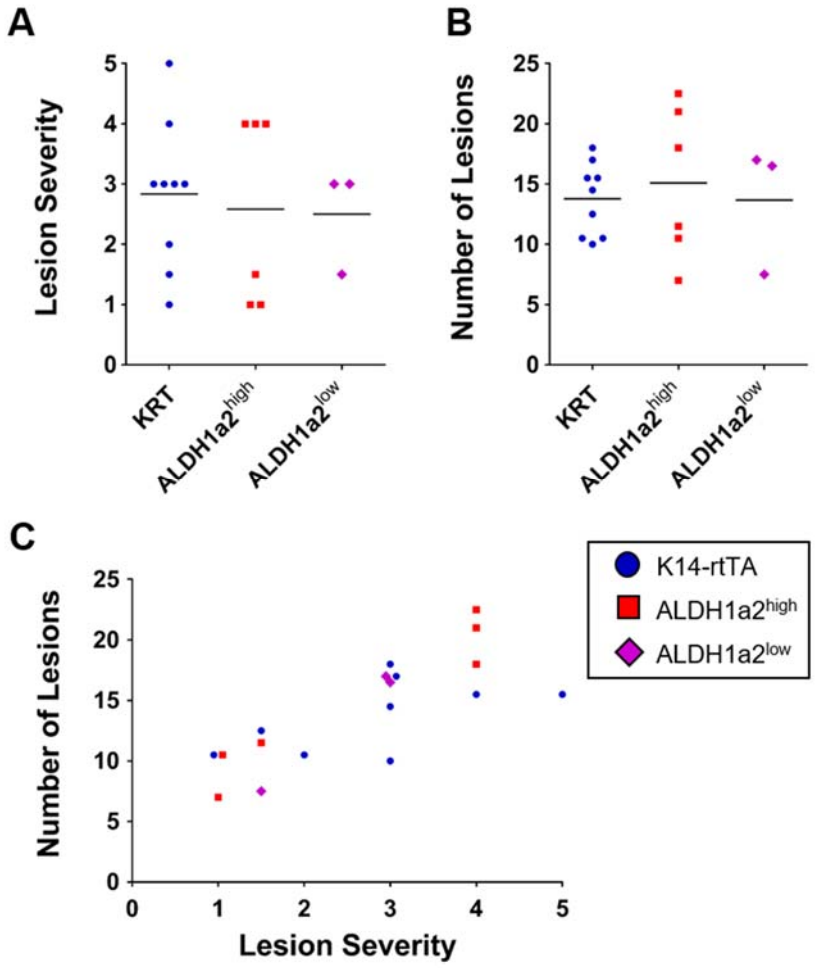

Figure 4.9: Lesion severity and number in ALDH1a2^{high} and ALDH1a2^{low} *KRT/ALDH* mice following 4-NQO treatment. Mice were treated with dox (2 mg/mL) and 4-NQO (100 µg/mL) for 10 weeks before being switched to dox alone (2 mg/mL) for another 11 weeks. Tongues were dissected and photographed immediately following sacrifice. The grossly visible lesions on the whole tongues were counted and graded in a blinded manner. *KRT/ALDH* mice were designated ALDH1a2^{high} (n=6) and ALDH1a2^{low} (n=3) according to ALDH1a2 mRNA and protein expression as determined by RT-PCR and IHC, respectively (Figures 4.3,4.4, Table 4.3). (A) Lesion severity observed in 4-NQO-treated mice. All mice were graded in a blinded manner on a scale of 1-5 (5 being the most severe). (B) Number of observable tongue lesions of mice treated with 4-NQO. (C) Lesion severity of each mouse graphed relative to observed lesion number. Each data point represents an individual mouse. Bars in (A,B) represent mean, determined using GraphPad Prism 6.0 software.

or invasive SCC). Representative pictures of each histopathologic stage are shown in Figure 4.10. Of the 4N+Dox mice, we found that 56% of *KRT* mice (n=5) and 44% of *KRT/ALDH* mice (n=4) exhibited histopathology indicative of low-risk of oral carcinogenesis (normal, hyperplasia, mild-moderate dysplasia), and that 44% of *KRT* mice (n=4) and 56% of *KRT/ALDH* mice exhibited histopathology indicative of high risk of oral carcinogenesis (severe dysplasia, carcinoma *in situ*/superficial SCC, invasive SCC) (Supplemental Table 4.1)[24]. Because only one 7μm section per mouse tongue was analyzed, these histopathology classifications are not necessarily representative of the whole tongue phenotype. For example, *KRT* mouse #11-186, which was graded as having a lesion severity of 3 and presented with a medium-large gross lesion on the left dorsal side of the tongue, was evaluated as having a normal histopathology (Supplemental Figure 4.1). Histopathological analysis of additional tongue sections from each mouse could yield additional insights on differences between the *KRT* and *KRT/ALDH* mice. In the present study we have chosen to focus on lesion grade as a readout of disease severity, as it is representative of the whole tongue. Histopathologic stage was used to categorize the tongue sections themselves and inform the analysis as described in Part I of this chapter.

DISCUSSION PART II: PHENOTYPIC CHANGES

Previous research in our lab has explored the role of RA signaling in the 4-NQO murine model of OSCC carcinogenesis. Transgenic mouse experiments in which LRAT was constitutively overexpressed specifically in oral basal epithelial cells revealed that this overexpression makes the cells more sensitive to carcinogenesis induced by 4-NQO[26]. In addition, treatments with exogenous retinoids including RA (100 μg/kg body weight and 1 mg/kg body weight), bexarotene (a RXR agonist), and CD1530 (a RARγ selective agonist) were found to reduce incidence of oral cavity

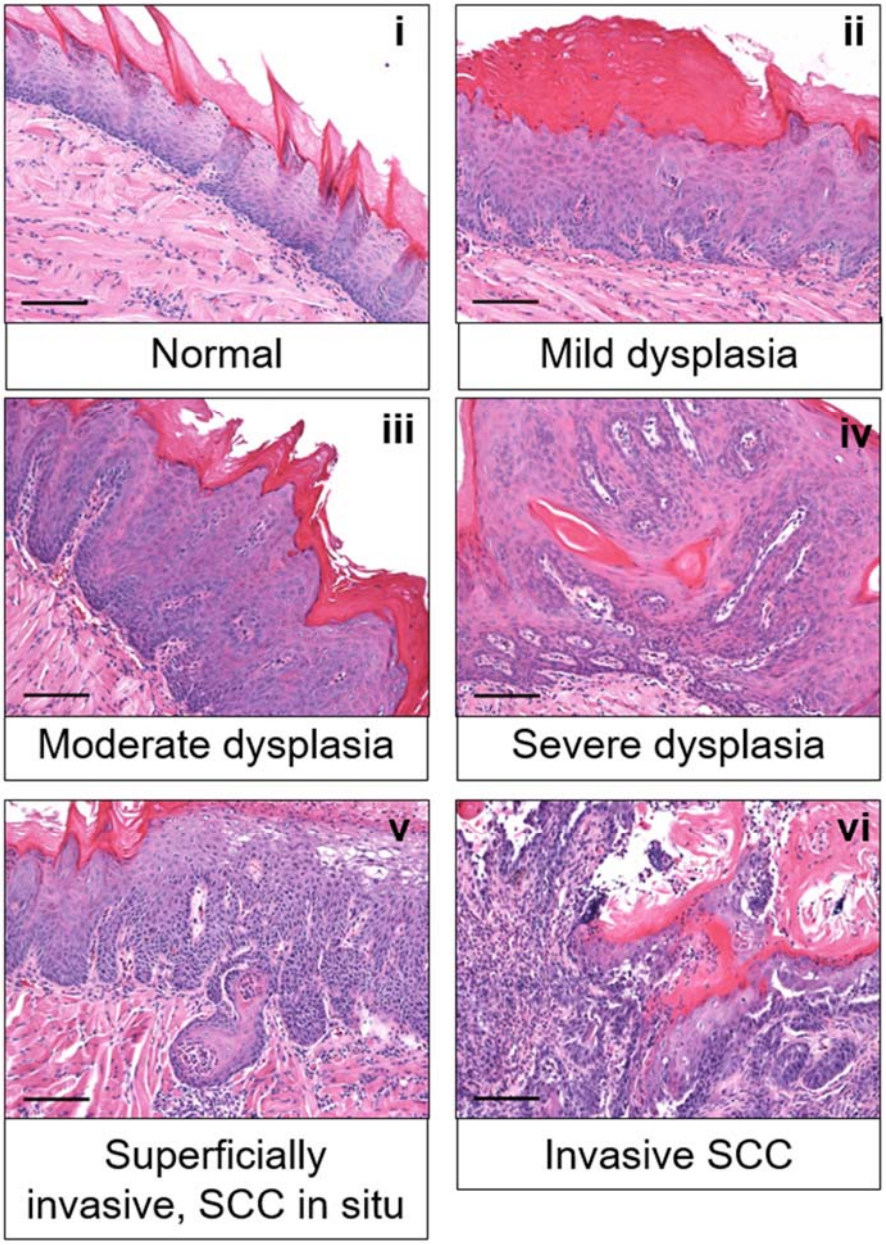

Figure 4.10: Histopathology of carcinogenesis in the 4-NQO murine model of OSCC. Immediately following sacrifice, mouse tongues were dissected, fixed (4% PFA overnight at 4°C), embedded, sectioned (7µm), and stained with hematoxylin and eosin (H&E). One tongue section from each 4-NQO-treated mouse was analyzed by a certified pathologist as described in the Materials and Methods (n=18 mice total; n=9 *KRT* and n=9 *KRT/ALDH*. Representative pictures of pathology, images were taken at 200X and scale bar represents 100µm. (i) normal; (ii) mild hyperplasia with marked hyperkeratosis; (iii) moderate dysplasia; (iv) severe dysplasia; (v) superficially-invasive, SCC *in situ*; (vi) invasive SCC. A representative image from the only mouse classified as having hyperplasia is shown in Supplemental Figure 4.4.

carcinogenesis induced by 4-NQO as measured by the multiplicity and severity of gross observable lesions[24, 25]. In contrast, we did not observe a significant change in the mean lesion severity or multiplicity in *KRT/ALDH* mice compared to *KRT* control mice, though we did observe a trend towards increased incidence of low grade tumors (grade <2) (Figure 4.8). There are numerous potential explanations for why ectopic ALDH1a2 expression did not decrease mean lesion severity and grade in this study like treatment with exogenous retinoids did in previous studies. First, VC+Dox and 4N+Dox *KRT/ALDH* mice varied significantly in the level of ALDH1a2 mRNA and protein induction by dox ($ALDH1a2^{high}$ vs. $ALDH1a2^{low}$ groups; Figures 4.3, 4.4). In addition, strong ALDH1a2 protein expression in $ALDH1a2^{high}$ *KRT/ALDH* mice was present in only certain regions of the tongue epithelium (Figure 4.4), as discussed in Discussion Part I. It is worth speculating that the effect of exogenous ALDH1a2 expression on gross lesion development would be more pronounced in transgenic mice with less intra-group and intra-tongue variation in ALDH1a2 expression. Lastly, 4N+Dox *KRT/ALDH* mice, which have a genetic background of 50/50 C57Bl/6/FVB, exhibited accelerated tumor development as compared to previous experiments in which mice of other genetic backgrounds were treated with the same concentration of 4-NQO (100 μg/mL)[23, 24, 26, 27, 55]. In xenograft experiments by Seidensaal *et al*., knockdown of ALDH1a2 in HNSCC cells prior to injection resulted in accelerated tumor growth but did not change the overall incidence of tumors[21]. Therefore, additional experimentation with *KRT/ALDH* mice using an earlier treatment endpoint or consistent monitoring of tumor growth over time might yield additional insights.

We observed two distinct sub-populations of 4N+Dox $ALDH1a2^{high}$ *KRT/ALDH* mice (n=6 total): mice with high grade/high multiplicity (n=3) and mice

with low grade/low multiplicity (n=3) (Figure 4.9C). This result suggests that expression of ectopic ALDH1a2 during carcinogenesis can have two disparate effects. We hypothesize that this may be because these sub-populations differ in their expression of proteins downstream of ALDH1a2 in the RA signaling pathway. Researchers recently observed that HNSCC patients with tumors with high ALDH1a2 protein expression ($ALDH1a2^{high}$) have a more favorable clinical outcome than patients with $ALDH1a2^{low}$ tumors, but only in the presence of CRABP2 ($ALDH1a2^{high}CRABP2^{high}$)[21]. In contrast, patients with $ALDH1a2^{high}CRABP2^{low}$ tumors had a worse overall survival probability comparable to patients with $ALDH1a2^{low}$ tumors[21]. In the absence of transport protein CRABP2, the intracellular RA synthesized by ALDH1a2 is free to be shuttled by a different lipid transporter, such as fatty acid binding protein 5 (FABP5). Unlike CRABP2, which preferentially delivers RA to RAR/RXR heterodimers for downstream signaling, FABP5 favors activation of RAR/peroxisome proliferator-activated receptor (PPAR) heterodimers[56]. While RAR/RXR signaling is known to promote differentiation, cell cycle arrest, apoptosis, and/or inhibition of cell growth, RAR/PPAR signaling promotes the expression of pro-survival factors such as survivin or components of the PDK-1/Akt pathway[56, 57]. Thus, RA signaling (and synthesis of RA by ALDH1a2) can activate opposing signaling pathways and have diverse effects on cell growth depending on the status of CRABP2, FABP5, and nuclear receptor expression. Indeed, it is hypothesized that expression of RARβ is a major contributing factor to how HNSCC patients respond to treatment with classical retinoids[12]. It is therefore feasible that the high grade/high multiplicity sub-population of $ALDH1a2^{high}$ *KRT/ALDH* mice have a high FABP5/CRABP2 ratio or reduced expression or activity of one or more RARs; this hypothesis could be addressed by analyzing the relative expression of other members of the retinoid signaling pathway in each $ALDH1a2^{high}$ *KRT/ALDH* mouse.

CONCLUSIONS

Based on these findings, we speculate that ALDH1a2 suppresses tumor cell EMT during OSCC carcinogenesis *in vivo*. Future experiments will investigate whether this observation translates to inhibition of distant metastases, which would be of clinical significance. We also observed that expression of endogenous ALDH1a2 is reduced following carcinogen-induced OSCC (Figure 4.2). These data, taken together with our data on HNSCC cell lines as described in Chapter 2, provide evidence that ALDH1a2 has tumor suppressive functions in HNSCC. Interestingly, our results also suggest that enhanced ALDH1a2 expression during OSCC carcinogenesis can have two disparate effects on lesion severity and multiplicity (Figure 4.9). Future experiments will determine if this phenomenon is due to the relative activity of the proteins downstream of ALDH1a2 in the RA signaling pathway (Figure 1.2).

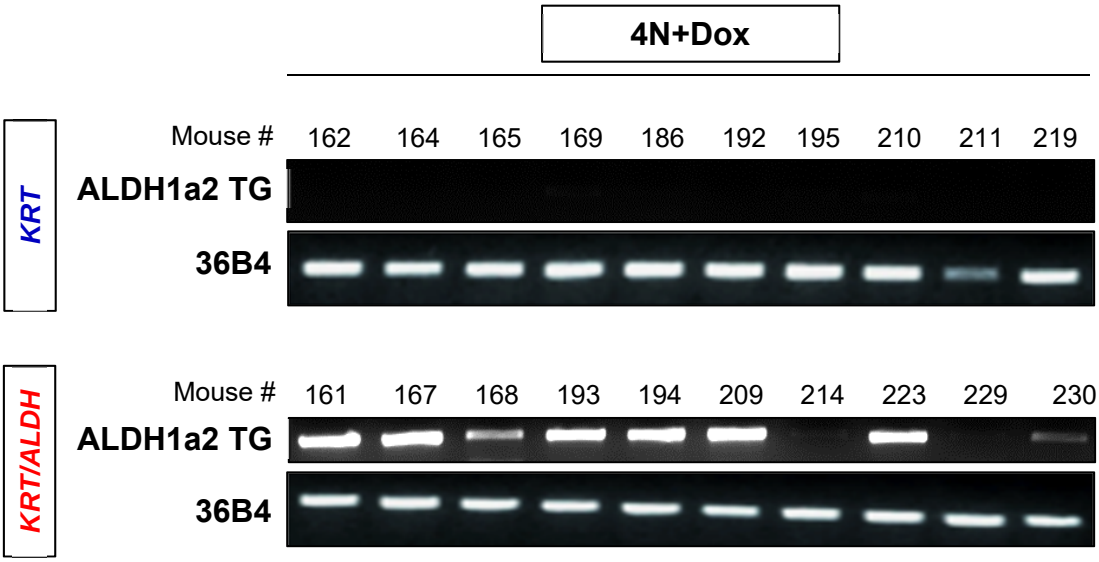

Supplemental Figure 4.1: Verification of ALDH1a2 transcript induction after 4-NQO treatment. Ear snips were collected from all mice at the close of the 10-week dox plus 4-NQO treatment (4N+Dox) (n=20, n=10 *KRT* and n=10 *KRT/ALDH*). We conducted RT-PCR analysis of transgenic ALDH1a2 transcript, and confirmed that transgenic ALDH1a2 (ALDH1a2 TG) was induced in *KRT/ALDH* mice and not *KRT* mice. 36B4 represents the loading control gene. This result suggests that ALDH1a2 induction by doxycycline was not impeded by co-treatment with 4-NQO. Faint ALDH1a2 TG bands were just visible in the lanes for *KRT/ALDH* mice #214 and 229. The variation of intensity of ALDH1a2 induction in *KRT/ALDH* mice is addressed more thoroughly in Figures 4.3 and 4.4. All primer sequences are provided in Table 4.2.

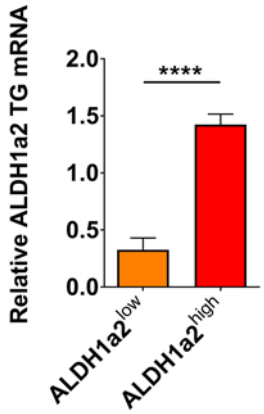

Supplemental Figure 4.2: Quantification of the ALDH1a2 TG bands observed in *KRT/ALDH* tongues in Figure 4.3A,B using Image J software. Values are normalized to 36B4. Mice were sorted into ALDH1a2^{high} and ALDH1a2^{low} groups based on the results in Figure 4.3 and in conjunction with IHC results as shown in Figure 4.4. See Table 4.3. Bars represent mean±SEM; **** indicates $p<0.0001$.

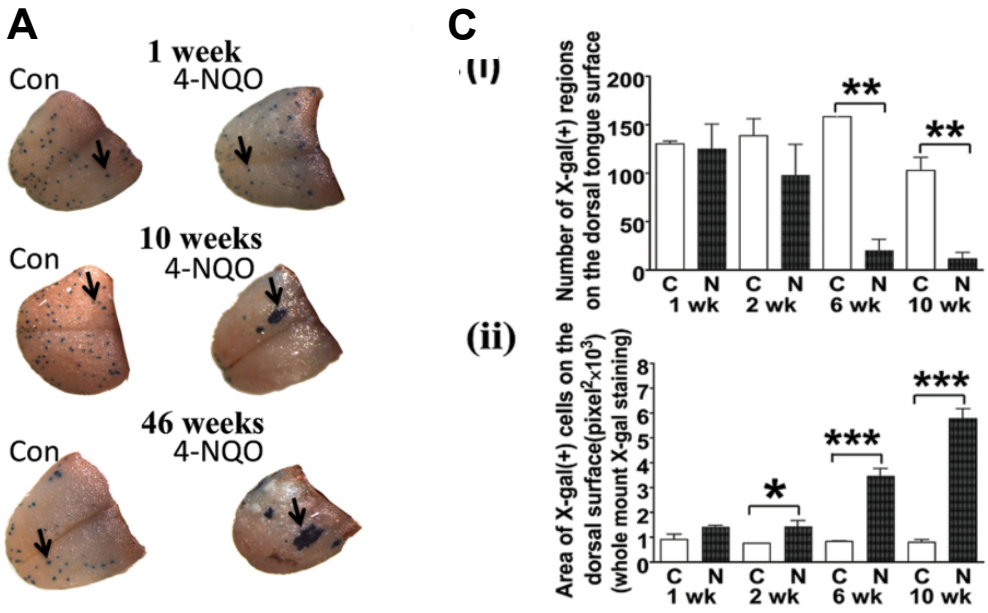
A
1 week
Con
4-NQO
10 weeks
Con
4-NQO
46 weeks
Con
4-NQO
C
(i)
Number of X-gal(+) regions on the dorsal tongue surface
200
150
100
50
0
**
**
C N C N C N C N
1 wk 2 wk 6 wk 10 wk
(ii)
Area of X-gal(+) cells on the dorsal surface(pixel²×10³) (whole mount X-gal staining)
8
7
6
5
4
3
2
1
0
*
***
***
C N C N C N C N
1 wk 2 wk 6 wk 10 wk

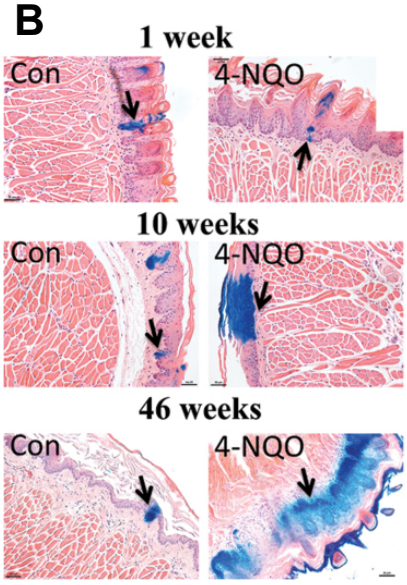
B
1 week
Con
4-NQO
10 weeks
Con
4-NQO
46 weeks
Con
4-NQO

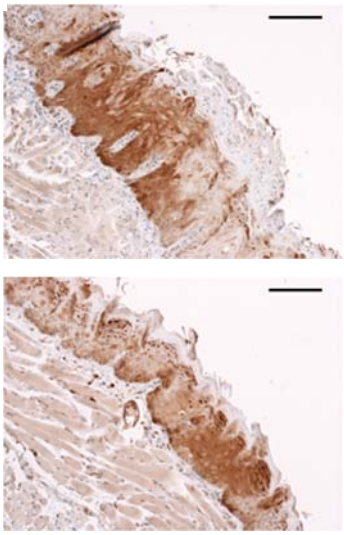
D

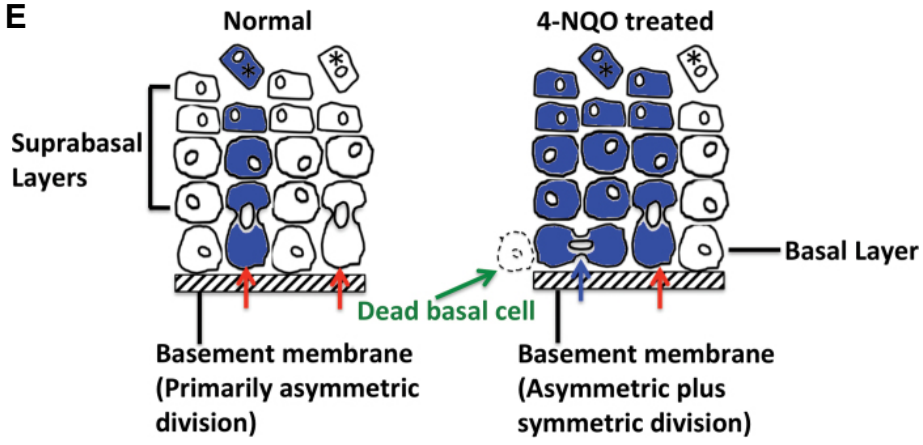
E
Normal
4-NQO treated
Suprabasal Layers
Basal Layer
Dead basal cell
Basement membrane (Primarily asymmetric division)
Basement membrane (Asymmetric plus symmetric division)

Supplemental Figure 4.3 (adapted from Tang *et al*., 2013): Expansion of clonal cell populations following 4-NQO treatment. (A-C) K14-CreER^{TAM}/ROSA26 mice received tamoxifen treatment (4mg/mouse/day) by intraperitoneal injections on two consecutive days four weeks prior to the start of treatment. Mice (n≥3 per group) were then treated with 4-NQO (100 μg/mL) or vehicle control for various times (as indicated). After dissection, tongues were stained with X-Gal as described. (A) Whole-mount X-Gal staining of mouse tongues. Images taken at 8X. (B) H&E-stained sections from X-gal-stained tongues. Images taken at 200X, scale bar represents 50 μm. (C) Quantification of the number of X-Gal(+) populations on the dorsal side of the tongue and the areas (ii) of the biggest X-Gal(+) populations on the dorsal side of each tongue. (D) Images of tongue sections from n=2 4N+Dox ALDH1a2^{high} *KRT/ALDH* mice stained with 1:200 ALDH1a2. Images taken at 200X, scale bar represents 100 μm. (E) Model of tongue epithelia homeostasis generated by Tang *et al*. Under normal conditions (left panel) basal stem cells undergo asymmetric division (red arrows). Treatment with 4-NQO (right panel) results in the death of some basal stem cells and the expansion of others via symmetric division (blue arrows).

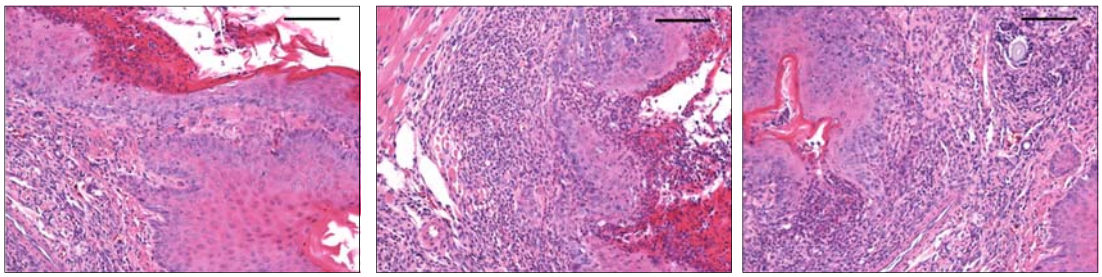

Supplemental Figure 4.4: Additional histopathology. Immediately following sacrifice, mouse tongues were dissected, fixed (4% PFA overnight at 4°C), embedded, sectioned (7μm), and stained with hematoxylin and eosin (H&E). One tongue section from each 4-NQO-treated mouse was analyzed by a certified pathologist as described in the Materials and Methods (n=18 mice total; n=9 *KRT* and n=9 *K14-rtTA/TRE-ALDH1a2*). Representative pictures of pathology of mouse #11-165: hyperplastic squamous mucosa with acute and chronic inflammation. Images were taken at 200X and scale bar represents 100μm.

	Gross Lesions		Histopathology		
Mouse	**Grade**	**Number**	**Tongue**	**Esophagus**	
KRT					
162	3	10	Normal	Normal	
164	1.5	12.5	SCC in-situ with superficial invasion	No mucosa to evaluate	
165	3	14.5	Hyperplastic squamous mucosa with acute and chronic inflammation	Normal	
169	2	10.5	Focal moderate to severe dysplasia	Normal	
186	3	18	Normal	No mucosa to evaluate	
192	3	17	Mild dysplasia	Normal	
195	4	15.5	Invasive SCC	Normal	
210	5	15.5	Invasive SCC	Normal	
211	1	10.5	Moderate dysplasia	Normal	
KRT/ALDH					**ALDH1a2**
167	1.5	11.5	Severe dysplasia	Normal	high
168	4	21	Severe dysplasia	Normal	high
193	4	18	Superficially invasive SCC	Normal	high
194	1	10.5	Moderate dysplasia to focal severe dysplasia	Acute and chronic inflammation	high
209	1	7	Mild dysplasia	Mild hyperplasia	high
214	3	17	Moderate dysplasia	Normal	low
223	4	22.5	Invasive SCC	Normal	high
229	3	16.5	Superficially invasive SCC and SCC in-situ	Normal	low
230	1.5	7.5	Normal	Normal	low

Supplemental Table 4.1: Examination of the tongues of mice after treatment with 4N+Dox.

REFERENCES

1. Jemal A, Bray F, Center MM, Ferlay J, Ward E, Forman D. Global cancer statistics. CA Cancer J Clin. 2011;61: 69-90.

2. Leemans CR, Braakhuis BJ, Brakenhoff RH. The molecular biology of head and neck cancer. Nat Rev Cancer. 2011;11: 9-22.

3. Sacco AG, Cohen EE. Current Treatment Options for Recurrent or Metastatic Head and Neck Squamous Cell Carcinoma. J Clin Oncol. 2015;33: 3305-3313.

4. Curado MP, Hashibe M. Recent changes in the epidemiology of head and neck cancer. Curr Opin Oncol. 2009;21: 194-200.

5. Brinkman BM, Wong DT. Disease mechanism and biomarkers of oral squamous cell carcinoma. Curr Opin Oncol. 2006;18: 228-233.

6. Lee JJ, Wu X, Hildebrandt MA, et al. Global assessment of genetic variation influencing response to retinoid chemoprevention in head and neck cancer patients. Cancer Prev Res (Phila). 2011;4: 185-193.

7. Mongan NP, Gudas LJ. Diverse actions of retinoid receptors in cancer prevention and treatment. Differentiation. 2007;75: 853-870.

8. Lotan R. Suppression of squamous cell carcinoma growth and differentiation by retinoids. Cancer Res. 1994;54: 1987s-1990s.

9. Giannini F, Maestro R, Vukosavljevic T, Pomponi F, Boiocchi M. All-trans, 13-cis and 9-cis retinoic acids induce a fully reversible growth inhibition in HNSCC cell lines: implications for in vivo retinoic acid use. Int J Cancer. 1997;70: 194-200.

10. Zou CP, Clifford JL, Xu XC, et al. Modulation by retinoic acid (RA) of squamous cell differentiation, cellular RA-binding proteins, and nuclear RA receptors in human head and neck squamous cell carcinoma cell lines. Cancer Res. 1994;54: 5479-5487.

11. Khuri FR, Lee JJ, Lippman SM, et al. Randomized phase III trial of low-dose isotretinoin for prevention of second primary tumors in stage I and II head and neck cancer patients. J Natl Cancer Inst. 2006;98: 441-450.
12. Freemantle SJ, Dragnev KH, Dmitrovsky E. The retinoic acid paradox in cancer chemoprevention. J Natl Cancer Inst. 2006;98: 426-427.
13. Tang XH, Gudas LJ. Retinoids, retinoic acid receptors, and cancer. Annu Rev Pathol. 2011;6: 345-364.
14. Napoli JL. Physiological insights into all-trans-retinoic acid biosynthesis. Biochim Biophys Acta. 2012;1821: 152-167.
15. Zhao D, McCaffery P, Ivins KJ, et al. Molecular identification of a major retinoic-acid-synthesizing enzyme, a retinaldehyde-specific dehydrogenase. Eur J Biochem. 1996;240: 15-22.
16. Niederreither K, Subbarayan V, Dollé P, Chambon P. Embryonic retinoic acid synthesis is essential for early mouse post-implantation development. Nat Genet. 1999;21: 444-448.
17. Touma SE, Perner S, Rubin MA, Nanus DM, Gudas LJ. Retinoid metabolism and ALDH1A2 (RALDH2) expression are altered in the transgenic adenocarcinoma mouse prostate model. Biochem Pharmacol. 2009;78: 1127-1138.
18. Kim H, Lapointe J, Kaygusuz G, et al. The retinoic acid synthesis gene ALDH1a2 is a candidate tumor suppressor in prostate cancer. Cancer Res. 2005;65: 8118-8124.
19. Williams SJ, Cvetkovic D, Hamilton TC. Vitamin A metabolism is impaired in human ovarian cancer. Gynecol Oncol. 2009;112: 637-645.
20. Kostareli E, Holzinger D, Bogatyrova O, et al. HPV-related methylation signature predicts survival in oropharyngeal squamous cell carcinomas. J Clin Invest. 2013;123: 2488-2501.

21. Seidensaal K, Nollert A, Feige AH, et al. Impaired aldehyde dehydrogenase 1 subfamily member 2A-dependent retinoic acid signaling is related with a mesenchymal-like phenotype and an unfavorable prognosis of head and neck squamous cell carcinoma. Mol Cancer. 2015;14: 204.
22. Wu S, Xue W, Huang X, et al. Distinct prognostic values of ALDH1 isoenzymes in breast cancer. Tumour Biol. 2015;36: 2421-2426.
23. Tang XH, Knudsen B, Bemis D, Tickoo S, Gudas LJ. Oral cavity and esophageal carcinogenesis modeled in carcinogen-treated mice. Clin Cancer Res. 2004;10: 301-313.
24. Tang XH, Albert M, Scognamiglio T, Gudas LJ. A DNA methyltransferase inhibitor and all-trans retinoic acid reduce oral cavity carcinogenesis induced by the carcinogen 4-nitroquinoline 1-oxide. Cancer Prev Res (Phila). 2009;2: 1100-1110.
25. Tang XH, Osei-Sarfo K, Urvalek AM, Zhang T, Scognamiglio T, Gudas LJ. Combination of bexarotene and the retinoid CD1530 reduces murine oral-cavity carcinogenesis induced by the carcinogen 4-nitroquinoline 1-oxide. Proc Natl Acad Sci U S A. 2014;111: 8907-8912.
26. Tang XH, Su D, Albert M, Scognamiglio T, Gudas LJ. Overexpression of lecithin:retinol acyltransferase in the epithelial basal layer makes mice more sensitive to oral cavity carcinogenesis induced by a carcinogen. Cancer Biol Ther. 2009;8: 1212-1213.
27. Osei-Sarfo K, Tang XH, Urvalek AM, Scognamiglio T, Gudas LJ. The molecular features of tongue epithelium treated with the carcinogen 4-nitroquinoline-1-oxide and alcohol as a model for HNSCC. Carcinogenesis. 2013;34: 2673-2681.
28. Laursen KB, Wong PM, Gudas LJ. Epigenetic regulation by RARα maintains ligand-independent transcriptional activity. Nucleic Acids Res. 2012;40: 102-115.

29. Nguyen H, Rendl M, Fuchs E. Tcf3 governs stem cell features and represses cell fate determination in skin. Cell. 2006;127: 171-183.
30. Fuchs E, Green H. Changes in keratin gene expression during terminal differentiation of the keratinocyte. Cell. 1980;19: 1033-1042.
31. Kannan S, Balaram P, Chandran GJ, et al. Differential expression of cytokeratin proteins during tumour progression in oral mucosa. Epithelial Cell Biol. 1994;3: 61-69.
32. Kim KH, Schwartz F, Fuchs E. Differences in keratin synthesis between normal epithelial cells and squamous cell carcinomas are mediated by vitamin A. Proc Natl Acad Sci U S A. 1984;81: 4280-4284.
33. Chu PG, Lyda MH, Weiss LM. Cytokeratin 14 expression in epithelial neoplasms: a survey of 435 cases with emphasis on its value in differentiating squamous cell carcinomas from other epithelial tumours. Histopathology. 2001;39: 9-16.
34. Benoit YD, Laursen KB, Witherspoon MS, Lipkin SM, Gudas LJ. Inhibition of PRC2 histone methyltransferase activity increases TRAIL-mediated apoptosis sensitivity in human colon cancer cells. J Cell Physiol. 2013;228: 764-772.
35. Cao W, Feng Z, Cui Z, et al. Up-regulation of enhancer of zeste homolog 2 is associated positively with cyclin D1 overexpression and poor clinical outcome in head and neck squamous cell carcinoma. Cancer. 2012;118: 2858-2871.
36. Li Z, Wang Y, Qiu J, et al. The polycomb group protein EZH2 is a novel therapeutic target in tongue cancer. Oncotarget. 2013;4: 2532-2549.
37. Eriksson JE, Dechat T, Grin B, et al. Introducing intermediate filaments: from discovery to disease. J Clin Invest. 2009;119: 1763-1771.
38. Liu LK, Jiang XY, Zhou XX, Wang DM, Song XL, Jiang HB. Upregulation of vimentin and aberrant expression of E-cadherin/beta-catenin complex in oral

squamous cell carcinomas: correlation with the clinicopathological features and patient outcome. Mod Pathol. 2010;23: 213-224.
39. Lotan R. Roles of retinoids and their nuclear receptors in the development and prevention of upper aerodigestive tract cancers. Environ Health Perspect. 1997;105 Suppl 4: 985-988.
40. Guo X, Gudas LJ. Metabolism of all-trans-retinol in normal human cell strains and squamous cell carcinoma (SCC) lines from the oral cavity and skin: reduced esterification of retinol in SCC lines. Cancer Res. 1998;58: 166-176.
41. Yang Q, Wang R, Xiao W, Sun F, Yuan H, Pan Q. Cellular Retinoic Acid Binding Protein 2 Is Strikingly Downregulated in Human Esophageal Squamous Cell Carcinoma and Functions as a Tumor Suppressor. PLoS One. 2016;11: e0148381.
42. Guo X, Ruiz A, Rando RR, Bok D, Gudas LJ. Esterification of all-trans-retinol in normal human epithelial cell strains and carcinoma lines from oral cavity, skin and breast: reduced expression of lecithin:retinol acyltransferase in carcinoma lines. Carcinogenesis. 2000;21: 1925-1933.
43. Xu XC, Ro JY, Lee JS, Shin DM, Hong WK, Lotan R. Differential expression of nuclear retinoid receptors in normal, premalignant, and malignant head and neck tissues. Cancer Res. 1994;54: 3580-3587.
44. Hu L, Crowe DL, Rheinwald JG, Chambon P, Gudas LJ. Abnormal expression of retinoic acid receptors and keratin 19 by human oral and epidermal squamous cell carcinoma cell lines. Cancer Res. 1991;51: 3972-3981.
45. Osanai M, Lee GH. Increased expression of the retinoic acid-metabolizing enzyme CYP26A1 during the progression of cervical squamous neoplasia and head and neck cancer. BMC Res Notes. 2014;7: 697.
46. Klaassen I, Brakenhoff RH, Smeets SJ, Snow GB, Braakhuis BJ. Enhanced turnover of all-trans-retinoic acid and increased formation of polar metabolites in head

and neck squamous cell carcinoma lines compared with normal oral keratinocytes. Clin Cancer Res. 2001;7: 1017-1025.

47. Tang XH, Scognamiglio T, Gudas LJ. Basal stem cells contribute to squamous cell carcinomas in the oral cavity. Carcinogenesis. 2013;34: 1158-1164.

48. Thiery JP, Sleeman JP. Complex networks orchestrate epithelial-mesenchymal transitions. Nat Rev Mol Cell Biol. 2006;7: 131-142.

49. Kim KH, Kim L, Choi SJ, et al. The clinicopathological significance of epithelial mesenchymal transition associated protein expression in head and neck squamous cell carcinoma. Korean J Pathol. 2014;48: 263-269.

50. Nijkamp MM, Span PN, Hoogsteen IJ, van der Kogel AJ, Kaanders JH, Bussink J. Expression of E-cadherin and vimentin correlates with metastasis formation in head and neck squamous cell carcinoma patients. Radiother Oncol. 2011;99: 344-348.

51. Wang C, Liu X, Chen Z, et al. Polycomb group protein EZH2-mediated E-cadherin repression promotes metastasis of oral tongue squamous cell carcinoma. Mol Carcinog. 2013;52: 229-236.

52. Chang JW, Gwak SY, Shim GA, et al. EZH2 is associated with poor prognosis in head-and-neck squamous cell carcinoma via regulating the epithelial-to-mesenchymal transition and chemosensitivity. Oral Oncol. 2016;52: 66-74.

53. Kidani K, Osaki M, Tamura T, et al. High expression of EZH2 is associated with tumor proliferation and prognosis in human oral squamous cell carcinomas. Oral Oncol. 2009;45: 39-46.

54. Yan M, Zhang Y, He B, et al. IKKα restoration via EZH2 suppression induces nasopharyngeal carcinoma differentiation. Nat Commun. 2014;5: 3661.

55. Liu L, Tang XH, Scognamiglio T, Gudas LJ. Oral carcinogenesis induced by 4-nitroquinoline 1-oxide in lecithin:retinol acyltransferase gene knockout mice. J Nutr Biochem. 2010;21: 975-982.

56. Schweitzer A, Knauer SK, Stauber RH. Nuclear receptors in head and neck cancer: current knowledge and perspectives. Int J Cancer. 2010;126: 801-809.
57. Schug TT, Berry DC, Shaw NS, Travis SN, Noy N. Opposing effects of retinoic acid on cell growth result from alternate activation of two different nuclear receptors. Cell. 2007;129: 723-733.

CHAPTER FIVE

CONCLUSIONS AND FUTURE DIRECTIONS

K14-rtTA/TRE-ALDH1a2 murine model of inducible ALDH1a2 expression

We have developed the first murine model for inducible ALDH1a2 expression. In our Tet-On system, ALDH1a2 is inducibly and reversibly expressed in certain squamous epithelial tissues: the tongue, skin, and esophagus (Figures 3.2, 3.3). Because of the importance of endogenous RA signaling in both normal and disease states of the epithelium, such a model will be a valuable experimental system for future experiments.

The effect of TG ALDH1a2 expression on retinoid signaling

One of the goals of this project was to determine how overexpression of ectopic ALDH1a2 affects RA signaling in the epithelium. Preliminary data from human SCC cell lines infected with ALDH1a2-containing retrovirus suggest that ALDH1a2 overexpression increases the expression of certain other RA signaling pathway genes in transformed keratinocytes (see Appendix, Figure A.1). We also observed that TG ALDH1a2 increased CRABP2 protein levels and decreased EZH2 protein levels in the tongue epithelia of *K14-rtTA/TRE-ALDH1a2* (*KRT/ALDH*) mice (Figure 3.5B). These data indirectly evidence that ectopic ALDH1a2 stimulates RA signaling, however future work should be done to confirm this directly. While we were ultimately unsuccessful in using LC-MS to measure retinoid levels following TG ALDH1a2 induction by dox due to technical issues, we are optimistic that these issues can be resolved in future LC-MS

experiments (see Appendix, Figures A.2, A.3). Ideally, this future work will delineate the effects of ectopic ALDH1a2 expression on total intracellular RA levels, which would greatly inform our results as well as the field of retinoid synthesis and metabolism.

The effect of TG ALDH1a2 on EZH2 and PRC2 activity

We were intrigued to observe that TG ALDH1a2 decreases EZH2 protein levels in the tongue epithelia of *KRT/ALDH* mice treated with dox (Figures 3.7, 4.6). We intend to follow up on this observation with numerous additional analyses. Endogenous EZH2 is a methyltransferase that functions as a core component of the Polycomb Repressive Complex 2 (PRC2), and catalyzes the trimethylation of lyine 27 on histone H3 (H3K27me3)[1]. We therefore will evaluate the levels of H3K27me3 and the levels of other members of PRC2 (such as Suz12 and Eed) in dox-treated *KRT/ALDH* mice to further our understanding of how TG ALDH1a2 affects the functions of EZH2 and PRC2.

EZH2 plays a critical role in the differentiation of embryonic basal epithelial progenitor cells[2]. We therefore plan to investigate whether the decreased EZH2 protein levels in tongue epithelia of dox-treated *KRT/ALDH* mice are associated with changes in the differentiation of the basal stem cell population. To assess this, we will look at markers of epithelial terminal differentiation – such as loririn and filaggrin – in dox-treated *KRT* and *KRT/ALDH* transgenic mice. In addition, we will continue our ongoing experiments with *K14-CreER$^{TAM+/-}$/ROSA26$^{+/-}$/K14-rtTA$^{+/-}$/TRE-ALDH1a2$^{+/-}$* quadruple-transgenic mice, as described in the Appendix. In this work, we are utilizing

a lineage-tracing approach to evaluate how TG ALDH1a2 expression affects the tongue stem/progenitor cell profile. These experiments will illuminate how TG ALDH1a2 repression of EZH2 expression affects basal epithelial cell differentiation in the tongue.

ALDH1a2 as a putative tumor suppressor in head and neck cancer

We have demonstrated that endogenous ALDH1a2 mRNA and protein expression is reduced in human HNSCC compared to normal tissue, cultured human HNSCC cell lines compared to a non-transformed line, and the tongues of carcinogen-treated mice compared to control-treated mice in the 4-NQO murine model of OSCC (Figures 2.1, 2.2, 4.2). Together, these results indicate that decreased ALDH1a2 levels are a common event in HNSCC. Furthermore, there is a logical pathogenic connection between loss of ALDH1a2 expression and HNSCC carcinogenesis since ALDH1a2 synthesizes intracellular RA, a known signaling molecule for growth arrest, apoptosis, and differentiation[3]. We have also shown that ectopic ALDH1a2 expression decreases the proliferation and colony formation of human SCC cells (Figures 2.4, 2.5). Together these data indicate that ALDH1a2 acts as a tumor suppressor in HNSCC.

ALDH1a2 as an inhibitor of tumor cell migration and metastasis

We observed that ectopic ALDH1a2 decreased known markers of EMT – vimentin and EZH2 – in the tongue epithelia of 4-NQO-treated mice (Figures 4.5, 4.6). This is an intriguing finding which suggests that ALDH1a2 inhibits tumor migration and metastasis during OSCC carcinogenesis. However more research should be conducted to confirm this hypothesis. This could be investigated using cellular migration and invasion assays of control- and ALDH1a2-infected SCC cell lines *in vitro*

and analyzing the cell lines for expression of EMT markers. In addition, by injecting the SCC cell lines into oral cavities of immunocompromised mice, we could test the ability of ALDH1a2-infected lines to develop SCCs and metastases *in vivo*[4].

In Chapter 4, we utilized a 4-NQO-induced murine model of OSCC in which mice are administered 100 μg/mL 4-NQO (plus dox) in the drinking water for 10 weeks. Following 10 weeks of 4-NQO treatment, mice are switched to drinking water containing dox alone and monitored for cancerous lesion development. Though mice in this model develop lesions that are histologically and molecularly similar to those observed in human OSCC, they generally do not develop lymph node metastases, which is a common feature of the human disease[5]. In 2013, Li *et al*. reported that treating mice with a higher dose of 4-NQO (200 μg/mL) for a longer period of time (20 weeks) resulted in a high rate of lymph node metastases[6]. Therefore in order to evaluate whether ectopic, TG ALDH1a2 inhibits metastasis development in 4N+Dox *KRT/ALDH* mice, we could conduct additional experiments in which *KRT* and *KRT/ALDH* mice are treated with higher dose 4-NQO (plus dox) for a longer period of time and assessed for regional lymph node metastases.

Lastly, we would also like to investigate whether TG ALDH1a2 affects the expression of E-cadherin in addition to vimentin. While vimentin is mesenchymal marker, E-cadherin is an epithelial marker, and both of these proteins are well-characterized as markers of EMT. Increased vimentin expression and decreased E-cadherin expression are observed in HNSCC patient tumors, and associate with poor prognostic factors such as recurrence, reduced overall survival, and lymph node

metastases[7]. In addition, knockdown of EZH2 in HNSCC cell lines FaDu and SNU1041 increased E-cadherin expression and decreased vimentin expression[8]. We therefore intend to evaluate the E-cadherin protein levels in the tongue epithelia of our VC+Dox and 4N+Dox *KRT* and *KRT/ALDH* mice, to further characterize how ectopic ALDH1a2 affects EMT in this tissue during 4-NQO-induced carcinogenesis.

ALDH1a2: a putative drug target?

Increasing intracellular RA signaling through a means other than application of exogenous retinoids is still for the most part an unexplored and unexploited avenue for HNSCC therapy. Studies have shown that the cellular localization of RA, and the efficacy of stimulated gene expression, can differ depending on whether RA is added externally or is generated endogenously. For example, inhibition of RA catabolism to increase intracellular RA was shown to be effective in breast cancer cells, whereas application of exogenous RA was not[9]. To date the limited efficacy of exogenous retinoid treatment is largely attributed to rapid metabolism – both on a cellular level via CYP26A1, and on an organismal level via the liver[9]. An ALDH1a2-based therapy could potentially exhibit different metabolic properties and be more efficacious and/or less toxic than delivery of exogenous RA. Furthermore, the ALDH family of enzymes is amenable to activation via small molecules, which can be identified via adaptation of an already established high throughput screen, making development of a therapeutic strategy to increase ALDH1a2 activity in tumors a future possibility[10]. Lastly, there is evidence that ALDH1a2 and other key members of the RA signaling pathway exhibit reduced expression in HNSCC due to promoter hypermethylation[11, 12]. Therefore,

should future experimentation on ALDH1a2 in HNSCC prove promising, combination therapy of an ALDH1a2-activator and a DNA methyltransferase inhibitor could be an attractive chemotherapeutic strategy.

REFERENCES

1. Cao R, Wang L, Wang H, et al. Role of histone H3 lysine 27 methylation in Polycomb-group silencing. Science. 2002;298: 1039-1043.

2. Ezhkova E, Pasolli HA, Parker JS, et al. Ezh2 orchestrates gene expression for the stepwise differentiation of tissue-specific stem cells. Cell. 2009;136: 1122-1135.

3. Mongan NP, Gudas LJ. Diverse actions of retinoid receptors in cancer prevention and treatment. Differentiation. 2007;75: 853-870.

4. Simon C, Nemechek AJ, Boyd D, et al. An orthotopic floor-of-mouth cancer model allows quantification of tumor invasion. Laryngoscope. 1998;108: 1686-1691.

5. Leemans CR, Braakhuis BJ, Brakenhoff RH. The molecular biology of head and neck cancer. Nat Rev Cancer. 2011;11: 9-22.

6. Li J, Liang F, Yu D, Qing H, Yang Y. Development of a 4-nitroquinoline-1-oxide model of lymph node metastasis in oral squamous cell carcinoma. Oral Oncol. 2013;49: 299-305.

7. Kim KH, Kim L, Choi SJ, et al. The clinicopathological significance of epithelial mesenchymal transition associated protein expression in head and neck squamous cell carcinoma. Korean J Pathol. 2014;48: 263-269.

8. Chang JW, Gwak SY, Shim GA, et al. EZH2 is associated with poor prognosis in head-and-neck squamous cell carcinoma via regulating the epithelial-to-mesenchymal transition and chemosensitivity. Oral Oncol. 2016;52: 66-74.

9. Belosay A, Brodie AM, Njar VC. Effects of novel retinoic acid metabolism blocking agent (VN/14-1) on letrozole-insensitive breast cancer cells. Cancer Res. 2006;66: 11485-11493.

10. Budas GR, Disatnik MH, Mochly-Rosen D. Aldehyde dehydrogenase 2 in cardiac protection: a new therapeutic target? Trends Cardiovasc Med. 2009;19: 158-164.

11. Kostareli E, Holzinger D, Bogatyrova O, et al. HPV-related methylation signature predicts survival in oropharyngeal squamous cell carcinomas. J Clin Invest. 2013;123: 2488-2501.

12. Youssef EM, Lotan D, Issa JP, et al. Hypermethylation of the retinoic acid receptor-beta(2) gene in head and neck carcinogenesis. Clin Cancer Res. 2004;10: 1733-1742.

APPENDIX

CHANGES IN RA TARGET GENES IN SCC-25 CELLS AS MEASURED BY RT-PCR

In our experiments described in Chapter 2, we analyzed the phenotypic effects of transgenic (TG) ALDH1a2 overexpression in cultured human SCC cell lines. We also carried out analysis of transcript levels of known RA target genes following retroviral infection of SCC-25 cells with pQC (empty vector) or pQC-ALDH1a2. The pQC-ALDH1a2 vector drives constitutive overexpression of ALDH1a2 (Supplemental Figure 2.1). These RT-PCR analyses, repeated n=2 times, provided preliminary evidence that overexpression of TG ALDH1a2 increased transcript expression of retinoic acid receptor γ (RARγ) and cytochrome P450 enzymes CYP26A1 and CYP26B1 in SCC-25 cells (Figure A.1). Cells infected with the empty vector and treated with exogenous RA (1 μM) (+pQC +RA) were used as a positive control. We also observed increased CYP26A1 and CYP26B1 transcript levels in ALDH1a2-infected SCC-9 cells (n=2, data not shown).

The retinoic acid receptors, including RARγ, are bound and activated by RA to initiate changes in gene transcription that control many key cellular processes[1]. Cytochrome P450 family 26 (CYP26) enzymes metabolize RA and are highly inducible by RA in many cellular contexts, including in keratinocytes[2, 3]. Therefore these preliminary results suggest that overexpression of TG ALDH1a2 is sufficient to increase RA signaling in this transformed oral keratinocyte line. Future experiments will confirm these results in this and other HNSCC cell lines, and delineate the effect of ectopic ALDH1a2 expression on other known RA signaling genes (e.g. RARβ$_2$) compared to

treatment with exogenous RA. Such results would be highly informative to the study of retinoid signaling in the context of epithelial carcinomas.

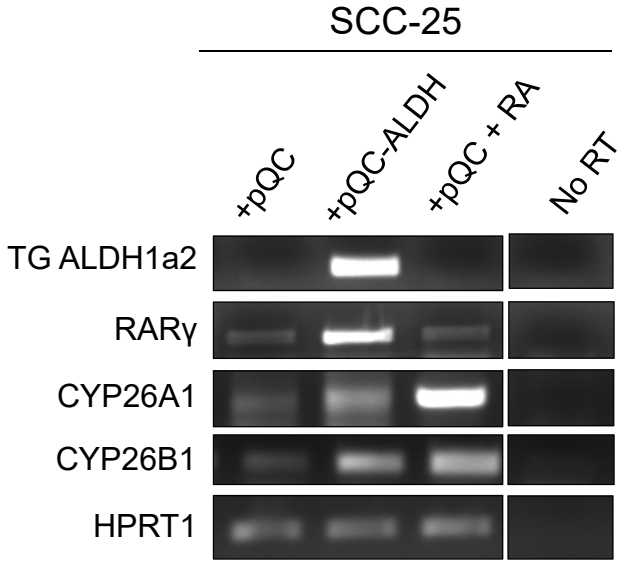

Figure A.1: mRNA expression of RA signaling genes in infected SCC-25 cells. **S**CC-25 cells were infected overnight with either empty vector (pQC) or a vector driving constitutive expression of ALDH1a2 (pQC-ALDH1a2, Supplemental Figure 2.1) and selected 7-10 days with puromycin. Cells were then plated for experiments and treated with vehicle control (DMSO) or 1μM RA for 7 days. We then harvested cells and performed RNA isolation according to the manufacturer's protocol. RT-PCR protocol is described in the Materials and Methods of Chapters 2-4. TG ALDH1a2 results shown here are representative of n≥3 biological repeats. RARγ, CYP26A1 and CYP26B1 RT-PCR results shown here are representative of n=2 biological repeats. HPRT1 was used as a loading control. All primers used in this figure are described in Table A.1.

Table A.1: Primer sequences used for RT-PCR

Gene	Forward Primer (5'-3')	Reverse Primer (5'-3')	Product Size
ALDH1a2 TG	gacttgtagcagctgtcttcact	tcacccatttctctcccatttcc	160 bp
CYP26A1	gaggggagagcggctggaca	agcaacccgaaaccctcctgg	292 bp
CYP26B1	tgggcttcccgctcatcgga	ctcacgaggtggtgctcgcc	181 bp
RARγ	aatgacaagtcctctggctaccac	cagatccagctgcacgcggtggtc	393 bp
HPRT1	tgaggatttggaaagggtgt	aatccagcaggtcagcaaag	155 bp

REFERENCES

1. Tang XH, Gudas LJ. Retinoids, retinoic acid receptors, and cancer. Annu Rev Pathol. 2011;6: 345-364.

2. Pavez Loriè E, Li H, Vahlquist A, Törmä H. The involvement of cytochrome p450 (CYP) 26 in the retinoic acid metabolism of human epidermal keratinocytes. Biochim Biophys Acta. 2009;1791: 220-228.

3. Loudig O, Babichuk C, White J, Abu-Abed S, Mueller C, Petkovich M. Cytochrome P450RAI(CYP26) promoter: a distinct composite retinoic acid response element underlies the complex regulation of retinoic acid metabolism. Mol Endocrinol. 2000;14: 1483-1497.

THE EFFECTS OF ECTOPIC (TG) ALDH1A2 EXPRESSION ON RETINOID LEVELS IN THE STRATIFIED SQUAMOUS EPITHELIUM

Endogenous ALDH1a2 plays a critical role in retinoid signaling and metabolism, as it catalyzes the synthesis of intracellular RA[1, 2]. Therefore, we anticipated that the induction of exogenous (TG) ALDH1a2 using our Tet-On expression system would result in increased intracellular all-*trans* retinoic acid (RA) in target tissues. In addition, absolute quantitation of RA following expression of TG ALDH1a2 would provide direct evidence that ALDH1a2 overexpression increases RA signaling through increased RA synthesis. In preliminary experiments in our lab, using reverse phase high-performance liquid chromatography (HPLC), we could not detect retinol or RA in mouse tongue and skin samples from either *K14-rtTA* (*KRT*) or *K14-rtTA/TRE-ALDH1a2* (*KRT/ALDH*) mice treated with dox for 72 hrs (data not shown). Consequently, we next tried using liquid chromatography-mass spectrometry (LC-MS), which has a lower limit of detection[3]. These experiments are detailed below.

MATERIALS AND METHODS

Liquid chromatography-mass spectrometry (LC-MS) analysis of retinoid levels

We treated *K14-rtTA*$^{(+/-)}$*/TRE-ALDH1a2*$^{(+/-)}$ (*KRT/ALDH*) mice and *K14-rtTA*$^{(+/-)}$ (*KRT*) littermate mice with dox for 72 hours before sacrifice. All mice were from the #11 line. We dissected whole tongue (60-100 mg each) and skin (~100 mg each) from each mouse, and snap froze and weighed each tissue sample before homogenization in 500 µL PBS. As an internal control of extraction efficiency, we added 25 µL of a 100 µM stock of retinyl acetate, which is not present endogenously in

these tissues. We then extracted retinoids as previously described[4, 5]. Briefly, we added 350 µL of acetonitrile:butanol (50:50, v/v) to each sample and vortexed for 45 seconds. We then added 300 µL of a saturated K_2HPO_4 solution (~1.3 Kg/L), vortexed again, and centrifuged 10 minutes at 14,000 rpm. The upper organic layer was collected, dried down, and placed under argon before shipping to the Metabolite Profiling Core Facility at the Whitehead Institute for Biomedical Research (affiliated with the Massachusetts Institute of Technology) for LC-MS analysis. In our first LC-MS experiment, each individual tissue was analyzed separately (i.e. the retinoid extract of n=1 mouse tongue = 1 sample analyzed by LC-MS). In our second LC-MS experiment, we pooled the tissue retinoid extracts in triplicate (i.e. the retinoid extracts from n=3 mouse tongues = 1 sample analyzed by LC-MS) before drying them down for shipping. Retinoic acid and retinol were measured using an RP-Amide column with a gradient of water/0.1% formic acid and acetonitrile/0.1% formic acid, as previously described[3]. Retinyl palmitate and retinyl acetate were measured using a C18 column, as previously described[6]. Retinoid levels were normalized to starting tissue weight and retinyl acetate detection, as indicated. Work at the Whitehead Institute was conducted by Dr. Elizaveta Freinkman. Dr. Freinkman, the director of this facility, left the Whitehead Institute in the fall of 2016 and there was a search for a new director.

RESULTS

The effect of ectopic ALDH1a2 expression on retinoid levels in the stratified squamous epithelium

Using LC-MS as described in the Materials and Methods, we measured the levels of RA in the tongues and skin of n=3 *KRT/ALDH* mice and n=3 *KRT* mice treated with dox for 72 hours (6 tongue and 6 skin samples analyzed, 1 tongue and 1 skin per mouse). We also analyzed the levels of retinol and retinyl palmitate (a retinyl ester), to ascertain how dox induction of TG ALDH1a2 affected the retinoid pathway and overall retinoid status of target cells. In our initial LC-MS run we could not detect retinyl palmitate in the majority of the samples (detected in 3/6 tongue and 1/6 skin samples; data not shown). In addition, we detected very low levels of RA in both tongue and skin samples (ranging from 0.0008 to 0.066 pmol/mg tissue; RA in one *KRT/ALDH* tongue sample was undetectable) (Figure A.2). Furthermore, both RA and retinol levels were variable within each group of mice, complicating further analysis (Figure A.2).

We therefore conducted a larger experiment in which we treated n=18 mice (n=9 *KRT/ALDH*, n=9 *KRT*) for 72 hours with dox, and extracted retinoids from tongue and skin tissue as before. We then pooled the retinoid extracts from n=3 individual tissue samples to generate larger samples for analysis (i.e. the n=9 tongues from each group were pooled in triplicate to generate 3 separate samples for LC-MS). Unfortunately, due to a technical failure at the facility, RA levels were undetectable in all samples, including the standard curve samples. This experiment could not be repeated in the fall of 2016 because of the departure of Dr. Freinkman. However we were able to detect

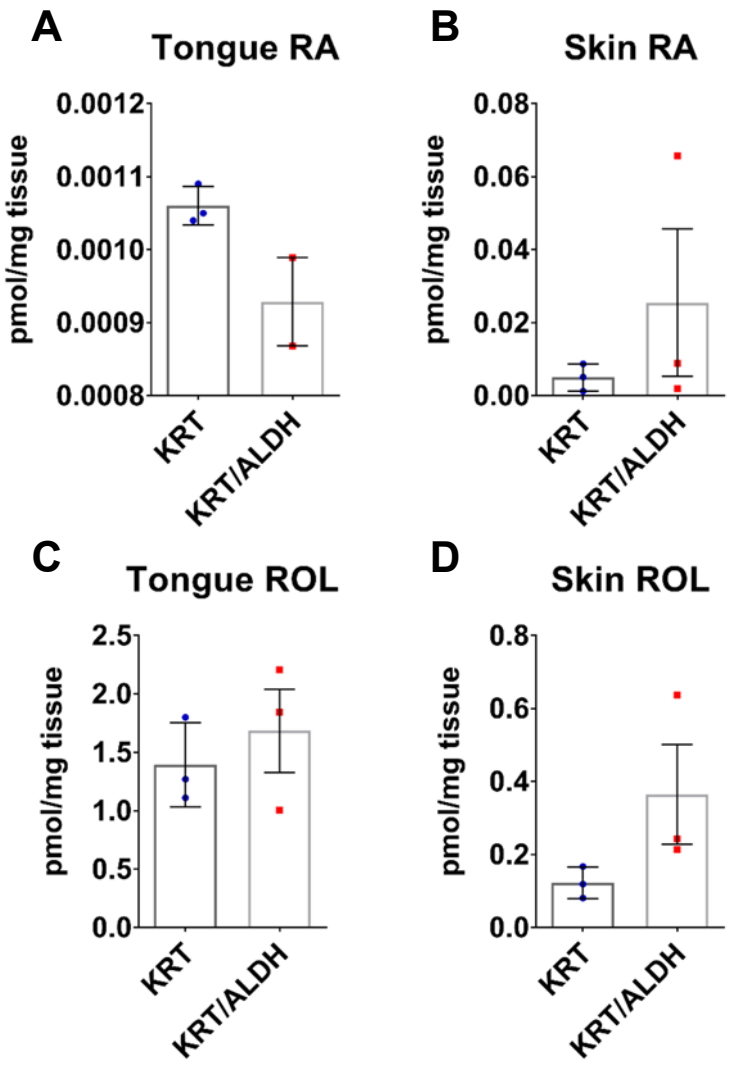

Figure A.2: LC-MS of retinoids in the tongues and skin of n=6 dox-treated *KRT* and *KRT/ALDH* mice. Six 6-8 week-old #11 line mice (n=3 *KRT, n*=3 *KRT/ALDH*) were treated with dox for 72 hrs before sacrifice and tissue dissection. Whole tongues (~60-100 mg) and skin (~100 mg) were weighed, snap frozen, and homogenized in PBS. Retinoids were extracted according to standard protocol, dried down, and shipped on dry ice to the Whitehead Institute for LC-MS analysis. (A,B) Analysis of tissue retinoic acid levels. (C,D) Analysis of tissue retinol levels. All results shown are normalized to starting tissue weight and retinyl acetate concentration. Error bar represents ±SEM as calculated by GraphPad Prism 6.0 software.

retinyl palmitate in all of the tongue and skin samples, and we detected no statistical differences in the average retinyl palmitate levels of dox-treated *KRT* and *KRT/ALDH* mice (Figures A.3A,B). Retinol levels also exhibited no significant differences in the mean in the tongue and skin samples (Figures A.3C,D). However, retinol levels in the tongue and skin samples from *KRT/ALDH* mice exhibited greater variation than those from *KRT* mice; using an F test to compare variances, we found that there was a statistical difference in the variance (p=0.0003) of tongue retinol levels in *KRT/ALDH* mice compared to *KRT* mice.

DISCUSSION

We investigated how induced expression of TG ALDH1a2 modulates intracellular retinoid levels using LC-MS. Ultimately we were unable to obtain a conclusive result for RA levels in the tongues and skin of *KRT* and *KRT/ALDH* mice. Future experiments with these mice will seek to achieve this, as RA levels are a key measurement in determining how expression of TG ALDH1a2 affects intracellular RA synthesis and signaling. Using HPLC, researchers in our lab were previously able to detect tongue retinol levels of 0.06±0.02 pmol/mg in control-fed wild type mice (normalized to starting tissue weight)[7]. In our first LC-MS experiment (1 tongue = 1 sample analyzed), we detected tongue retinol levels of 1.393±0.2086 pmol/mg (normalized to starting tissue weight and retinyl acetate concentration) (Figure A.2). In our second LC-MS experiments (3 tongues = 1 sample analyzed) we detected tongue retinol levels of 0.1045±0.0002 (normalized to starting tissue weight and retinyl acetate

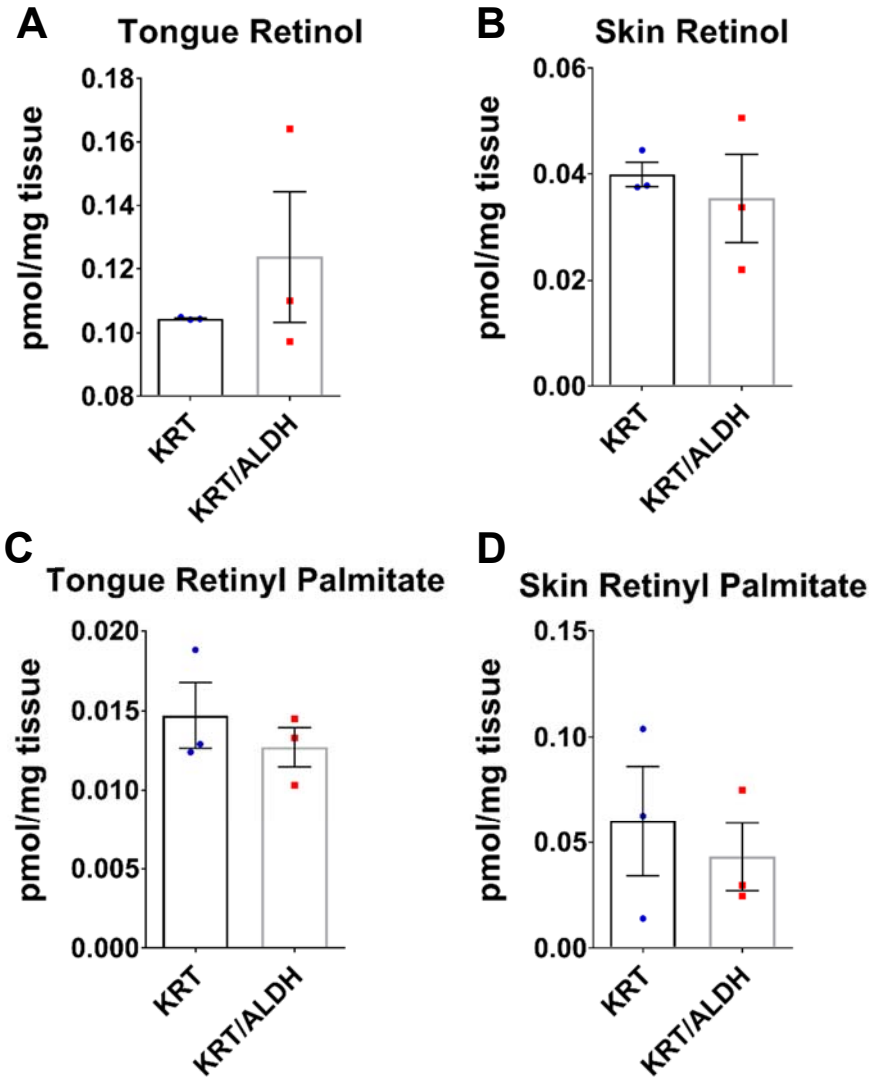

Figure A.3: LC-MS of retinoids in the tongues and skin of n=18 dox-treated *KRT* and *KRT/ALDH* mice. Eighteen 6-8 week-old mice (n=9 *KRT, n*=9 *KRT/ALDH*; all #11 line) were treated with dox for 72 hrs before sacrifice and tissue dissection. Whole tongues (~60-100 mg) and skin (~100 mg) were weighed, snap frozen, and homogenized in PBS. Retinoids were extracted according to standard protocol, pooled in triplicate, dried down, and shipped on dry ice to the Whitehead Institute for LC-MS analysis. (A,B) Analysis of tissue retinol levels. (C,D) Analysis of tissue retinyl palmitate levels. All results shown are normalized to starting tissue weight and retinyl acetate concentration. Error bar represents ±SEM as calculated by GraphPad Prism 6.0 software.

concentration) (Figure A.3). Therefore our second experiment, in which we used tissue samples pooled in triplicate, was more consistent with previous data on retinoid levels in these tissues (Figure A.3).

We did not observe any statistical difference in the mean levels of retinyl palmitate or retinol (Figure A.2, A.3). Of course, we would not expect a difference in retinyl palmitate or retinol since the levels of these retinoids are much higher than those of RA in most tissues[7, 8]. However, with respect to tongue retinol levels, there was a statistically significant difference in the variance between *KRT* mice and *KRT/ALDH* mice. This was unexpected since each sample analyzed was a combination of three whole tongues from different mice. While the meaning of this result is inconclusive, it could suggest that ALDH1a2-inducing *KRT/ALDH* mice exhibit greater variation in tongue vitamin A status as compared to control mice. Future experiments will seek to clarify the effect of ectopic TG ALDH1a2 expression on retinoid levels in these tissues.

REFERENCES

1. Gudas LJ. Emerging roles for retinoids in regeneration and differentiation in normal and disease states. Biochim Biophys Acta. 2012;1821: 213-221.

2. Zhao D, McCaffery P, Ivins KJ, et al. Molecular identification of a major retinoic-acid-synthesizing enzyme, a retinaldehyde-specific dehydrogenase. Eur J Biochem. 1996;240: 15-22.

3. Kane MA, Napoli JL. Quantification of endogenous retinoids. Methods Mol Biol. 2010;652: 1-54.

4. Tang XH, Su D, Albert M, Scognamiglio T, Gudas LJ. Overexpression of lecithin:retinol acyltransferase in the epithelial basal layer makes mice more sensitive to oral cavity carcinogenesis induced by a carcinogen. Cancer Biol Ther. 2009;8: 1212-1213.

5. Tang XH, Suh MJ, Li R, Gudas LJ. Cell proliferation inhibition and alterations in retinol esterification induced by phytanic acid and docosahexaenoic acid. J Lipid Res. 2007;48: 165-176.

6. Bird SS, Marur VR, Sniatynski MJ, Greenberg HK, Kristal BS. Serum lipidomics profiling using LC-MS and high-energy collisional dissociation fragmentation: focus on triglyceride detection and characterization. Anal Chem. 2011;83: 6648-6657.

7. Liu L, Gudas LJ. Disruption of the lecithin:retinol acyltransferase gene makes mice more susceptible to vitamin A deficiency. J Biol Chem. 2005;280: 40226-40234.

8. Liu L, Tang XH, Gudas LJ. Homeostasis of retinol in lecithin: retinol acyltransferase gene knockout mice fed a high retinol diet. Biochem Pharmacol. 2008;75: 2316-2324.

USING A CELL LINEAGE TRACING APPROACH TO INVESTIGATE THE EFFECT OF TRANSGENIC ALDH1A2 ON STEM CELL DIVISION

Previously, researchers in our lab have utilized *K14-CreER^{TAM}/ ROSA26* transgenic mice to identify and track K14+ epithelial stem cells[1, 2]. Using this transgenic expression system, we are able to permanently mark stem/progenitor cells in the mouse tongue epithelia and visualize clonal cell populations using X-gal staining. In my experiments, we observed that increased transgenic (TG) ALDH1a2 decreased EZH2 protein expression in normal and 4-NQO-treated tongue epithelia (Chapters 3, 4). EZH2 is a known orchestrator of gene expression in the differentiation of embryonic epithelial stem cells[3]. We therefore wanted to investigate whether inducible TG ALDH1a2 expression affects the stem/progenitor profile in normal and carcinogen-treated tongue epithelia.

We crossed a *K14-rtTA$^{+/-}$/TRE-ALDH1a2$^{+/-}$* mouse with a *K14-CreER$^{TAM+/-}$/ROSA26$^{+/-}$* mouse to generate a *K14-CreER$^{TAM+/-}$/ROSA26$^{+/-}$/K14-rtTA$^{+/-}$/TRE-ALDH1a2$^{+/-}$* line. The pups resulting from this cross were genotyped for the presence of each of the four transgenes using RT-PCR as previously described (Chapter 3, 4)[1]. Mice from this line that possess all four transgenes will have ALDH1a2 expression (following doxycycline (dox) treatment) and LacZ expression (following tamoxifen treatment) specifically in the basal layer of the epithelium.

We treated n=22 mice of various genotypes. N=6 were positive for all four transgenes, n=5 positive for *K14-CreER$^{TAM+/-}$/ROSA26$^{+/-}$*, n=3 positive for *K14-rtTA$^{+/-}$/TRE-ALDH1a2$^{+/-}$*, and the remainder positive for other gene combinations that will not result in any TG ALDH1a2 expression or positive X-gal staining. All mice received tamoxifen (4mg/mouse/day) by intraperitoneal injections on two consecutive days two

weeks prior to the start of treatment. Mice were then treated with vehicle control plus dox (2 mg/mL; Sigma) (VC+Dox) or 4-NQO (100 100 µg/mL; Sigma) plus dox (2 mg/mL) (4N+Dox) for 10 weeks. We sacrificed mice at the 12 week time point, and carried out X-gal staining as previously described[1, 2].

We aimed to analyze the resulting blue signal and compare: a) VC+Dox *K14-CreER$^{TAM+/-}$/ROSA26$^{+/-}$/K14-rtTA$^{+/-}$/TRE-ALDH1a2$^{+/-}$* and *K14-CreER$^{TAM+/-}$/ROSA26$^{+/-}$* mice, which would reveal how TG ALDH1a2 affects the stem/progenitor profile in non-transformed tongues, and b) 4N+Dox *K14-CreER$^{TAM+/-}$/ROSA26$^{+/-}$/K14-rtTA$^{+/-}$/TRE-ALDH1a2$^{+/-}$* and *K14-CreER$^{TAM+/-}$/ROSA26$^{+/-}$* mice, which would reveal how TG ALDH1a2 affects the stem/progenitor profile in tongues undergoing 4-NQO-induced carcinogenesis. Analysis has been complicated by genotyping errors which were discovered after sacrifice. These errors resulted in n<3 mice in some of the key treatment groups. Future experiments will remedy this, and currently analysis of this experiment is still underway. Representative images of X-gal stained tongues from some of the groups are shown in Figure A.4.

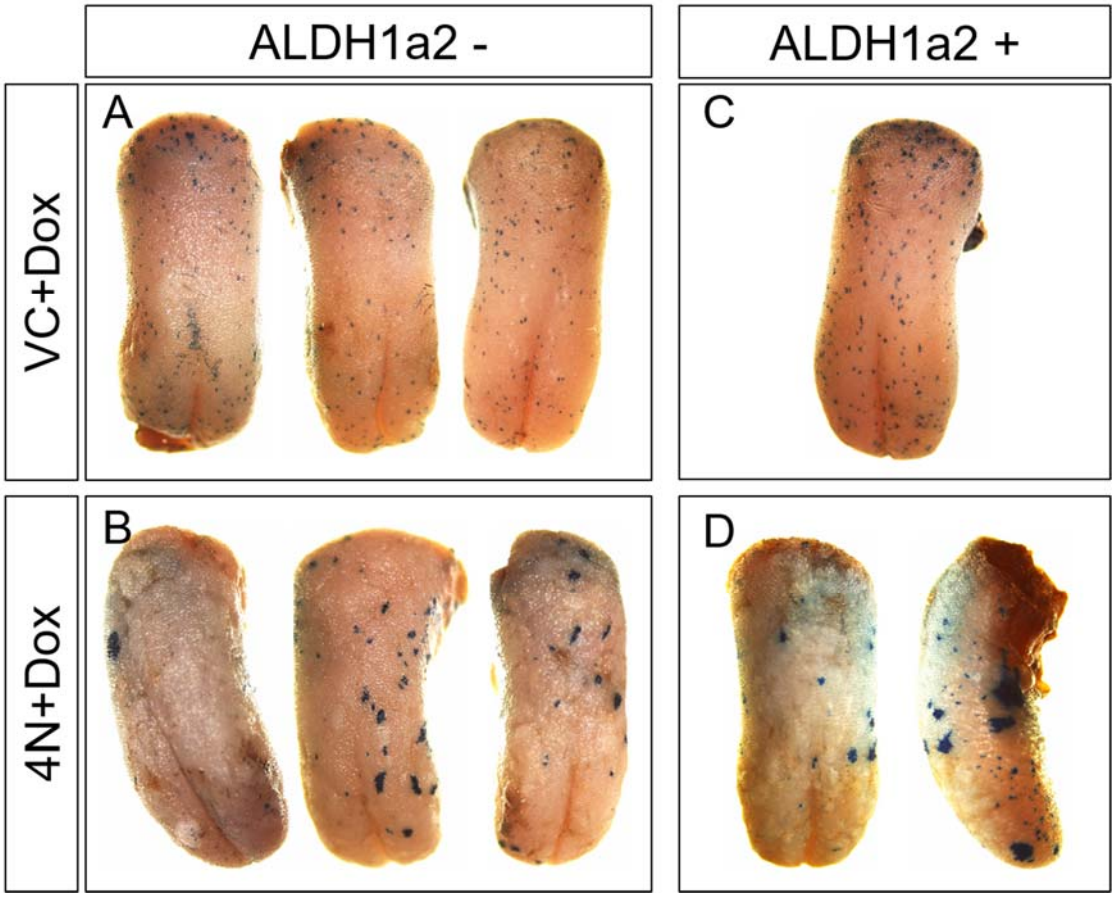

Figure A.4: Representative photomicrographs of whole mount X-gal-stained tongues to visualize a representative population of stem cells. (A) VC+Dox-treated mice (n=3) positive for *K14-CreER^{TAM}/ROSA26* (ALDH1a2-); (B) 4N+Dox-treated mice (n=3) positive for *K14-CreER^{TAM}/ROSA26* (ALDH1a2-); (C) VC+Dox-treated mouse (n=1) positive for *K14-CreER^{TAM}/ROSA26/K14-rtTA/TRE-ALDH1a2* (ALDH1a2+); (D) 4N+Dox-treated mouse (n=1) positive for *K14-CreER^{TAM}/ROSA26/K14-rtTA/TRE-ALDH1a2* (ALDH1a2+) (two views shown). Magnification, ×4.

REFERENCES

1. Tang XH, Scognamiglio T, Gudas LJ. Basal stem cells contribute to squamous cell carcinomas in the oral cavity. Carcinogenesis. 2013;34: 1158-1164.

2. Osei-Sarfo K, Tang XH, Urvalek AM, Scognamiglio T, Gudas LJ. The molecular features of tongue epithelium treated with the carcinogen 4-nitroquinoline-1-oxide and alcohol as a model for HNSCC. Carcinogenesis. 2013;34: 2673-2681.

3. Ezhkova E, Pasolli HA, Parker JS, et al. Ezh2 orchestrates gene expression for the stepwise differentiation of tissue-specific stem cells. Cell. 2009;136: 1122-1135.